Thin-Walled Structures

Using laminate hybridisation (CFRP-GFRP) and shaped CFRP plies to increase plate post-buckling strain to failure under shear loading

--Manuscript Draft--

Manuscript Number:	TWST-D-20-01039R1
Article Type:	Research Paper
Keywords:	shear buckling; Laminated Composites; hybrid composites; post-buckling behaviour; Nonlinear behaviour; failure criterion
Corresponding Author:	mahdi damghani University of the West of England - Frenchay Campus: University of the West of England Bristol, UNITED KINGDOM
First Author:	mahdi damghani, PhD
Order of Authors:	mahdi damghani, PhD
	Christopher Wallis
	Jerzy Bakunowicz, PhD
	Adrian Murphy, PhD
Manuscript Region of Origin:	Europe
Abstract:	Previous works have established the response and failure behaviour of hybrid (CFRP-GFRP) laminates when subjected to a wide range of destabilising loads. However, to date no works have quantified the influence of selective laminate shapes and hybridisation on plate post-buckling strain to failure. Thus, this paper investigates the plate collapse behaviour of a novel X-braced hybrid (CFRP-GFRP) twill woven laminate, subjected to in-plane shear loading. An experimental and numerical investigation is undertaken, including the consideration of a baseline pure CFRP laminate design. The experimental results illustrate that despite having less CFRP material, a hybrid laminate design with shaped CFRP plies can exhibit a greater strain to failure and buckling to failure load ratio, with only a marginally lower initial plate buckling load. Additionally, the experimental and numerical analysis reveals that the failure mechanism of the hybrid laminate is dominated by shear damage and fibre compressive breakage, whereas compressive and tensile fibre breakage dominate the conventional baseline laminate behaviour. Due to the prevalence of the shear damage and hence cracking and plastic deformation of the matrix, the novel hybrid laminate demonstrates a more gradual failure than the standard baseline laminate design, with failure strains significantly higher than that of the baseline laminate design.
Suggested Reviewers:	Carol Featherston, PhD professor, Cardiff University featherstonca@cf.ac.uk expert
	David Kennedy, PhD Professor, Cardiff University kennedyd@cf.ac.uk Expert
	Richard Butler, PhD Professor, University of Bath R.Butler@bath.ac.uk expert
Response to Reviewers:	

Dr. Mahdi Damghani

(CEng MIMechE, PhD, MSc, BSc)
Senior Lecturer in Composites and Aero-structures
Room 3D26
Engineering Design and Mathematics Department
University of the West of England (UWE)
Frenchay Campus
Coldharbour Lane
Bristol
BS16 1QY
Tel: 0117 328 7369
Email: Mahdi.Damghani@uwe.ac.uk

Date: 06/01/2021

Dear Editor,

I am pleased to submit an original research article titled “Using laminate hybridisation (CFRP-GFRP) and shaped CFRP plies to increase plate post-buckling strain to failure under shear loading” by Mahdi Damghani [1], Christopher Wallis [2], Jerzy Bakunowicz [3] and Adrian Murphy [4] for consideration for publication in the *Journal of Thin Walled Structures*. This article is prepared by people who are actively involved in the design and analysis of composite aerospace structures having considerable experience with industrial leaders such as Airbus UK and Rolls-Royce. This article combines experiments with numerical validation using fully characterised and calibrated material model for woven fabric composites providing unique perspective to the scientists and engineers on the advantages of the use of light weighting and hybridisation of composite laminates for enhancing their buckling and postbuckling response under shear loading.

This article has not been published and is not under consideration for publication elsewhere.

Thank you for your consideration.

Yours’ Sincerely

Dr. Mahdi Damghani

---

[1] Senior Lecturer in University of the West of England (UWE), Tel: +4411732 87369, Email: Mahdi.Damghani@uwe.ac.uk
[2] Researcher in University of the West of England (UWE)
[3] Senior Lecturer in University of the West of England (UWE)
[4] Professor in University of Queen’s Belfast (QUB)

Reviewers' comments:

Reviewer #1:

The authors present an experimental and numerical investigation on novel hybrid laminates. The work is very interesting, and the paper is well written. This reviewer proposes the publication of the article following minor revisions according to the remarks below.

General comments:

Remark #1: The authors only tested 2 specimens of the novel hybrid laminates proposed. This seems far too little for this relatively small-scale testing. Although it does not necessarily invalidate the publishing of the results, this limitation should be clearly stated and the conclusions should be taken with some reserve.

Response: This was mentioned at the end of the Introduction section as highlighted in yellow on page 4. However, the end section of conclusion is reworded to reflect the reviewer's comment.

Remark #2: Given the lower buckling mode of the novel laminates, when compared to the traditional ones, there are well-founded doubts regarding their cyclic response. This should be acknowledged and, perhaps, further investigation on the topic should be proposed in future research.

Response: The authors greatly appreciate this comment. A sentence is added at the end of the conclusions section to reflect the reviewer's comment and we will study this is a later research.

Reviewer #2:

Remark #1: Section 3, paragraph 1: I believe there is a typo, where it reads: "the load bearing capacity of the GFRP plies are typically ignored", it should read: "the load bearing capacity of the GFRP plies is typically ignored".

Response: Incorporated and highlighted as green

Remark #2: Section 3: it would be interesting to state the comparison between the benchmark laminate and the X-bracing hybrid with W=60 mm.

Response: Figure 2 shows the comparison of results between type 1 and type 2 laminates for both buckling performance and mass addition. The authors did attempt to limit the amount of content given the fact that the paper already stand as 40 pages. However, a statement is added on page 9 to reflect this comment.

Remark #4: Section 4: the inputs used for the failure model are not clear.

Response: A sentence is added on page 10 and therefore an appendix is included demonstrating all the damage parameters used for the model.

Remark #5: Section 6, page 23: There is an automated reference error, likely referring to Table 2.

Response: Incorporated and highlighted as green

Remark #6: Section 6, Table 2: this reviewer does not understand how the authors retrieved the standard deviation out of two samples.
Response: The standard deviation is removed from the table is highlighted in green.

Remark #7: Section 6, page 27: In the sentence "Examination of the predicted damage from the simulation, just before failure and throughout the failure process, shows that shear damage (SDV5) occurs far in advance of any damage mechanism and is present throughout the failure process as shown in Figure 17" do the authors mean "… in advance of any axial damage mechanism"?

Response: As shown in section 5, damage is associated to both the fibre failure and shear damage. Therefore, by any other damage we mean fibre failure. To avoid further ambiguity by the reader we have added a statement in the same location to clarify what is meant by any other damage. This is highlighted in green.

Remark #8: Section 6, page 29: in the first sentence after Figure 14, the used of both "although" and "but" seem awkward.

Response: This is reworded and amended and is highlighted in green.

Remark #8: Section 7: the authors state that both laminate types failed for ~1.6 times the buckling load. However, plate type 1 failed for ~1.3 of the buckling load (arguably, a further advantage of the hybrid laminates proposed).

Response: I greatly appreciate this as the reviewer is correct. Therefore, several corrections are made throughout the document (including the conclusions section and abstract) to reflect this benefit and are highlighted in green. These include on pages 1, 24 and 34

Using laminate hybridisation (CFRP-GFRP) and shaped CFRP plies to increase plate post-buckling strain to failure under shear loading

Mahdi Damghani [a,*], Christopher Wallis [a], Jerzy Bakunowicz [a], Adrian Murphy [b]

[a] Department of Engineering, Design and Mathematics (EDM), University of the West of England (UWE), Bristol, BS16 1QY, UK

[b] School of Mechanical and Aerospace Engineering, Queen's University Belfast (QUB), Belfast, BT9 5AG, UK

Abstract

Previous works have established the response and failure behaviour of hybrid (CFRP-GFRP) laminates when subjected to a wide range of destabilising loads. However, to date no works have quantified the influence of selective laminate shapes and hybridisation on plate post-buckling strain to failure. Thus, this paper investigates the plate collapse behaviour of a novel X-braced hybrid (CFRP-GFRP) twill woven laminate, subjected to in-plane shear loading. An experimental and numerical investigation is undertaken, including the consideration of a baseline pure CFRP laminate design. The experimental results illustrate that despite having less CFRP material, a hybrid laminate design with shaped CFRP plies can exhibit a greater strain to failure and buckling to failure load ratio, with only a marginally lower initial plate buckling load. Additionally, the experimental and numerical analysis reveals that the failure mechanism of the hybrid laminate is dominated by shear damage and fibre compressive breakage, whereas compressive and tensile fibre breakage dominate the conventional baseline laminate behaviour. Due to the prevalence of the shear damage and hence cracking and plastic deformation of the matrix, the novel hybrid laminate demonstrates a more gradual failure than the standard baseline laminate design, with failure strains significantly higher than that of the baseline laminate design.

Keywords: shear buckling, laminated composites, hybrid composites, post-buckling behaviour, nonlinear behaviour, failure criterion

* Corresponding author. Tel.: +4411732 87369
Email address: Mahdi.Damghani@uwe.ac.uk

1 Introduction

In recent years, there has been a significant increase in the use of Carbon Fibre Reinforced Polymer (CFRP) and Glass Fibre Reinforced Polymer (GFRP) in the design of highly loaded structural components, e.g. aircraft wing primary structure, and wind turbine blades. For instance, the Boeing 787 Dreamliner and the Airbus 350 XWB are reported to have respectively 52 and 53 per cent of their total weight resulting from the use of CFRP material. This is a markedly more substantial proportion than reported for the previous generation of aircraft, for example, 12 per cent for the Boeing 777 [1]. This marked increase is due to the superior strength/weight and stiffness/weight ratios of such material systems compared to conventional homogeneous isotropic materials, e.g. aluminium alloy [2]. Moreover, these materials also demonstrate enhanced fatigue performance [3] and corrosion resistance [4], particularly crucial for high-performance structures with long service life.

In aerospace applications, wing and fuselage CFRP panels are subjected to significant loading resulting from a vast range of combined aerodynamic pressures, manoeuvre induced inertial loads, and environmental fluctuations, e.g. temperature changes. Such panels are typically thin-walled, to minimise structural mass, but have large surface areas to generate the required lift or enclose the payload, crew, systems and fuel. Additionally, stiffness is a key requirement for such panels to maintain an aerodynamic form. As a result, wing skin and fuselage panels have their stressed skin supported and divided by internal stiffeners (stringers and ribs in a wing structure and stringers and frames in a fuselage). With the skin assumed as thin-walled plate elements between stiffeners, they need to resist significant direct and shear membrane loading [5]. Thus, understanding the behaviour of skin panel elements under various membrane loading actions is key to achieving a low mass design.

Skin panel elements under direct and shear stresses are prone to buckling instability [6], [7]. This topic is an essential area of research because it significantly influences design and structural mass. Furthermore, one of the leading design strategies generally adopted by the industry is to size structural components using simplified analysis assumptions [8]–[10] which generally give lower-bound buckling solutions. Hence, they give conservative (upper-bound) solutions in design. This is, of course, appropriate for conservative structural design and initial sizing, but where the

structure is weight critical, it is important to investigate lightweight structural configurations that have large strength reserves after structural buckling.

There is a large body of research which establishes the response and failure behaviour of hybrid (CFRP-GFRP) laminates when subjected to a wide range of destabilising loads [11]–[14]. However, these typically consider only complete plies and do not examine the tailoring of individual ply shapes. There is no works to date which investigate the benefits of combine selective laminate shapes and hybridisation to increase strain to failure and delay plate post-buckling collapse. In addition, most preceding work considers only plate compression and does not consider shear loading of plates which is a critical loading condition for many structures. Thus, this paper aims to examine if a hybrid CFRP-GFRP laminate with selective CFRP laminate shapes may be used to increase strain to failure and delay plate post-buckling collapse. However, it is necessary, that such additional post-buckling reserve is achieved without significantly impacting the load to cause initial plate buckling or to increase the unit mass of the plate (comparing against standard CFRP laminate stacking sequence designs).

To achieve the stated aim and quantify the potential for improved post-buckling reserve, an experimental program will be undertaken to compare a conventional laminate design against a CFRP-GFRP laminate with selective ply shapes. This will identify whether the condition of equivalent or equal initial buckling can be achieved while also achieving an increase in post-buckling reserve. Next, a finite element simulation will be developed to understand the damage mechanisms which occur between initial buckling and collapse. The purpose of the modelling work is to develop further understanding of the internal damage behaviour not visible/captured during the physical testing, and establish a method for future work to optimise the shape of plies and the laminate stacking sequence design. To represent the bi-directional nature of the twill materials employed in the experimental study, a novel constitutive material model from the literature, developed for fabric reinforced composites, is used. This approach is required because the most common material criteria in the simulation literature, for example criteria such as Hashin, which were originally developed for uni-directional polymeric composites, are not appropriate for fabric plies. The fabric ply failure model is necessarily implemented within a built-in VUMAT user subroutine in ABAQUS/Explicit. A single standard specimen will be tested (as there is established

understanding on standard laminate strength and stiffness repeatability), however for the novel laminate design two specimens will be tested to initially understand the repeatability of the novel hybrid laminate behaviour.

2 Literature review

There is a considerable body of literature about buckling and post-buckling behaviour of composite laminate structures. Early investigations on the shear buckling performance of composite panels took place in the early 1980s [11], [15], [16]. Since the late 1980s, most of the literature proposes efficient analytical methods or numerical methods and many works present accompanying validation experiments. Amongst the analytical methods is the work of Loughlan [7], who characterised the buckling behaviour of CFRP plates with an efficient Finite Strip Method (FSM). Fazzolari et al. [17] developed an exact dynamic stiffness theory for composite plate elements, using higher-order shear deformation theory, and studied the buckling behaviour of complex structures modelled as plate assemblies. Zhao et al. [18] used exact strip analysis to study post-buckling behaviour of anisotropic plates under shear loading. In this analysis, the mode shapes were assumed to be the sum of sinusoidal responses with different half-wavelengths, which were coupled together to satisfy the boundary conditions at the longitudinal ends. The resultant predictions demonstrated good agreement with Finite Element Analysis (FEA). Damghani et al. [19], [20] used a smeared method based on exact stiffness analysis derived from analytical solutions of the governing differential equations. Global buckling behaviour of delaminated rectangular composite plates were predicted and found to be in good agreement with FEA predictions. Wu et al. [21] developed a semi-analytical variational approach to perform post-buckling analysis of Variable Angle Tow (VAT) plates under uniform axial compression loading. They demonstrated that VAT laminates outperformed straight fibre laminates. The advantage of analytical, semi-analytical and strip analysis methods is their low computational expense (in comparison to FEA analysis). However, such methods are less appropriate for non-prismatic plate and panel geometries and the representation of progressive material damage, which will be studied herein.

Since the 1990s, combined numerical modelling and experimental studies have for decades enabled a better understanding of buckling and post-buckling behaviour of laminated composite structures. Such works have considered both damaged

(delaminated) and undamaged laminates. For example, Kolanu et al. [22] carried out an experimental and numerical study of a quasi-isotropic CFRP laminate under positive and negative shear loading. The study considered laminate collapse to understand the combined stability behaviour and material failure mechanisms. They used non-contact techniques like digital image correlation (DIC), Air-coupled ultrasonics and infrared thermography (IR) and other in situ damage monitoring techniques like acoustic emission (AE) for better understanding of the structural behaviour and complex damage characteristics of composite laminates. Zhang et al. [23] conducted experiments subjecting stiffened composite panels to shear loading. The study illustrated the potential for good agreement between FEA predictions and well controlled experiments. Reinoso et al. [24] carried out an experimental investigation on buckling and post-buckling behaviour of a stiffened cylindrical composite panel under uniform pressure load. Significantly, the study showed that no damage was developed in the structure up to 3.5 times the first buckling load and collapse only occurred after 4.1 times the design buckling load. Kumar et al. [25], [26] investigated the buckling and post-buckling responses, failure loads and failure characteristics of a simply-supported quasi-isotropic laminate under shear loading and combined in-plane loading. An extensive review of the buckling and post-buckling response of composite laminates is given in [27].

Despite considerable attempts in the literature, such as those mentioned above, the application of post-buckling design with composite structures has been limited, as current industrial analysis tools are not capable of accurately representing the damage mechanisms that lead to structural collapse.

Focusing on the hybridisation of composites, this topic has drawn the attention of many researchers for over four decades, with the objective to create composites possessing high strength, stiffness, toughness and thermal resistance [13]. The advantage of hybridisation on post-buckling performance of thin-walled laminated composite structures was demonstrated by Burgueno et al. [14]. They presented numerical and experimental studies that evaluated the elastic response of thin-walled laminated composite cylindrical shells in their post-buckling regime under axial loading and unloading. Two structural prototypes were considered: (1) a carbon/epoxy cylindrical shell and (2) a hybrid carbon/E-glass/epoxy cylindrical shell with various carbon ply shapes. The study illustrates the well-known challenges of predicting and

controlling cylindrical shell buckling and post-buckling response because of their high sensitivity to imperfections. Interestingly, the study demonstrates that by hybridising the cylindrical shell, the structure was able to withstand a load 1.26 times greater than the buckling load. Kubiak et al. [12] studied experimental and numerical post-buckling behaviour of thin-walled channel columns. The columns were made as a hybrid of Fibre Metal Laminate (FML) and GFRP. The failure loads of the hybrid columns were two times that of the GFRP columns. Al-Azzawi et al. [28], [29] established the potential for good agreement between numerical predictions of the instability behaviour of hybrid FML-Glare laminates and experimental tests. Petkune et al. [30] used hybridisation of shear walls in civil engineering, revealing that a hybrid of carbon and glass were superior to pure steel under repeated shear loading in terms of load bearing capacity, energy absorption and dynamic stiffness degradation. In fact, in civil engineering, X-braced frames are an alternative to shear walls, capable of stabilising structures under seismic loading, but having low cost, low weight, and quickness in construction. Although there has been limited work on the post-buckling behaviour of hybridized composite laminates there has been considerable work in other structural topics and the reader is referred to [31] for a comprehensive review of hybrid composites.

In summary, it is evident from the literature that composite laminates have considerable strength reserve after buckling. However, this strength reserve is not used in aircraft design due to limited understanding, a lack of robust and rapid prediction methods for composite damage mechanisms after buckling, loading complexity, and aerodynamic considerations for some zones of the aircraft. Additionally, the success of any developed understanding, analysis/design methodology and the potential of post-buckling composite structures will have applications for the next generation of lightweight aerospace structures.

Despite the developed knowledge on the buckling and post-buckling behaviour of composite laminates, there is very limited work on the damage mechanisms of hybrid CFRP-GFRP woven fabric composite laminates designed for optimal weight under in-plane shear loading. In particular, for such loading, there are very few combined experimental studies and numerical works which fully characterise hybrid laminate post-buckling damage behaviour. Hence, this paper presents a combined experimental and numerical simulation study. A conventional laminate and a novel

CFRP-GFRP laminate with selective laminate shapes will be designed and tested. Buckling, post-buckling and collapse behaviour will be experimentally captured and simulation will further examine the different design post-buckling damage behaviours. This will identify whether the condition of equivalent or equal initial buckling can be achieved while also achieving an increase in post-buckling reserve, and how damage in the post-buckling regime influences this performance.

Based on the literature review the remaining paper content is arranged as follows: Section 3 introduces the design of the novel CFRP-GFRP laminate with selective laminate shapes, and an appropriate baseline laminate design. Section 4 presents the Finite Element modelling approach which will be used to understand the differences in post-buckling damage mechanisms between the conventional and novel laminate designs. The experimental procedure for material characterisation and the laminate post-buckling testing is presented in section 5. Finally, results and discussions are given in section 6 and conclusions are made in section 7.

3 Laminate design

In civil engineering applications, X-bracing of steel frame structures has long been used to withstand the shear loads resulting from either seismic activities or lateral wind forces [32]. On the other hand, the current industrial practice makes use of hybrid CFRP-GFRP laminates in aircraft wing construction, e.g. AIRBUS A350-XWB. From this perspective, 1 to 2 GFRP plies are placed on the outer mould surfaces of a purely CFRP laminate wing skin where these plies act as a protective layer for the CFRP laminates against accidental impact. However, as the primary purpose of these additional plies is to reduce damage from impact, the load bearing capacity of the GFRP plies is typically ignored, thus adding extra weight to the structure [33]. Hence, in this study, the concept of X-bracing for a hybrid CFRP-GFRP laminate subjected to pure shear loading is explored.

Two structural configurations are considered. In the first configuration (type 1), the entire laminate is made of woven twill CFRP with a stacking sequence of $\left[\pm 45/\pm 45/0/0\right]_S$. This is the benchmark laminate in which all CFRP plies have a square shape of $200\,mm \times 200\,mm$. The second configuration (type 2) is a hybrid laminate in which woven twill GFRP plies are placed at the outer and inner mould surfaces. This is to ensure that the hybrid laminate of study mimics a civil aircraft wing

laminate. In this hybrid laminate design both the GFRP and CFRP plies of 0^o angle have a square shape with size $200\,mm \times 200\,mm$. However, the CFRP plies at angle 45^o have a X shape, as shown in Figure 1. Thus, the stacking sequence for the type 2 laminate is $\left[45G/\pm 45_X/\pm 45_X/0/0\right]_S$. The X shape is chosen to not only provide stiffness for shear loading but also reduce some mass to compensate for the addition of the GFRP plies, compared to benchmark type 1. In order to establish an appropriate width of the X-bracing, a parametric study is initially carried out to complete the design. By changing the width (W) of the X-bracing, Figure 1, and finding the minimum W which gives an equal or higher buckling load (both under pure shear and axial load) compared to the benchmark laminate (type 1) will finalise the laminate design.

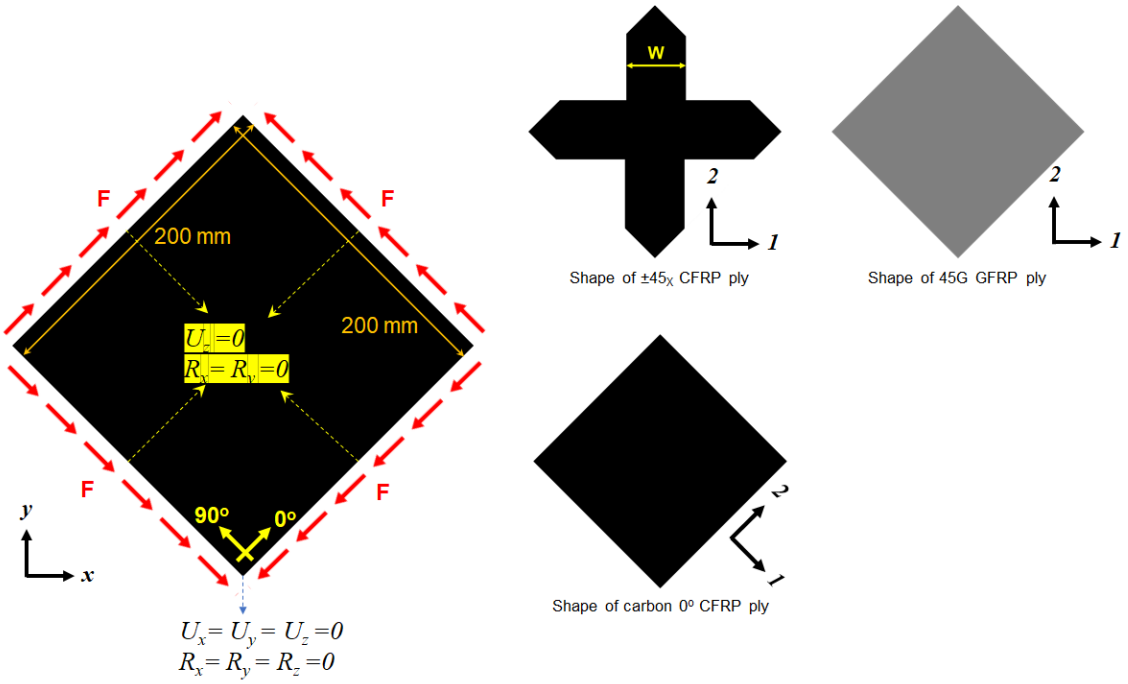

Figure 1: Loading (shear edge load in N/mm), boundary conditions and ply shapes of the laminates

The parametric study was carried out using ABAQUS software and linear eigenvalue analysis. S4R quadrilateral elements with reduced integration were used to model the laminate. Three integration points through the thickness were chosen for each ply. As shown in Figure 1, all edges of the laminates are constrained to displace in z direction and rotate about x and y axes. Multipoint constraints were incorporated on all four edges to ascertain they remain straight throughout the loading process [34]. Displacement and rotation of the node at the bottom of the laminate is constrained in all directions. The mesh used for the study is depicted in Figure 2a. As stated, the

objective was to match the buckling load of the hybrid laminate with the buckling load of the baseline laminate (type 1), whilst minimising mass. Figure 2 presents the simulation study results, with the non-dimensional buckling load plotted against the mass. Examining both the shear loading (Figure 2b) and compression loading (Figure 2c) it can be seen that a bracing width of $60\ mm$ yields slightly superior shear and axial buckling load of 1.05 and 1.12 times higher than type 1 laminate, respectively, and obviously with less mass compared to a width of $70\ mm$. Therefore, $W = 60\ mm$ is chosen to complete the hybrid laminate (type 2) design, which, together with the baseline laminate (type 1), will be manufactured, experimentally tested and its post-buckling behaviour modelled.

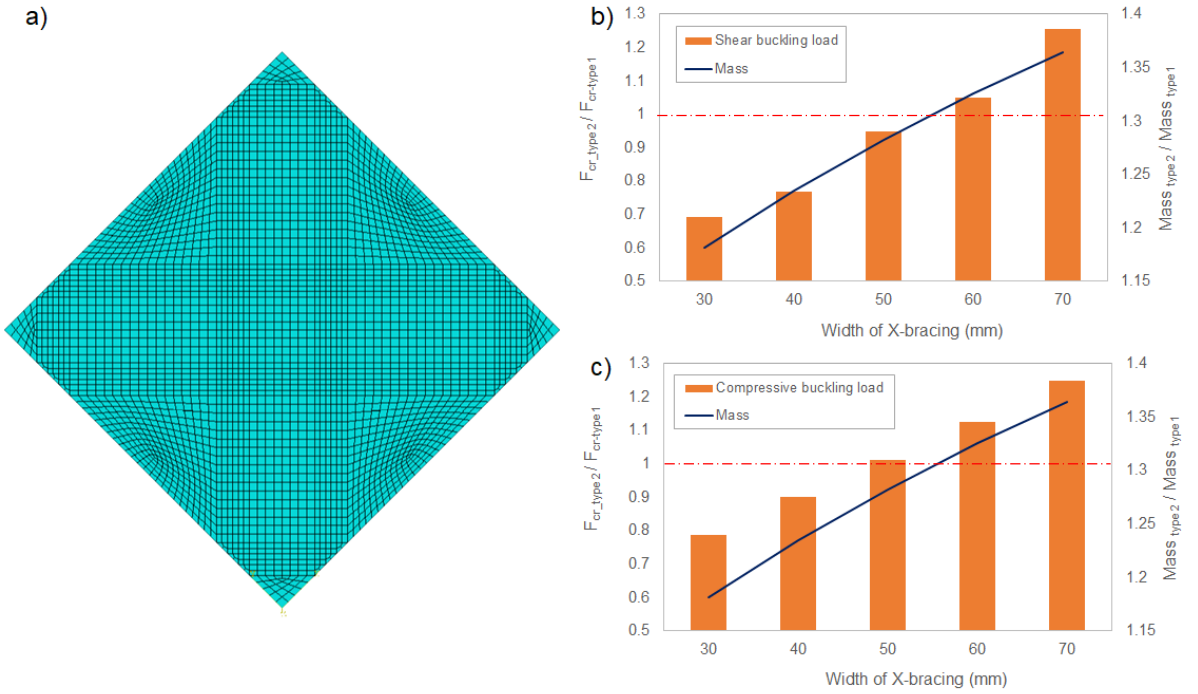

Figure 2: Meshing and critical buckling load of laminates; a) Mesh density; Ratios of buckling load of type 2 / buckling load of type 1 and mass of type 2 / mass of type 1 vs width of X-bracing subjected to b) shear loading only and c) axial compressive loading

4 Numerical analysis

4.1 Material model

The bi-directional nature of the twill materials employed in the study means that common conventional material failure criteria such as Hashin, which were originally developed for uni-directional polymeric composites, are not appropriate. Thus, a constitutive material model from the literature, developed for fabric reinforced composites, is used. The fabric ply failure model is necessarily implemented within a built-in VUMAT user subroutine in ABAQUS/Explicit.

Within the selected model, the fabric-reinforced ply is represented as a homogenous orthotropic elastic material, with the potential to sustain progressive stiffness degradation because of fibre and matrix cracking and plastic deformation under shear loading. Thus, it is assumed that there are two main failure mechanisms: fibre dominated failure in tension or compression in the two fibre directions; and matrix dominated failure in in-plane shear. The mechanisms of failure are discussed hereafter and further detailed in [35]. Furthermore, a summary of damage parameters used in this study are provided in the Appendix.

4.1.1 Elastic stress-strain relationship

The elastic stress-strain relations are given by orthotropic damaged elasticity. The relation is formulated in a local coordinate system aligned with the fibre direction as follows;

$$\begin{bmatrix} \varepsilon_{11} \\ \varepsilon_{22} \\ \varepsilon_{12}^{el} \end{bmatrix} = \begin{bmatrix} \frac{1}{(1-d_1)E_1} & \frac{-\upsilon_{12}}{E_1} & 0 \\ \frac{-\upsilon_{21}}{E_2} & \frac{1}{(1-d_2)E_2} & 0 \\ 0 & 0 & \frac{1}{(1-d_{12})2G_{12}} \end{bmatrix} \begin{bmatrix} \sigma_{11} \\ \sigma_{22} \\ \sigma_{12} \end{bmatrix} \quad (1)$$

where E_1 and E_2 are Young's moduli in the principal orthotropic directions, G_{12} is the in-plane shear modulus, and υ_{12} is the principal Poisson's ratio. Three scalar damage variables are used: d_1 $(0 \le d_1 \le 1)$ and d_2 $(0 \le d_2 \le 1)$ are associated to fibre fracture along the ply 1 and 2 directions, respectively; and d_{12} $(0 \le d_{12} \le 1)$ is related to matrix micro-cracking due to shear deformation. It is worth noting that fibre fracture damage variables consider the tensile and compressive fibre failure modes based on the stress state in the fibre direction.

4.1.2 Fibre response

The material response along the fibre directions is characterised with damage elasticity. It is assumed that the fibre damage variables are a function of the corresponding effective stresses as

$$
\begin{aligned}
d_{1+} &= d_{1+}\left(\overline{\sigma_{1+}}\right) \\
d_{1-} &= d_{1-}\left(\overline{\sigma_{1-}}\right) \\
d_{2+} &= d_{2+}\left(\overline{\sigma_{2+}}\right) \\
d_{2-} &= d_{2-}\left(\overline{\sigma_{2-}}\right)
\end{aligned}
\tag{2}
$$

where d_{1+}, d_{1-}, d_{2+} and d_{2-} are the tensile and compressive damages along the fibre in the ply directions 1 and 2, respectively. Effective stresses are updated stress states after damage initiation and are defined as

$$
\begin{aligned}
\overline{\sigma_{1+}} &= \frac{\sigma_{11}}{1-d_{1+}} \\
\overline{\sigma_{1-}} &= \frac{-\sigma_{11}}{1-d_{1-}} \\
\overline{\sigma_{2+}} &= \frac{\sigma_{22}}{1-d_{2+}} \\
\overline{\sigma_{2-}} &= \frac{-\sigma_{22}}{1-d_{2-}}
\end{aligned}
\tag{3}
$$

At any given time throughout the analysis, the elastic domain is defined in terms of the damage activation functions, F_i, as

$$
\begin{aligned}
F_i &= \phi_i - r_i \le 0 \\
\phi_i &= \frac{\overline{\sigma_i}}{X_i}; \left(i = 1+, 1-, 2+, 2-\right)
\end{aligned}
\tag{4}
$$

where X_i are the tensile (+) and compressive (-) strength for uniaxial loading along the fibre directions 1 and 2. The damage thresholds (r_i) are initially set to one. After damage activation ($\phi_i = 1$), the damage thresholds at any given time (t) increase based on

$$
r_i\left(t\right) = \max \phi_i\left(t^*\right); t^* \le t \tag{5}
$$

Thus, the model assumes that the ply material is non-healing. Therefore, on unloading, after damage, the damage parameters remain constant until a higher damaging load is re-applied. The evolution of damage variables are a function of the damage thresholds (r_i), the elastic energy density per unit volume at the point of

damage initiation (g_0^i), the fracture energy per unit area under uniaxial tensile/compressive loading (G_f^i) and the characteristic length of the FE mesh element (L_c). The damage variables are formulated as

$$d_i = 1 - \frac{1}{r_i} e^{\left(-\frac{2 g_0^i L_c}{G_f^i - g_0^i L_c} (r_i - 1) \right)} \tag{6}$$

The elastic energy density per unit volume at the point of damage initiation is given as

$$g_0^i = \frac{X_i^2}{2E_i} \tag{7}$$

In the current study, both carbon and glass fibres are assumed to behave in a brittle manner. Furthermore, $G_f^i \approx L_{\max} g_0^i$ where $L_{\max}$ is the maximum element length to avoid over prediction of energy dissipation. The reader may refer to [35] for further details.

4.1.3 Shear response

It is assumed that shear behaviour and the mechanism of ply in-plane shear degradation are mainly controlled by the resin [36]. Thus, in the adopted material model, fibre and shear damage modes are decoupled. The shear response is dominated by the nonlinear behaviour of the matrix, which may be inelastic and/or irreversible due to the presence of extensive matrix cracking or plasticity. On unloading, this can lead to permanent deformations in the ply. Various components of matrix elasticity, plasticity and evolution of damage are consequently modelled, each is described hereafter.

4.1.3.1 Elasticity

The elastic response of the matrix relates the effective stress to the elastic strain, as follows

$$\overline{\sigma_{12}} = \frac{\sigma_{12}}{1 - d_{12}} = 2G_{12}\varepsilon_{12}^{el} = 2G_{12}\left(\varepsilon_{12} - \varepsilon_{12}^{pl}\right) \tag{8}$$

where ε_{12}^{el} and ε_{12}^{pl} are elastic and plastic strains, respectively. It is worth noting that plasticity is only associated with the matrix and therefore, fibre plasticity is zero, i.e. $\varepsilon_{11}^{pl} = \varepsilon_{22}^{pl} = 0$.

4.1.3.2 Plasticity

An elastic domain function, otherwise known as a yield function, is introduced (F) that assumes only the effective shear stresses lead to plastic deformation, thus

$$F = \left|\overline{\sigma_{12}}\right| - R\left(\varepsilon^{pl}\right) \tag{9}$$

where $R\left(\varepsilon^{pl}\right)$ is an isotropic hardening function following a power rule, given as

$$R\left(\varepsilon^{pl}\right) = \overline{\sigma_{y0}} + C\left(\varepsilon^{pl}\right)^{p} \tag{10}$$

where $\overline{\sigma_{y0}}$ is the initial effective shear yield stress and C and p are coefficient and power terms in the hardening equation, respectively. It should be noted that the condition of $F < 0$ corresponds to stress states inside the elastic domain where the material undergoes elastic damage. Whereas $F = 0$ describes the plastic deformations. The evolution of the plastic work during yielding ($\dot{U}^{pl}$) is given as a function of the evolution of the plastic strain ($\dot{\varepsilon}_{12}^{pl}$), the shear damage parameter (d_{12}) and the effective shear stresses ($\overline{\sigma_{12}}$), as

$$\dot{U}^{pl} = 2\sigma_{12}\dot{\varepsilon}_{12}^{pl} = 2\left(1 - d_{12}\right)\overline{\sigma_{12}}\dot{\varepsilon}_{12}^{pl} \tag{11}$$

4.1.3.3 Damage

The elastic domain is defined in terms of the damage activation function (F_{12}) as

$$\begin{aligned} F_{12} &= \phi_{12} - r_{12} \le 0 \\ \phi_{12} &= \frac{\overline{\sigma_{12}}}{S} \end{aligned} \tag{12}$$

The function ϕ_{12} is the criteria for initiation of shear damage of the matrix and S is the shear strength of the ply. Damage thresholds (r_{12}) are initially set to one. After damage activation ($\phi_i = 1$), the damage thresholds at any given time (t) increase based on

$$r_{12}(t) = \max \phi_{12}(t^*); t^* \le t \tag{13}$$

It is assumed that the shear damage variable increases as a logarithm of r_{12} until a maximum value of $d_{12}^{\max}$ is reached. Thus

$$d_{12} = \min\left(\alpha_{12} \operatorname{Ln}(r_{12}), d_{12}^{\max}\right) \tag{14}$$

where $\alpha_{12} > 0$ and $d_{12}^{\max} \le 1$ are defined material properties.

4.2 Buckling and post-buckling analysis

In order to predict buckling, post-buckling behaviour and unstable collapse, eigenvalue buckling and explicit analysis were used. Initially, an eigenvalue buckling analysis is performed. The subspace method is used to extract the eigenvalues of the composite laminates, as the extraction of the eigenvalues in reduced space speeds convergence to the eigenvectors in full space. For the post-buckling prediction, geometric imperfections (typically less than 10% the thickness of laminates) are introduced to the model to trigger the unstable response within the explicit analysis. An initial qualitative comparison of the experimental buckling mode shapes and the eigenvalue mode shapes was undertaken (for both laminate types 1 and 2) to select the imperfections to be modelled. It was followed by a sensitivity study to select the imperfection magnitude.

Figure 3a shows that the type 1 laminate experimental out of plane deflections are symmetric about the centre line of the specimen and similar to the first numerical eigenvalue mode of the laminate, Figure 3b. Therefore, 10% of the laminate thickness times eigenvalue mode 1 is chosen as initial geometric imperfection after a series of imperfection sensitivity studies in which the minimum magnitude was identified which would produce the desired experimental mode shape. Similarly, close inspection of the experimental out of plane displacement for the type 2 laminate (see Figure 4a) shows that the displacements are un-symmetric with respect to the centre line of the specimen, and the mode shape has a larger wavelength on the left-hand side than the right-hand side of the geometric centreline. The sensitivity study identified that 8% laminate thickness of eigenvalue mode 2 (see Figure 4b) and 2% laminate thickness of eigenvalue mode 1 (see Figure 4c) was appropriate to recreate the experimental imperfection (see next Section).

Along with the initial imperfections, the material failure law, as defined in section 4.1, is used within each post-buckling analysis. Three integration points are considered for each ply for the calculation of stresses, strains and damage parameters. Elements are deleted when the damage parameter at all section points exceeds unity. For accuracy and efficiency, a quasi-static analysis was performed by applying the shear load using the ABAQUS/Explicit built-in load amplitude function called SMOOTH STEP. This uses a fifth order polynomial function to apply the load and eliminate significant energy changes at the start and end of loading. Additionally, mass scaling is employed to reduce the solution time without increasing the loading rate.

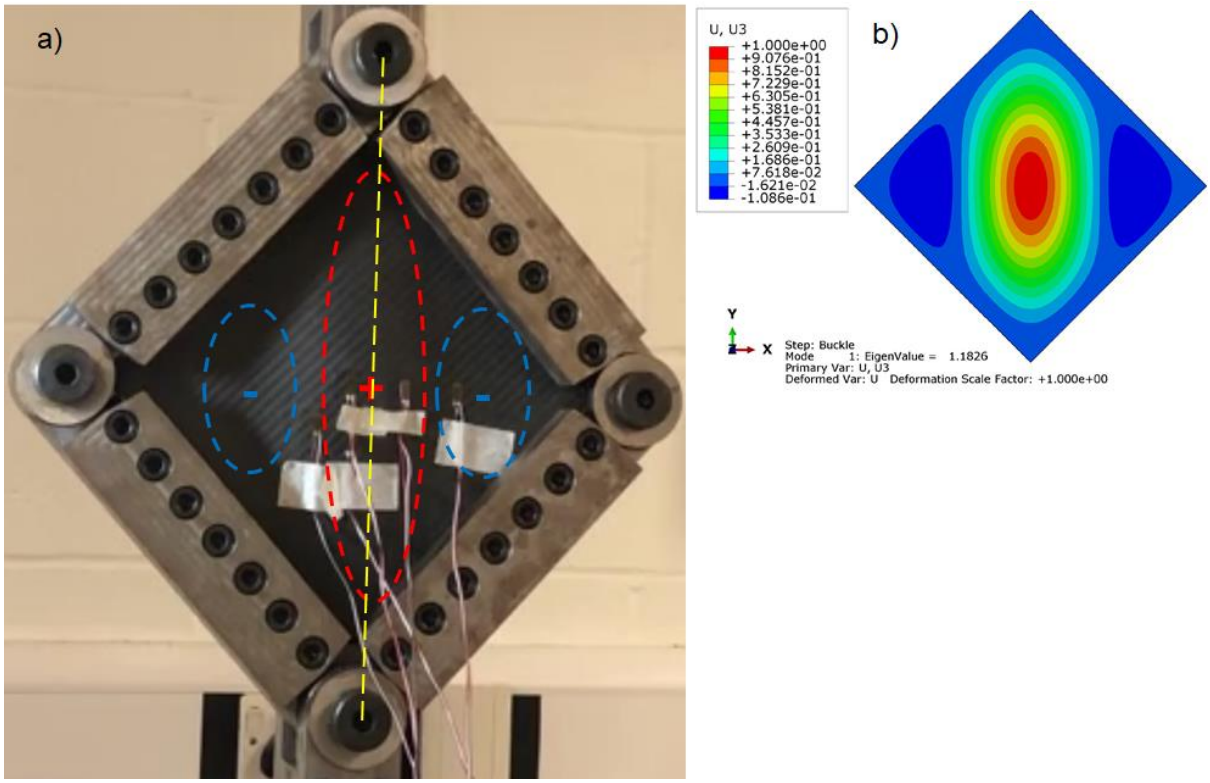

Figure 3: Qualitative comparison of experimental and numerical mode shapes for type 1 laminates; a) experimental mode shape, b) first mode shape (eigenvalue of 1.18) for applied shear load of $F = 100\ N/mm$

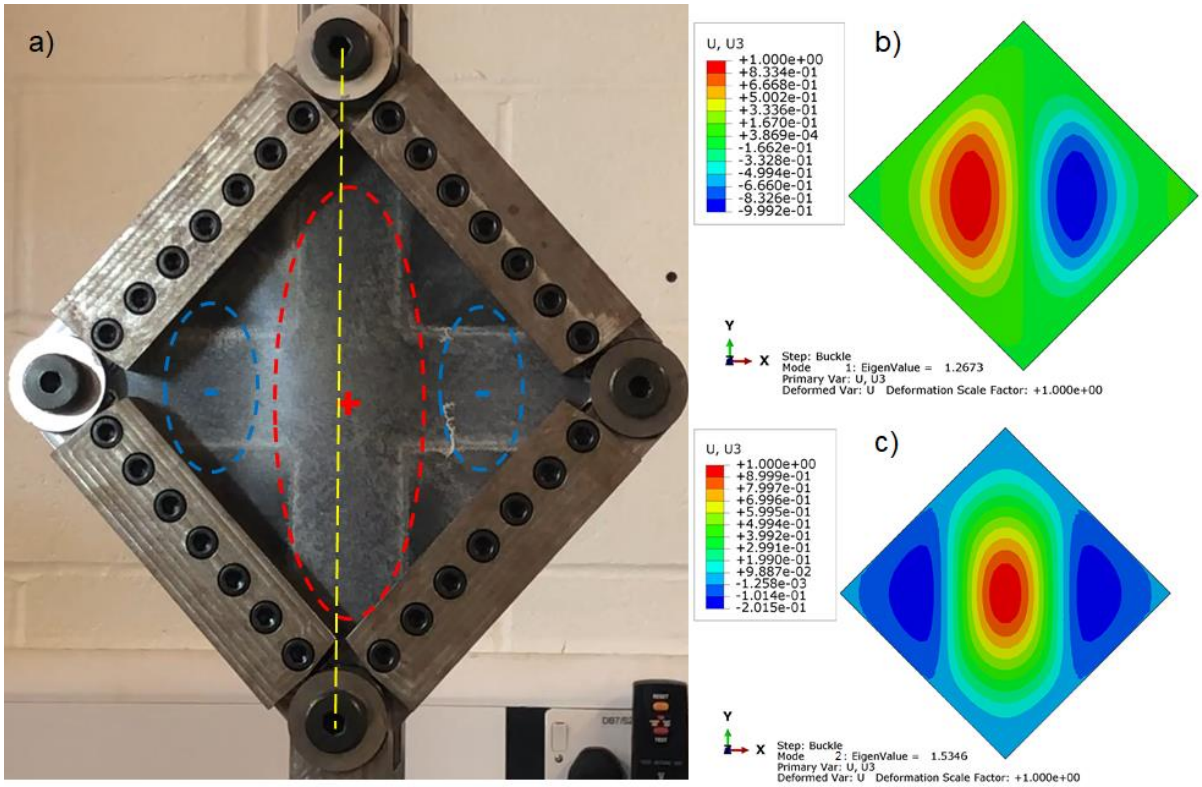

Figure 4: Qualitative comparison of experimental and numerical mode shapes for type 2 laminates; a) experimental mode shape, b) first mode shape (eigenvalue of 1.26) and c) second mode shape (eigenvalue of 1.53) for applied shear load of $F = 100\ N/mm$

5 Materials and experimental methods

5.1 Composite material and manufacture

The materials used in this study are twill woven pre-impregnated carbon fibre (AX-5180), and a twill woven pre-impregnated glass fibre (AX-3180) with mechanical properties given in Table 1. It is worth noting that in the absence of manufacturer's data, the mechanical properties have been obtained by the authors as detailed in the next section. Both carbon and glass prepregs consist of 54% fibre by volume (60% by weight) and have compatible resin contents enabling simultaneous hot press curing. Three laminates of each laminate type were initially hand laid to form a plate and cured in a heated press for an hour at 120^{O} Celsius under 1 bar pressure. The specimens were then abrasively cut to $200\ mm \times 200\ mm$.

Table 1: Mechanical properties of both woven CFRP (AX-5180) and GFRP (AX-3180) fabric plies

Mechanical properties	Units	AX-5180 CFRP	AX-3180 GFRP
$E_{11}=E_{22}$	MPa	67094.00	30083.00
G_{12}	MPa	4831.38	4954.60
S_t^*	MPa	595.50	437.16
S_c	MPa	393.00	306.00
S_s	MPa	87.00	62.00

Strain to failure	Strain	0.01	0.02
ϑ_{12} (Poisson's ratio)	N/A	0.04	0.14
t_{ply}^{**}	mm	0.224	0.288

* t, c and s subscripts denote the strength of ply in tensions, compression and shear respectively.
** cured ply thickness

5.2 Shear test

All testing was performed using a $100\ kN$ capacity INSTRON tensile machine and a picture frame test fixture. The laminate specimen is first clamped into the test fixture. On each edge the specimen is clamped via grip plates of width $10\ mm$, providing gauge dimensions of $180\ mm \times 180\ mm$. The specimen is held in position and loaded by constant static friction set initially by the clamping force of the bolts (which are set to a specific torque). The specimen and test fixture are located in the tensile machine, and a tensile load is applied under displacement control at a speed of 2 mm/min to the test fixture, as shown in Figure 5. This, in turn, induces a shear force on the test laminate. In addition, the test device is designed to ensure that the panel is under pure shear along the loading line.

To acquire strain data, the conventional laminate specimen and one of the novel laminate specimens were instrumented with six uniaxial Vishay strain-gauges (see Figure 5b). The locations of the strain gauges were determined based on the laminate eigenvalue simulations, with the areas of a high strain selected for gauging. Therefore, strain gauge 3 is positioned at the centre of the panel with strain gauge 6 on the opposite side to capture the effect of central laminate out of plane bending. All strain gauges measure strain in the y-direction (Figure 1), in the direction parallel to the applied tensile loading. Detailed positioning and spacing of each strain gauge and their numbering are given in Figure 5b.

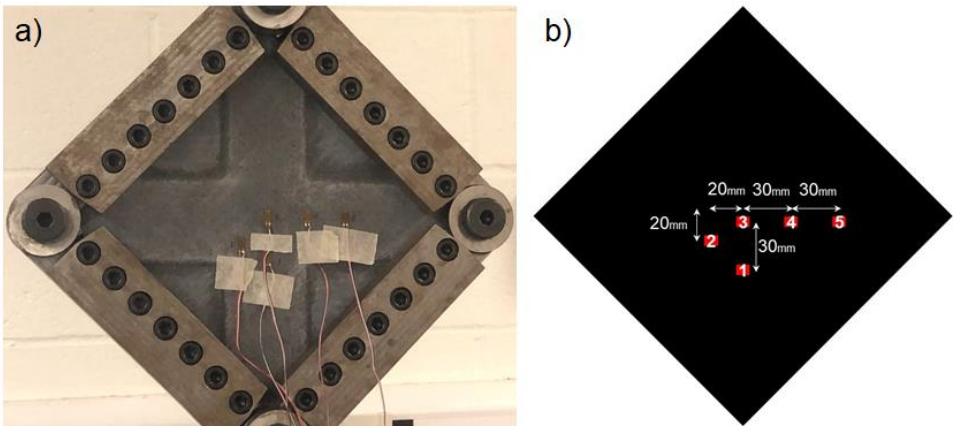

Figure 5: Shear test set-up; a) gauged type 2 and b) location of strain gauges and their numbering (strain gauge 6 is on the back of the laminate opposite to strain gauge 3)

5.3 Determination of fabric ply material model

In the absence of mechanical property data in the literature for the studied materials, and to find the material parameters for the material model proposed in section 4, a series of tensile and cyclic shear tests were performed. Incorporation of such data is expected to benefit future researchers in the field.

5.3.1 Tensile tests along the fibre

The parameters of the elastic damage model were derived from standard coupon tests under uniaxial tension/compression loading of $0/90$ laminates as summarised in Table 1. The compressive mechanical properties were estimated using data available in the literature [37]. The shear modulus values G_{12} were obtained from uniaxial tensile tests on ± 45 laminates, by calculating the Young' modulus (E_{45}) and using the equation [38]

$$\frac{1}{G_{12}} = \frac{4}{E_{45}} - \frac{1}{E_1} - \frac{1}{E_2} + 2\frac{\upsilon_{12}}{E_1} \tag{15}$$

The calibration of damage evolution in the fibre failure mode was not possible due to specimen abrupt and brittle failure for both the AX-5180 CFRP and the AX-3180 GFRP tests. Therefore, it can be assumed that $G_f^{\alpha} \approx 0$. However, for the stability of the post-buckling numerical model, the value of $G_f^{\alpha} = L_c g_0^{\alpha}$ will be used.

5.3.2 Cyclic shear tests

As a result of permanent plastic deformations, cyclic load, i.e. loading and unloading, an experimental test is required to characterise the shear response of both fabric materials. A typical idealised representation of a fabric laminate shear response is shown in Figure 6a. In order to obtain the damage parameters noted in Figure 6a, a tensile material specimen made of only angle plies, i.e. $\pm 45^o$, is tested. By testing such a material specimen, the strains along the fibre directions can be neglected. The resulting tensile test data is used to obtain the shear stresses and strains as below

$$\begin{aligned} \sigma_{12} &= \frac{\sigma_y}{2} = \frac{P}{2wt} \\ \varepsilon_{12} &= 0.5\left(1+\upsilon_{xy}\right)\varepsilon_y \end{aligned} \tag{16}$$

where P is the experimental tensile load, w and t are the laminate specimen width and thickness, respectively. ε_y is the experimental axial strain and υ_{xy} is the total homogenised Poisson's ratio of the cross-ply laminate (≈ 0.76 for carbon and 0.5 for glass laminates).

The calculated values of shear stresses against shear strains are plotted in Figure 6b-c for both CFRP and GFRP. The level of damage is measured from the ratio of unloading stiffness to the initial undamaged elastic stiffness. This allows the identification of a pair of (σ_{12}, d_{12}), for the unloading curve. This data is presented in terms of d_{12} and $\mathrm{Ln}\left(\overline{\sigma_{12}}\right)$ where $\overline{\sigma_{12}} = \sigma_{12} / (1 - d_{12})$. The linear fit of data then provides the parameters α_{12} and S. The schematic representation of this process is shown in Figure 7a. The experimental test results with all calculated damage parameters are shown in Figure 7b-c. Comparing the experimentally derived curves, it is clear that the GFRP plies are capable of sustaining more damage than the CFRP plies.

Finally, the plastic hardening function requires the calculation of the accumulated plastic strain. From the cyclic test data, it is possible to obtain a pair of $\left(\varepsilon_{12}^{pl}, \overline{\sigma_{12}}\right)$ to plot each hardening curve. The schematic representation of the hardening curve is illustrated in Figure 8a, and the experimentally determined hardening curves for CFRP and GFRP fabrics are shown in Figure 8b-c.

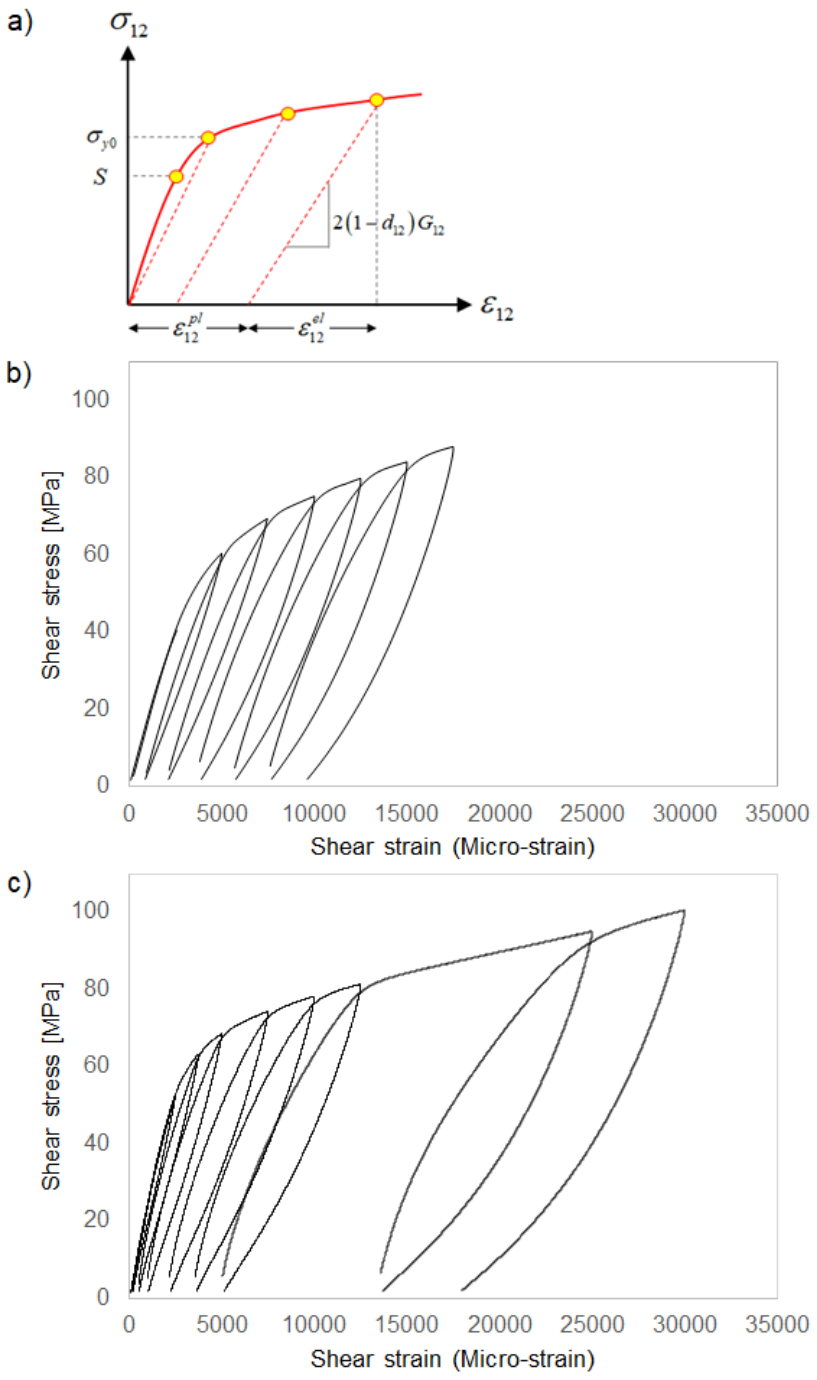

Figure 6: Shear response of a fabric reinforced composite. S is shear stress at the onset of damage and σ_{y0} is initial shear yield stress; a) schematic representation, b) experimental cyclic shear stress-strain for CFRP AX-5180 and c) experimental cyclic shear stress-strain for GFRP AX-3180.

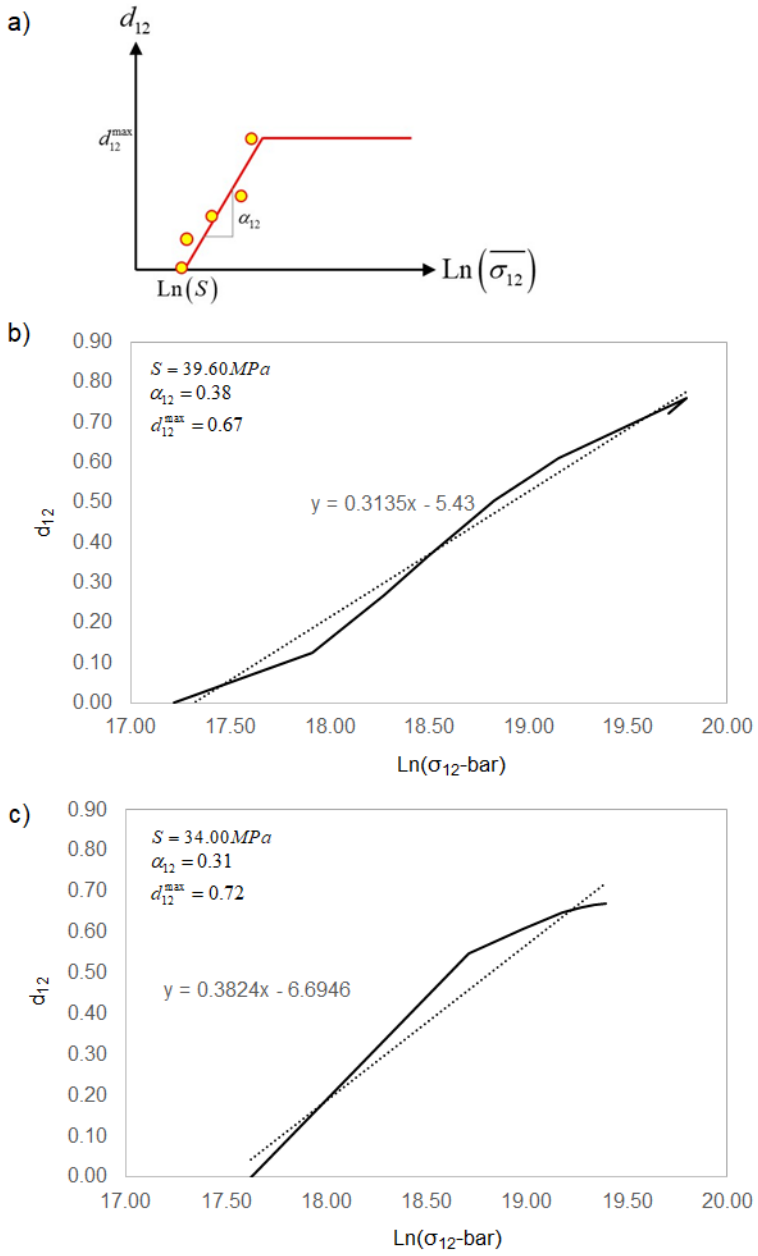

Figure 7: Shear damage parameters α_{12} and S ; a) schematic representation, b) experimental shear damage parameters for CFRP AX-5180 and c) experimental shear damage parameters for GFRP AX-3180

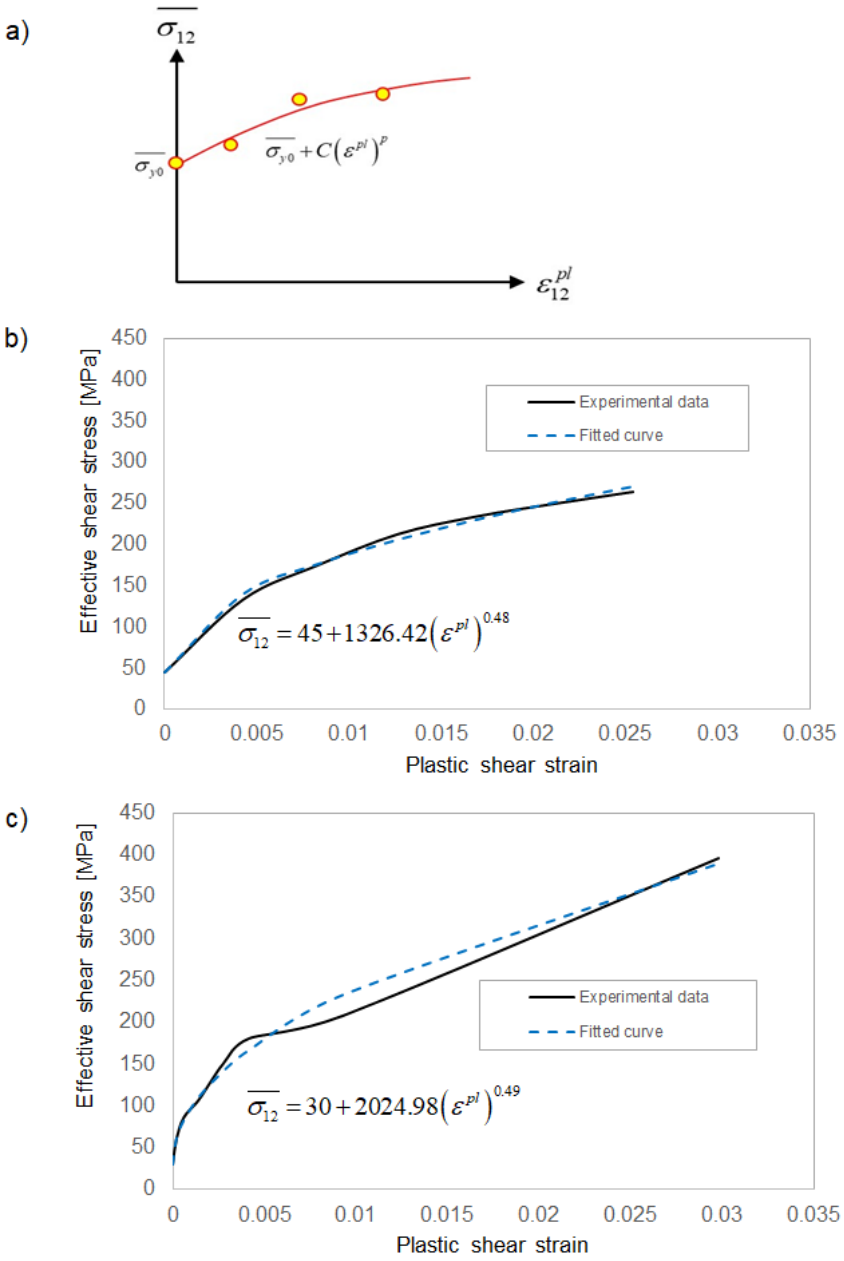

Figure 8: Shear hardening curve; a) schematic representation, b) experimental curve for CFRP AX-5180 and c) experimental curve for GFRP AX-3180.

6 Buckling/post-buckling results and discussions

Figure 9a demonstrates the theoretical plate buckling and post-buckling response for a composite laminate material. The behaviour is quite different from that of a homogenous isotropic material, due to the potential existence of specific composite laminate failure modes, i.e. delamination, fibre cracking, fibre debonding etc. In the theoretical illustration, the laminated composite deforms almost linearly up to the bifurcation point B. The bifurcation point corresponds to initial plate buckling and will lead to a collapse at A. However, the global buckling may be preceded or associated

with local buckling modes of delaminated sub-laminates, denoted by the point D. Additionally, the load path may be limited by material failure resulting from increasing deformations. Finally, the existence of geometric imperfections will influence each load path and the position of each point, i.e. A, B and D [27].

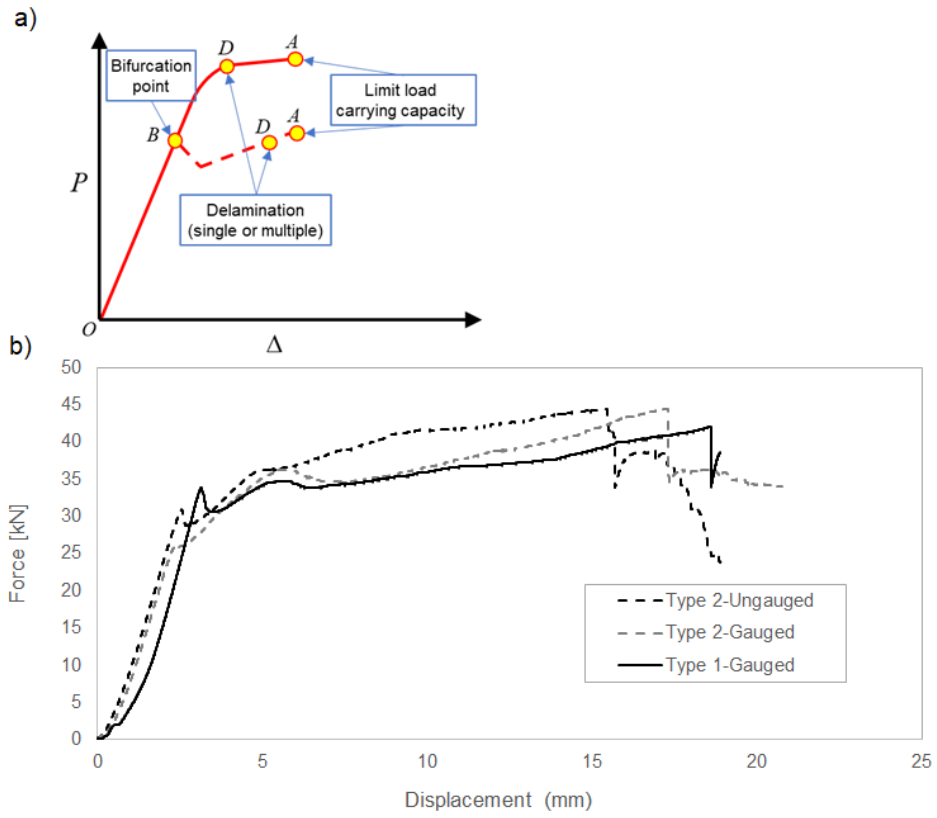

Figure 9: Buckling and post-buckling load-displacement curves for laminated composites; a) schematic representation for perfect structure (solid line) and structure with shape imperfections (dashed line), b) for type 1 and type 2 laminates of study under pure in-plane shear loading

The experimental load-displacement curves for the single conventional (type 1) and two novel (type 2) specimens are illustrated in Figure 9b. The measured load represents the tensile force applied to the test fixture, and the displacement is the resulting deflection at the loaded end of the test fixture. As expected, both laminate types, follow a linear equilibrium path up to the bifurcation point. The slopes of the linear portion of each curve (between 10-20kN) indicate specimen stiffnesses of $9.14\ kN/mm$ and $14.36\ kN/mm$ for type 1 and 2, respectively. For both laminate types, the applied shear force decreases immediately after buckling as a result of laminate out of plane bending. However, the force continues to increase up to the point of final collapse.

Table 2 summarises the experimental and numerical buckling and failure loads of both laminate configurations. It is worth noting that numerical strain values are extracted for elements and integration points associated to the location of strain gauges in the experiment. Both type 2 laminates exhibit a higher load bearing capacity than the type 1 laminate. The average failure load for the type 2 laminates was $43.94\ kN$, whereas the failure load for the gauged type 1 laminate was $41.8\ kN$. The average buckling load for the type 2 laminates was $27.9\ kN$, whereas the buckling load for the gauged type 1 laminate was $32.00\ kN$. Therefore, the hybrid X-braced laminate design (type 2) may have a marginally higher failure performance but a slightly lower buckling performance. The panels develop an approximate load carrying capacity of 1.3 and 1.6 times the critical buckling load for type 1 and type 2 laminates, respectively. This behaviour is similar to that of incomplete diagonal tension field panels for isotropic materials [5] in which the web of such beams retain, after buckling, some of their ability to support loads so that even near failure they are in a state of stress somewhere between that of pure diagonal tension and the pre-buckling stress. This underpins the importance of considering post-buckling behaviour for a lightweight design.

Table 2: Experimental and numerical buckling load

Laminate type	Number of specimens	Failure load (kN)	Average failure load (kN)	Numerical failure load (kN)	Experimental buckling load (kN)	Average experimental buckling load (kN)	Numerical buckling load (kN)
Type 1-Gauged	1	41.68	-	40.63	32.00	-	33.37
Type 2-Ungauged	1	44.30	43.94	46.45	29.80	27.90	35.84
Type 2-Gauged	1	43.58			26.00		

For a detailed analysis of the experimental post-buckling strain to failure, the measured strain gauge data is examined. Figure 10 presents strain gauge data for six locations (type 1 data in Figure 10a, type 2 data in Figure 10b). The numerical simulation results at extreme fibres are also shown on the figure as dashed lines. Based on the figures, the type 2 laminate endures greater strains than the type 1 laminate, due to the use of high strain to failure glass plies. For instance, as shown in Figure 11, strain gauge 3 on the type 2 laminate records a maximum strain of 7671 micro-strain, compared to a maximum of 5507 micro-strain for the type 1 laminate. This is a 40% higher failure strain. This demonstrates an improved strain to failure

response for the hybrid laminate over the pure CFRP laminate design. For both laminate types, there is good agreement between the numerical and experimental results up to the bifurcation point.

The prediction of failure load is in excellent agreement between the numerical and experimental results. It is observed that the predicted strain in the post-buckling region, at the strain gauge 4 location, shows a divergence from the measured strain results. This is due to the inability of the numerical model to capture the mode shape at failure fully. In the simulation, for the type 2 laminates, at the point close to collapse, the deflected shape tends to transit to the mode 1 shape with two lateral half wavelengths in the direction perpendicular to the loading direction (see Figure 4) which is not the case in the experiments. In fact, the change in the mode shape is not observed in the experiment. It is worth noting that consideration of a perturbed geometry (instead of the ideal perfect geometry) in the numerical model significantly contributes to a smoothing of the transition between the initial linear behaviour and the nonlinear post-buckling behaviour. In addition, it also smooths the transition between modes in the post-buckling regime, thus decreasing the severity of any convergence difficulties. This is in agreement with results obtained in [39], [40].

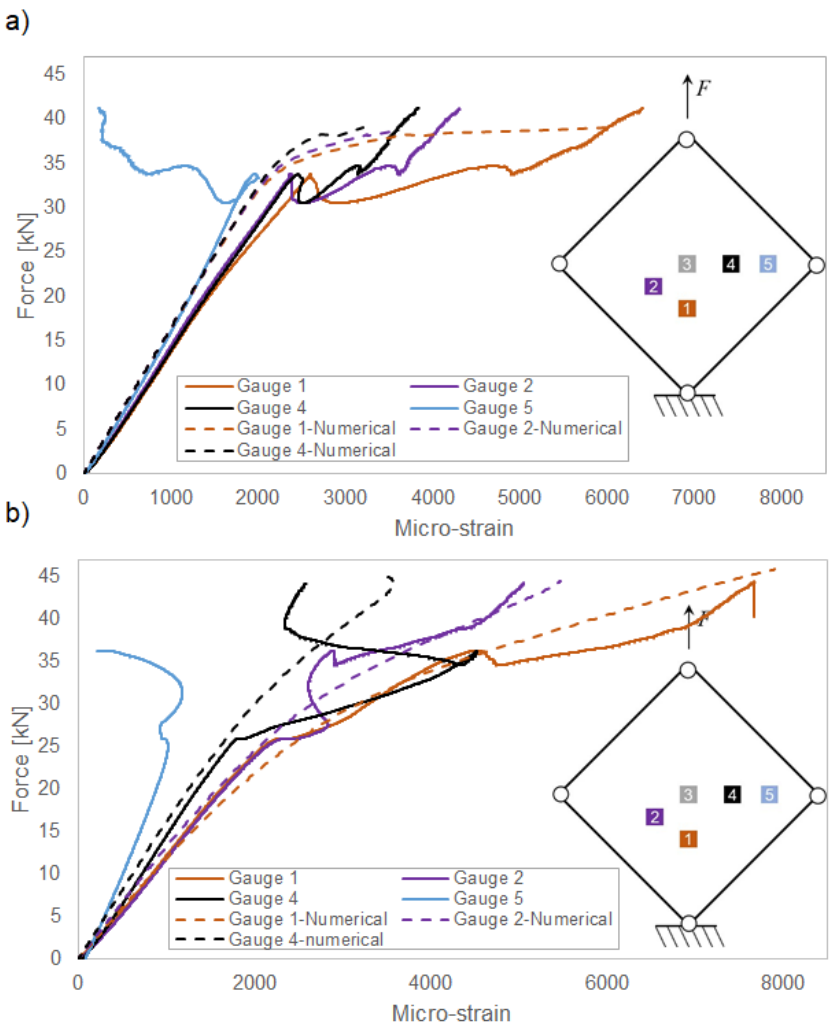

Figure 10: Experimental strain gauge readings and numerical values for; a) pure CFRP laminates (type 1) and b) X-braced hybrid laminates (type 2). FE results are extracted at through-thickness integration point locations equivalent to that of strain gauge locations in the experiment

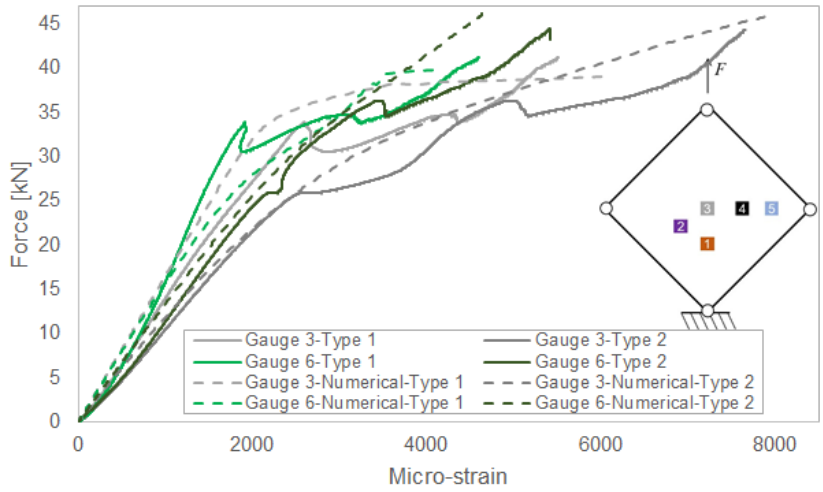

Figure 11: Experimental strains (solid lines) and numerical strains (dashed lines) for strain gauges 3 and 6 of both laminate types 1 and 2. Strain gauge 6 (green data) is on the opposite side of strain gauge 3

The numerical analysis has the advantage that it can provide insight into the internal specimen damage mechanisms, helping to identify differences in behaviour between the laminate designs. The failed specimens of type 1 and 2 laminates are shown in Figure 12 demonstrating a repeatable failure location and type for all specimens. Experimental examination of the failed laminates shows that the type 1 laminate failed along the centreline of the specimen, displaying a combination of matrix cracking and fibre breakage (see Figure 13). The failure in the direction of the main diagonal shows the well-known characteristic tension field panel behaviour under pure shear loading. A similar failure type is reported in [34]. After initial plate buckling, the specimen deforms into mode shape 1 (Figure 13a) and continues deforming in the same mode up to the point of failure (Figure 13c). As observed in the experiment, the fracture is sudden and brittle. Probing the numerical results suggests that although shear damage is present in the type 1 laminate (see Figure 14c), the failure is dominated by compressive and tensile fibre breakage along the local 2 direction of the outermost plies, i.e. plies 1 and 8 (see Figure 14a-b). In other words, the comparison of maximum and minimum principal stresses just before and after load drop (see Figure 15) for the outermost plies is comparable with those of material strength allowables ($595\,MPa$ for tensile and $393\,MPa$ for compressive strength) of Table 1. This shows that the initiation of damage is strongly correlated to the tensile damage of fibres focused along the geometric centreline of the tensile outermost ply in the laminate (ply 8). This is in good agreement with the observation of the experimental results.

Figure 16 illustrates the experimental failure process of the type 2 laminates. The experimental failure starts from the ply drop off of the X-brace CFRP plies (Figure 16a), which then joins up with the failure from the bottom grip location (Figure 16b). As the loading increases, the failure grows (Figure 16c-d) and reaches the top grip (Figure 16e-f). Examination of the predicted damage from the simulation, just before failure and throughout the failure process, shows that shear damage (SDV5) occurs far in advance of any damage mechanism, i.e. fibre tensile/compressive failure, and is present throughout the failure process as shown in Figure 17. Shear damage is mostly associated to the 0 deg carbon plies in the areas close to the boundaries of the laminate than the 45 deg carbon or glass plies. For the sake of brevity, shear stresses of the 0 deg carbon ply of the laminate are plotted in Figure 18 at various time steps.

Comparison of the numerical shear stresses of Figure 18 with those of Figure 8b illustrates the exceedance of shear stresses from $45\,MPa$ (threshold for plastic shear strain). This suggests that plastic deformation of the 0 deg carbon plies, under shear loading, could be a key contributing factor to the considerably higher strain to failure of the type 2 laminate design.

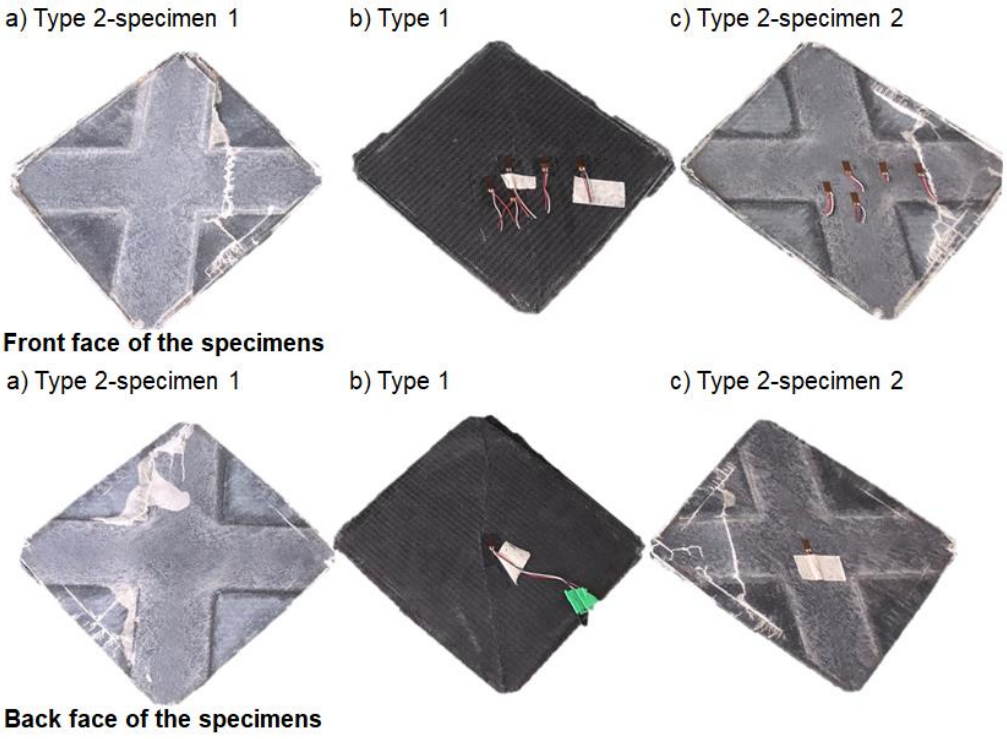

Figure 12: Failed specimens for type 1 and two of type 2 laminates. Top and bottom figures are for the front and back faces, respectively.

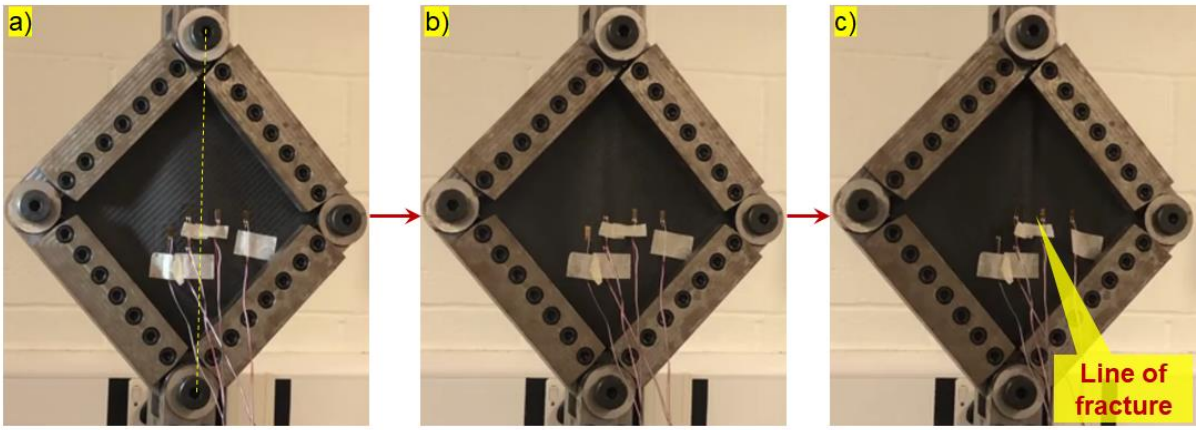

Figure 13: Experimental progression of failure in type 1 laminates (the yellow dashed line shows the centreline or axis of symmetry)

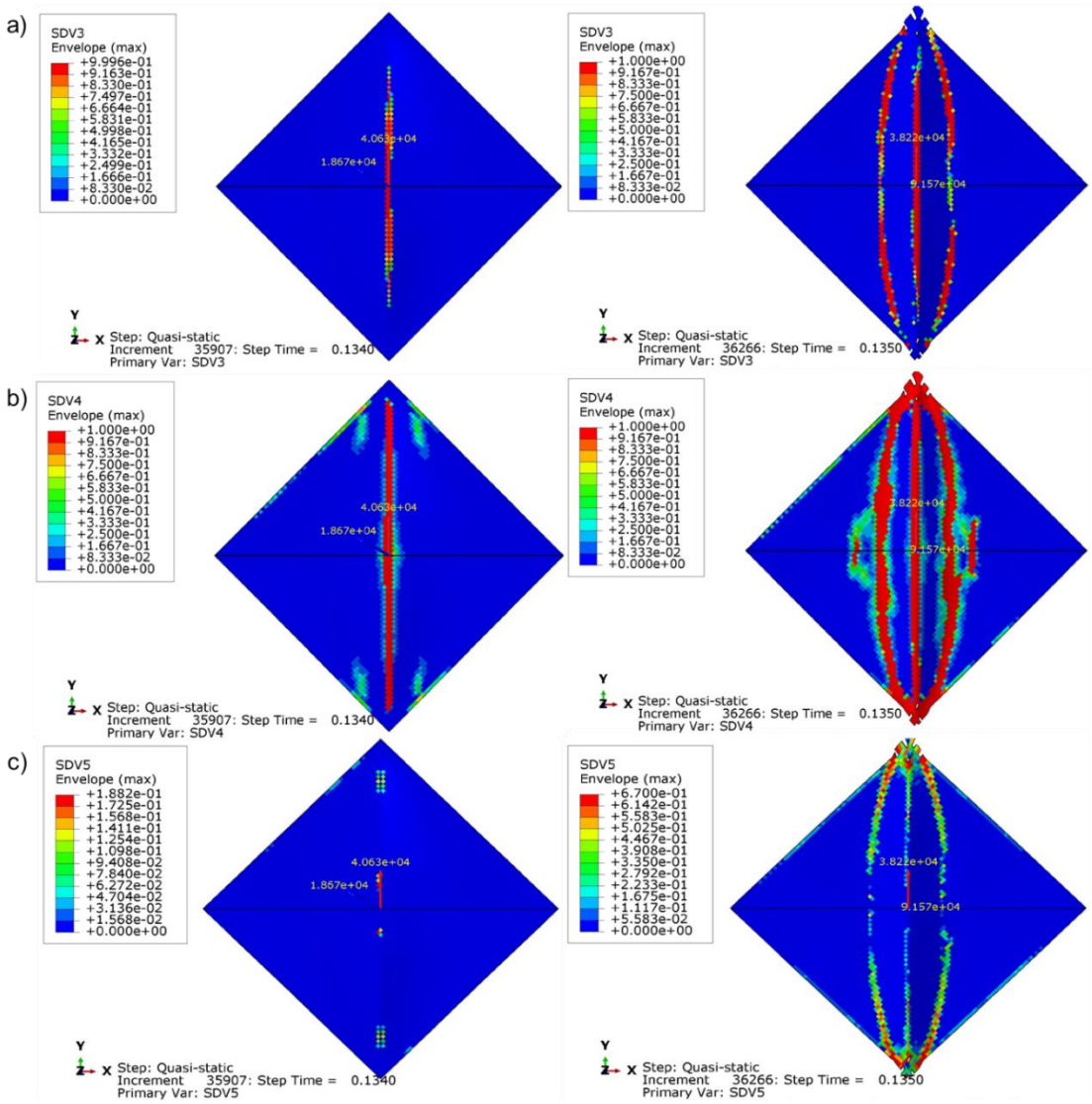

Figure 14: Damage parameters of type 1 laminates; a) fibre tensile damage in ply local direction 2, b) fibre compressive damage in ply local direction 2 and c) shear damage at the damage initiation (left images) and just prior to load drop and specimen collapse (right images)

It is worth noting that the shear damage parameter never exceeds 0.72 (maximum possible experimental shear damage parameter for CFRP and GFRP material as shown in Figure 7) and is present throughout the failure process. In fact, as shown in Figure 19, shear damage is often accompanied by a compressive failure (SDV4) of fibres along the 2 material direction. As shown in Figure 20, X shaped 45 deg carbon plies furthest away from the mid-plane of the laminates experience the highest compressive stresses as a result of out of plane bending deformation and fail first. Subsequently, the load is redistributed to the glass fibres located at the outer mould surfaces, giving rise to compressive stresses along the 2 material direction as shown in Figure 21. It is worth noting that, unlike the type 1 laminates, the numerical simulation does not predict tensile damage of the fibres, nor compressive damage in

the local 1 direction for the material. In general, the numerical model demonstrates good agreement with the experimental results, in terms of damage location, initiation and progression.

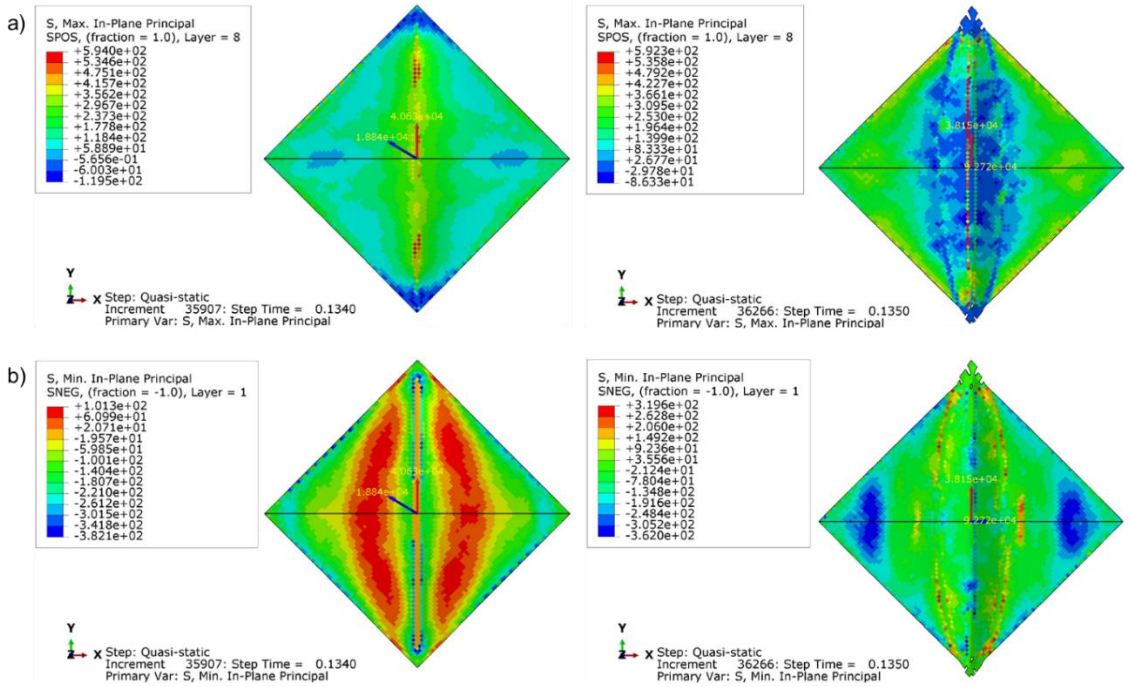

Figure 15: Principal stresses of type 1 laminates; a) maximum principal stress just before (left image) and after (right image) the load drop for tensile outermost ply (ply 8), b) minimum principal stress just before (left image) and after (right image) the load drop for compressive outermost ply (ply 1)

Unlike the conventional type 1 design, the type 2 laminates do not manifest the well-known characteristic behaviour of either complete or incomplete tension field plates. Instead, they demonstrate a gradual failure behaviour due to the dominance of the shear damage failure mechanism, as opposed to tension along the main diagonal of the plate and in the loading direction that could lead to sudden fibre breakage as evidenced in the type 1 design. This is a result of shear damage, cracking and plastic deformation of the matrix leading to a more gradual failure. It may be argued that this mode of failure is more desirable for flight critical components.

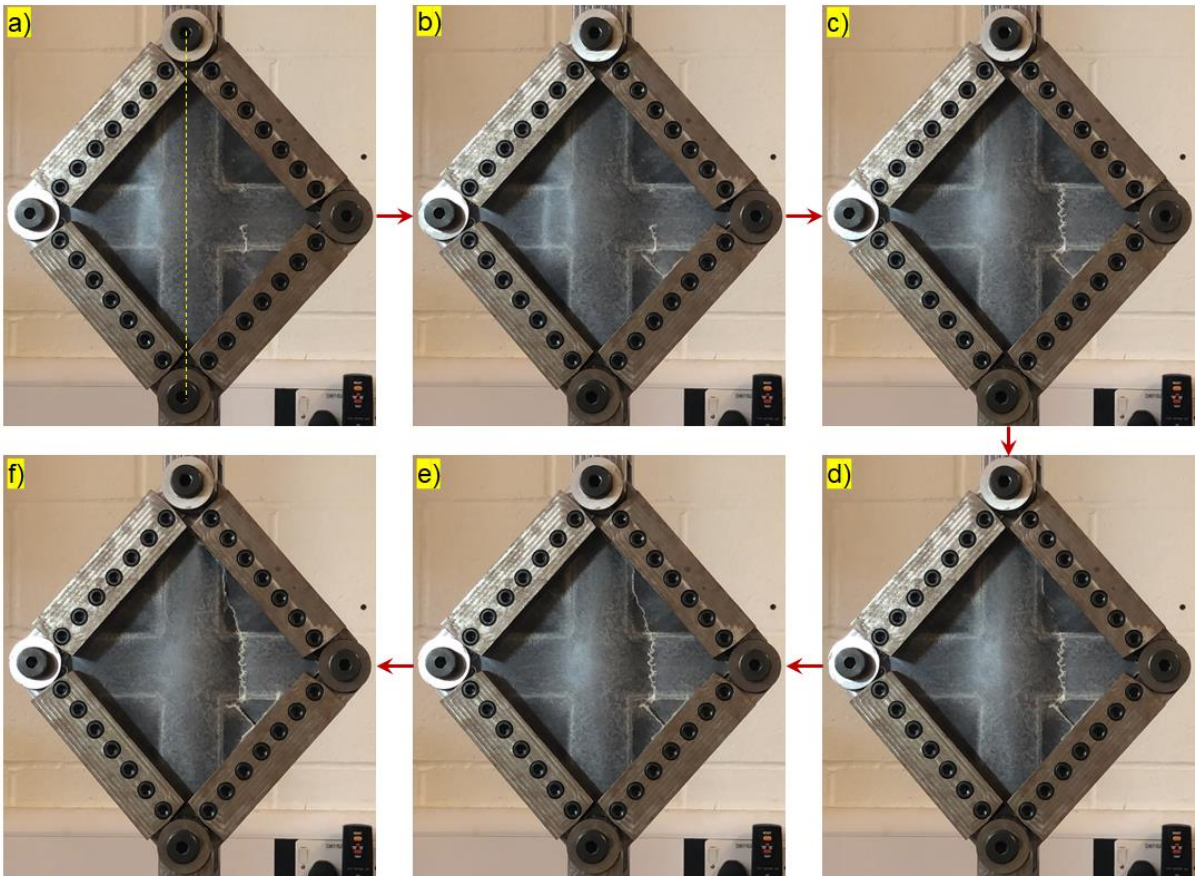

Figure 16: Experimental progression of failure in type 2 laminates (the yellow dashed line shows the centreline or axis of symmetry)

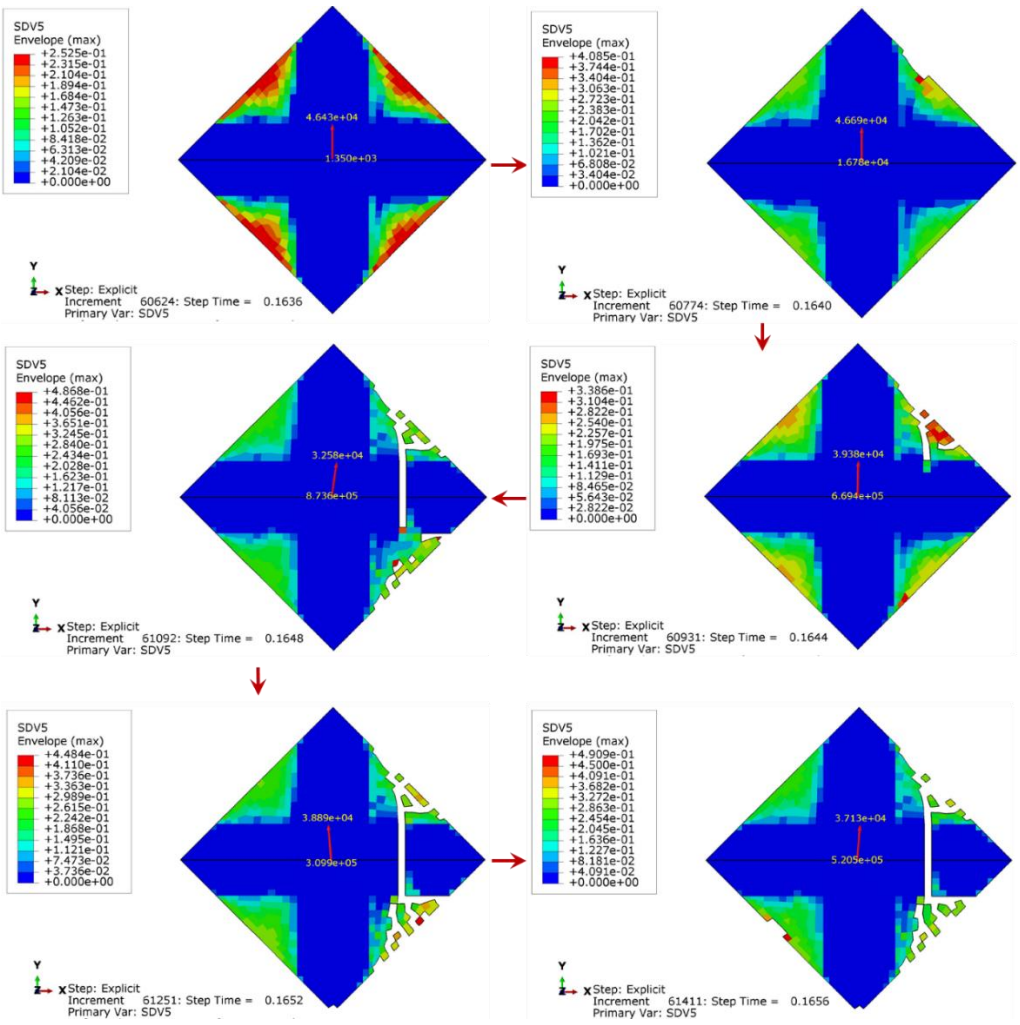

Figure 17: Progressive shear damage parameter (SDV5) for type 2 laminates throughout the failure process

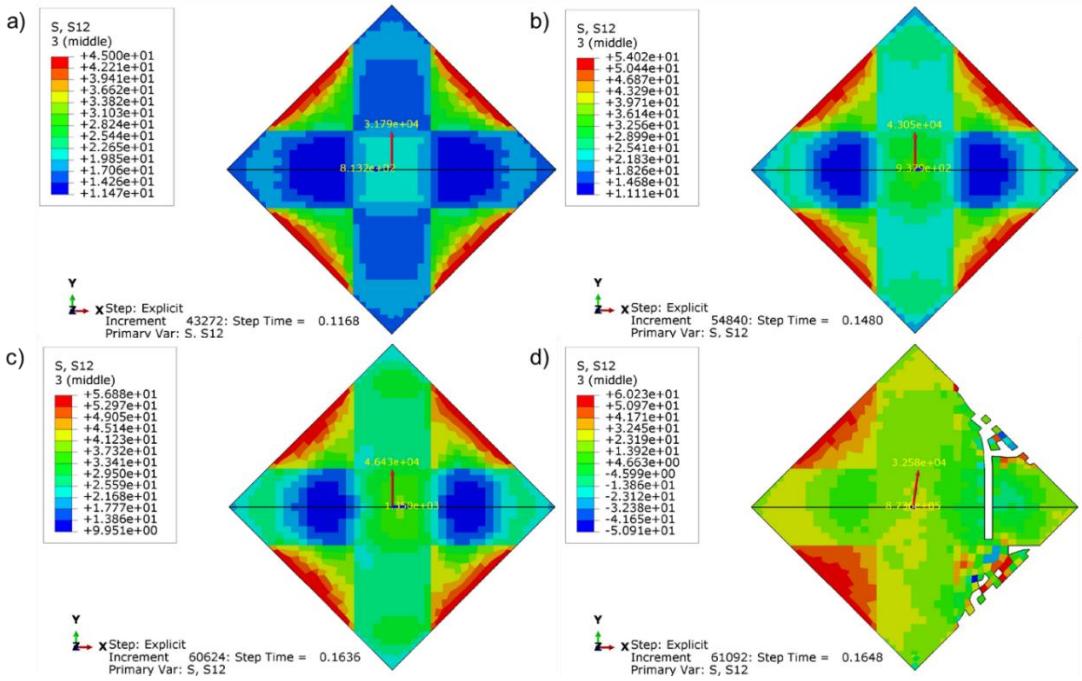

Figure 18: Progressive shear stresses of 0deg carbon plies for type 2 laminates before and throughout the failure process

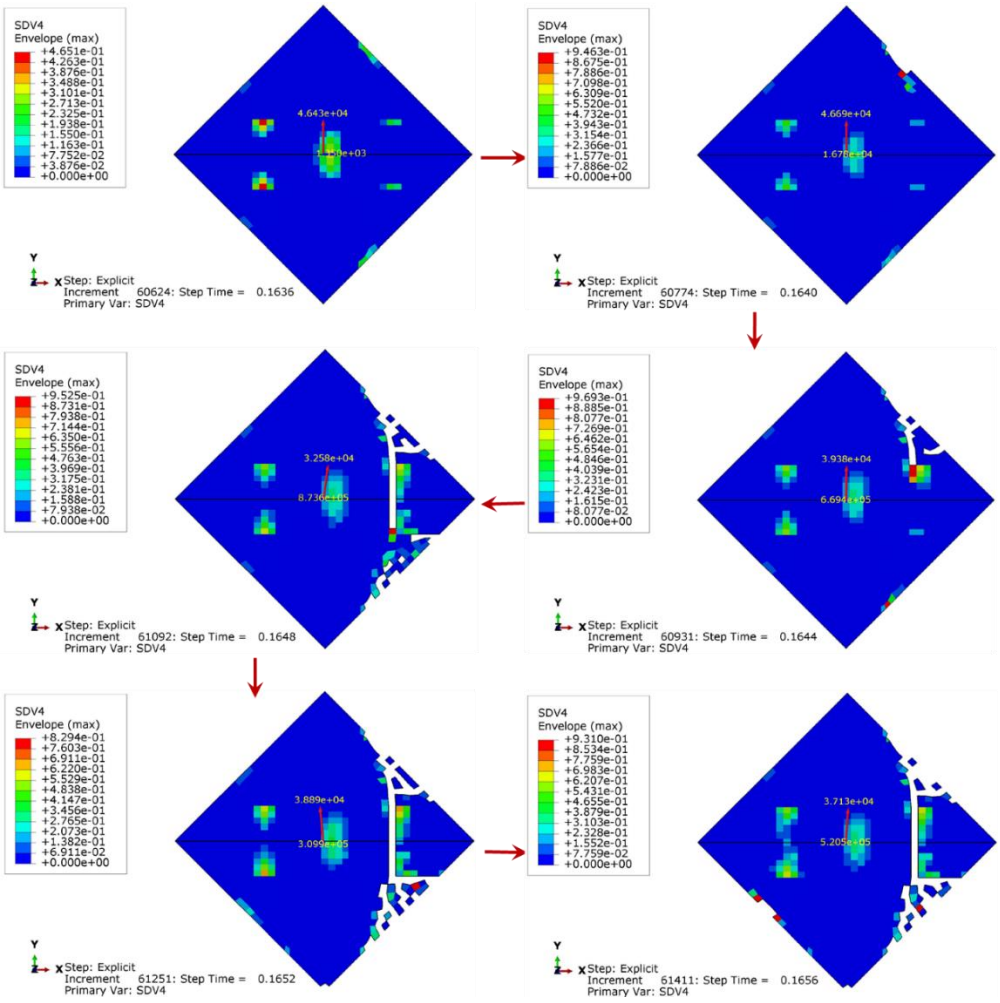

Figure 19: Progressive compressive damage parameter (SDV4) along fibre direction 2 for type 2 laminates throughout the failure process

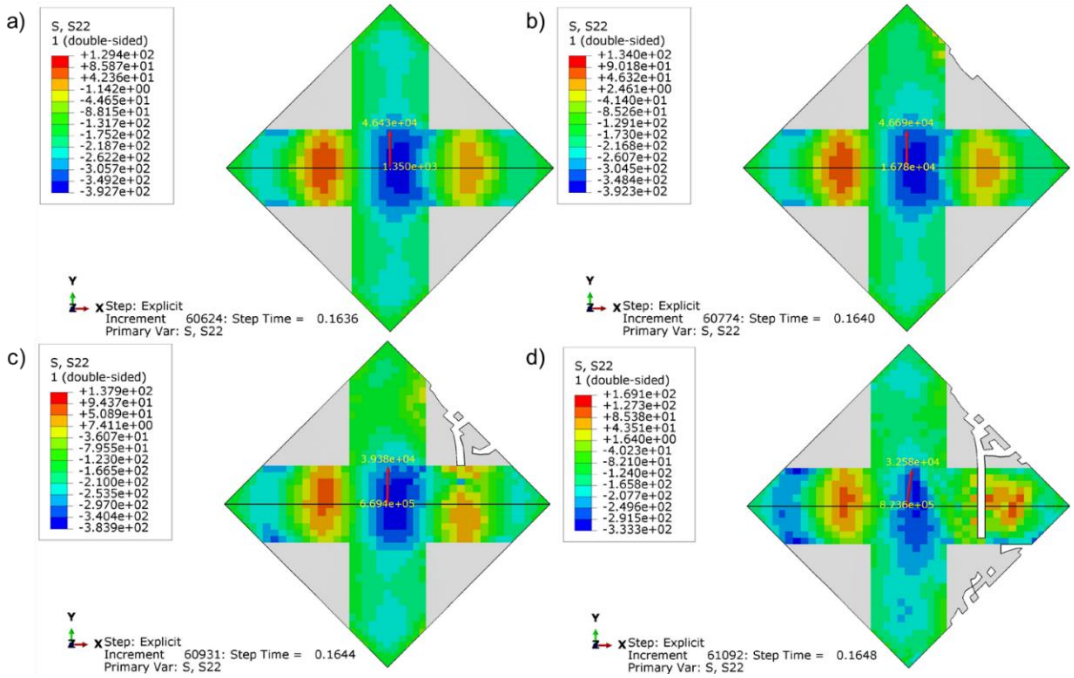

Figure 20: Progressive compressive stresses of X shaped carbon plies for type 2 laminates just before and throughout the failure process

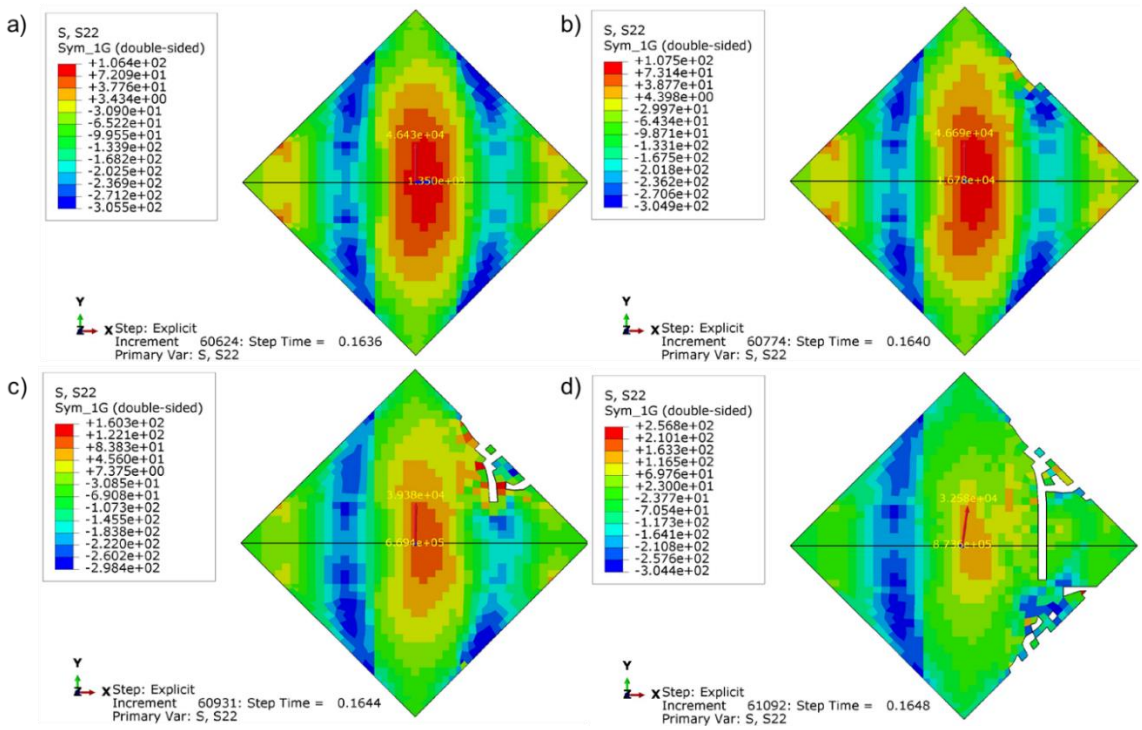

Figure 21: Progressive compressive stresses of glass plies for type 2 laminates just before and throughout the failure process

7 Conclusions

Buckling and post-buckling performance of pure twill woven CFRP (type 1) and a novel X-braced hybrid laminate design (type 2) have been investigated experimentally and numerically, considering pure shear loading. Type 1 and hybrid laminates failed at loads approximately 1.3 and 1.6 times higher than the initial plate buckling load, respectively, demonstrating the capability of composite laminates in resisting loads well beyond initial buckling. It is evident that the X-braced hybrid laminates benefit from 23% higher buckling to failure load ratio compared to type 1 laminate. The novel X-braced hybrid laminates, despite having less of the much stiffer CFRP plies, showed only marginally lower initial plate buckling performance and higher failure performance. In addition, the novel laminates also exhibited significantly higher strain to failure compared to the conventional laminates, thanks to the X-bracing concept and the plastic deformation of the 0 deg CFRP plies. The numerical models achieved close prediction of the experimental buckling and nonlinear post-buckling behaviour - predicting the bifurcation point, the failure load, the location of damage and the damage mechanisms all with reasonable accuracy. Due to the representation of initial imperfections within the numerical models, smooth transitions were consistently observed from the linear buckling to the post-buckling behaviour. Failure of the

conventional laminates was dominated by both tensile and compressive fibre damage in the local 2 direction of the outermost and innermost plies. Whereas the novel X-braced hybrid laminates failed with shear damage and compressive fibre breakage in the ply local 2 direction of the outermost plies. The combined experimental and numerical results illustrate the feasibility to tailor the shape of hybrid laminate plies to reduce weight and maximise their post-buckling strain to failure. Further studies and more test samples are required to evaluate the performance of such concepts under other loading conditions, particularly, their cyclic behaviour given the lower buckling mode of hybrid concept compared to the traditional type 1 laminate.

8 Declaration of conflicting interests

The authors declared no potential conflicts of interest with respect to the research, authorship, and/or publication of this article.

9 Acknowledgment

The authors received no financial support for the research, authorship, and/or publication of this article.

10 References

[1] Y. Feng, Y. He, X. Tan, T. An, and J. Zheng, “Experimental investigation on different positional impact damages and shear-after-impact (SAI) behaviors of stiffened composite panels,” *Compos. Struct.*, vol. 178, pp. 232–245, 2017, doi: 10.1016/j.compstruct.2017.06.053.

[2] D. G. Stamatelos, G. N. Labeas, and K. I. Tserpes, “Analytical calculation of local buckling and post-buckling behavior of isotropic and orthotropic stiffened panels,” *Thin-Walled Struct.*, vol. 49, no. 3, pp. 422–430, 2011, doi: https://doi.org/10.1016/j.tws.2010.11.008.

[3] M. Suresh Kumar, M. Ambresha, K. Panbarasu, I. Kishore, and V. R. Ranganath, “A comparative study of failure features in aerospace grade unidirectional and bidirectional woven CFRP composite laminates under four-point bend fatigue loads,” *Materwiss. Werksttech.*, vol. 46, no. 6, pp. 644–651, 2015, doi: 10.1002/mawe.201400278.

[4] M. H. Kabir, S. Fawzia, T. H. T. Chan, and M. Badawi, “Durability of CFRP strengthened steel circular hollow section member exposed to sea water,” *Constr. Build. Mater.*, vol. 118, pp. 216–225, 2016, doi: 10.1016/j.conbuildmat.2016.04.087.

[5] T. H. G. Megson, *Introduction to Aircraft Structural Analysis*. 2010.

[6] T. Kopecki, J. Bakunowicz, and T. Lisle, “Post-critical deformation states of composite thin-walled aircraft load-bearing structures,” *J. Theor. Appl. Mech.*, vol. 54, no. 1, pp. 195–204, 2016, doi: 10.15632/jtam-pl.54.1.195.

[7] J. Loughlan, “The buckling of CFRP composite plates in compression and shear and thin-walled composite tubes in torsion – The effects of bend-twist coupling and the applied shear direction on buckling performance,” *Thin-Walled Struct.*, vol. 138, pp. 392–403, 2019, doi: https://doi.org/10.1016/j.tws.2019.01.045.

[8] A. Murphy, F. Lynch, M. Price, and A. Gibson, “Modified stiffened panel analysis methods for laser beam and friction stir welded aircraft panels,” *Proc. Inst. Mech. Eng. Part G J. Aerosp. Eng.*, vol. 220, no. 4, pp. 267–278, 2006, doi: 10.1243/09544100JAERO51.

[9] D. Quinn, A. Murphy, and C. Glazebrook, “Aerospace stiffened panel initial sizing with novel skin sub-stiffening features,” *Int. J. Struct. Stab. Dyn.*, vol. 12, no. 5, p. 1250060, 2012, doi: 10.1142/S0219455412500605.

[10] X. Liu, C. A. Featherston, and D. Kennedy, “Buckling optimization of blended composite structures using lamination parameters,” *Thin-Walled Struct.*, vol. 154, p. 106861, 2020, doi: https://doi.org/10.1016/j.tws.2020.106861.

[11] B. E. Kaminski and J. E. Ashton, “Diagonal Tension Behavior of Boron-Epoxy Shear Panels,” *J. Compos. Mater.*, vol. 5, no. 4, pp. 553–558, Apr. 1971, doi: 10.1177/002199837100500416.

[12] T. Kubiak and R. J. Mania, “Hybrid versus FR laminate channel section columns – Buckling and postbuckling behaviour,” *Compos. Struct.*, vol. 154, pp. 142–149, 2016, doi: https://doi.org/10.1016/j.compstruct.2016.07.040.

[13] I. Papa, L. Boccarusso, A. Langella, and V. Lopresto, “Carbon/glass hybrid composite laminates in vinylester resin: Bending and low velocity impact tests,” *Compos. Struct.*, vol. 232, p. 111571, 2020, doi: https://doi.org/10.1016/j.compstruct.2019.111571.

[14] R. Burgueño, N. Hu, A. Heeringa, and N. Lajnef, “Tailoring the elastic postbuckling response of thin-walled cylindrical composite shells under axial compression,” *Thin-Walled Struct.*, vol. 84, pp. 14–25, 2014, doi: https://doi.org/10.1016/j.tws.2014.05.009.

[15] B. L. Agarwal, “Postbuckling Behavior of Composite Shear Webs,” *AIAA J.*, vol. 19, no. 7, pp. 933–939, Jul. 1981, doi: 10.2514/3.51022.

[16] S. Kosteletos, “Postbuckling response of laminated plates under shear load,” *Compos. Struct.*, vol. 20, no. 3, pp. 137–145, 1992, doi: https://doi.org/10.1016/0263-8223(92)90020-D.

[17] F. A. Fazzolari, J. R. Banerjee, and M. Boscolo, “Buckling of composite plate assemblies using higher order shear deformation theory—An exact method of solution,” *Thin-Walled Struct.*, vol. 71, pp. 18–34, 2013, doi: https://doi.org/10.1016/j.tws.2013.04.017.

[18] K. Zhao, D. Kennedy, and C. Featherston, “Exact strip postbuckling analysis of composite plates under compression and shear,” *Aeronaut. J.*, vol. 123, no. 1263, pp. 658–677, 2019, doi: https://doi-org.ezproxy.uwe.ac.uk/10.1017/aer.2019.27.

[19] M. Damghani, D. Kennedy, and C. Featherston, “Global buckling of composite plates containing rectangular delaminations using exact stiffness analysis and smearing method,” *Comput. Struct.*, vol. 134, pp. 32–47, Apr. 2014, doi: 10.1016/j.compstruc.2013.12.005.

[20] M. Damghani, D. Kennedy, C. C. A. C. Featherston, D. Kennedy, and C. C. A. C. Featherston, “Critical buckling of delaminated composite plates using exact stiffness analysis,” *Comput. Struct.*, vol. 89, no. 13–14, pp. 1286–1294, Jul. 2011, doi: 10.1016/j.compstruc.2011.04.003.

[21] Z. Wu, G. Raju, and P. M. Weaver, “Postbuckling analysis of variable angle tow composite plates,” *Int. J. Solids Struct.*, vol. 50, no. 10, pp. 1770–1780, 2013, doi: https://doi.org/10.1016/j.ijsolstr.2013.02.001.

[22] N. R. Kolanu, G. Raju, and R. M, “Post-buckling failure studies on quasi-isotropic CFRP panels under positive and negative in-plane shear loading,” *Compos. Struct.*, vol. 246, p. 112379, 2020, doi: https://doi.org/10.1016/j.compstruct.2020.112379.

[23] T. Zhang, S. Li, F. Chang, X. Shi, and L. Li, “An experimental and numerical analysis for stiffened composite panel subjected to shear loading in hygrothermal environment,” *Compos. Struct.*, vol. 138, pp. 107–115, 2016, doi: https://doi.org/10.1016/j.compstruct.2015.11.056.

[24] J. Reinoso, A. Blázquez, F. París, J. Cañas, and J. C. Meléndez, “Postbuckling behaviour of a pressurized stiffened composite panel – Part I: Experimental study,” *Compos. Struct.*, vol. 94, no. 5, pp. 1533–1543, 2012, doi: https://doi.org/10.1016/j.compstruct.2011.12.014.

[25] D. Kumar and S. B. Singh, “Postbuckling strengths of composite laminate with various shaped cutouts under in-plane shear,” *Compos. Struct.*, vol. 92, no. 12, pp. 2966–2978, 2010, doi: https://doi.org/10.1016/j.compstruct.2010.05.008.

[26] D. Kumar and S. B. Singh, “Stability and failure of composite laminates with various shaped cutouts under combined in-plane loads,” *Compos. Part B Eng.*, vol. 43, no. 2, pp. 142–149, 2012, doi: https://doi.org/10.1016/j.compositesb.2011.09.005.

[27] A. Muc, M. Chwał, and M. Barski, “Remarks on experimental and theoretical investigations of buckling loads for laminated plated and shell structures,” *Compos. Struct.*, vol. 203, pp. 861–874, 2018, doi: https://doi.org/10.1016/j.compstruct.2018.07.094.

[28] A. S. M. Al-Azzawi, L. F. Kawashita, and C. A. Featherston, “Buckling and postbuckling behaviour of Glare laminates containing splices and doublers. Part 2: Numerical modelling,” *Compos. Struct.*, vol. 176, pp. 1170–1187, 2017, doi:

https://doi.org/10.1016/j.compstruct.2017.04.063.

[29] A. S. M. Al-Azzawi, J. McCrory, L. F. Kawashita, C. A. Featherston, R. Pullin, and K. M. Holford, “Buckling and postbuckling behaviour of Glare laminates containing splices and doublers. Part 1: Instrumented tests,” *Compos. Struct.*, vol. 176, pp. 1158–1169, 2017, doi: https://doi.org/10.1016/j.compstruct.2017.04.030.

[30] N. Petkune, T. Donchev, H. Hadavinia, D. Wertheim, and M. Limbachiya, “Comparison of the behaviour of steel, pure FRP and hybrid shear walls under cyclic seismic loading in aspect of stiffness degradation and energy absorption,” *Constr. Build. Mater.*, vol. 165, pp. 621–630, 2018, doi: https://doi.org/10.1016/j.conbuildmat.2017.12.013.

[31] Y. Swolfs, L. Gorbatikh, and I. Verpoest, “Fibre hybridisation in polymer composites: A review,” *Compos. Part A Appl. Sci. Manuf.*, vol. 67, pp. 181–200, 2014, doi: 10.1016/j.compositesa.2014.08.027.

[32] E. A. Godínez-Domínguez and A. Tena-Colunga, “Behavior of ductile steel X-braced RC frames in seismic zones,” *Earthq. Eng. Eng. Vib.*, vol. 18, no. 4, pp. 845–869, 2019, doi: 10.1007/s11803-019-0539-0.

[33] M. Damghani, N. Ersoy, M. Piorkowski, and A. Murphy, “Experimental evaluation of residual tensile strength of hybrid composite aerospace materials after low velocity impact,” *Compos. Part B Eng.*, vol. 179, p. 107537, Dec. 2019, doi: 10.1016/J.COMPOSITESB.2019.107537.

[34] N. R. Kolanu, G. Raju, and M. Ramji, “Damage assessment studies in CFRP composite laminate with cut-out subjected to in-plane shear loading,” *Compos. Part B Eng.*, vol. 166, pp. 257–271, 2019, doi: 10.1016/j.compositesb.2018.11.142.

[35] A. F. Johnson, “Modelling fabric reinforced composites under impact loads,” *Compos. - Part A Appl. Sci. Manuf.*, 2001, doi: 10.1016/S1359-835X(00)00186-X.

[36] T. Lisle, C. Bouvet, M. L. Pastor, T. Rouault, and P. Marguerès, “Damage of woven composite under tensile and shear stress using infrared thermography and micrographic cuts,” *J. Mater. Sci.*, 2015, doi: 10.1007/s10853-015-9173-z.

[37] M.-G. Han and S.-H. Chang, “Draping simulation of carbon/epoxy plain weave fabrics with non-orthogonal constitutive model and material behavior analysis of the cured structure,” *Compos. Part A Appl. Sci. Manuf.*, vol. 110, pp. 172–182, 2018, doi: https://doi.org/10.1016/j.compositesa.2018.04.022.

[38] V. Munoz, M. Perrin, M. L. Pastor, H. Welemane, A. Cantarel, and M. Karama, “Determination of the elastic properties in CFRP composites: Comparison of different approaches based on tensile tests and ultrasonic characterization,” *Adv. Aircr. Spacecr. Sci.*, 2015, doi: 10.12989/aas.2015.2.3.249.

[39] K. A. Stevens, R. Ricci, and G. A. O. Davies, “Buckling and postbuckling of composite structures,” *Composites*, vol. 3, no. 26, pp. 189–199, 1995, doi:

10.1016/0010-4361(95)91382-F.

[40] A. Blázquez, J. Reinoso, F. París, and J. Cañas, “Postbuckling behavior of a pressurized stiffened composite panel - Part II: Numerical analysis. Effect of the geometrical imperfections,” *Compos. Struct.*, vol. 94, pp. 1544–1554, 2012, doi: 10.1016/j.compstruct.2011.12.013.

Appendix

The damage parameters used for the materials of study are obtained via experimental testing by the authors and are shown in Table A.

Table A: Damage parameters for the materials of study

Parameter	Unit	Description	Value	
			AX 5180	AX 3180
E_{1+}	MPa	Young's modulus along fibre direction 1 when $tr(\boldsymbol{\varepsilon}) \geq 0$ *	67094.00	30083.00
E_{2+}	MPa	Young's modulus along fibre direction 2 when $tr(\boldsymbol{\varepsilon}) \geq 0$	67094.00	30083.00
υ_{12+}	-	Poisson's ratio when $tr(\boldsymbol{\varepsilon}) \geq 0$	0.04	0.14
G_{12}	MPa	Shear modulus	4831.40	4954.60
E_{1-}	MPa	Young's modulus along fibre direction 1 when $tr(\boldsymbol{\varepsilon}) < 0$	67094.00	30083.00
E_{2-}	MPa	Young's modulus along fibre direction 2 when $tr(\boldsymbol{\varepsilon}) < 0$	67094.00	30083.00
υ_{12-}	-	Poisson's ratio when $tr(\boldsymbol{\varepsilon}) < 0$	0.04	0.14
X_{1+}	MPa	Tensile strength along fibre direction 1	595.00	437.16
X_{1-}	MPa	Compressive strength along fibre direction 1	393.00	306.00
X_{2+}	MPa	Tensile strength along fibre direction 2	595.00	437.16
X_{2-}	MPa	Compressive strength along fibre direction 2	393.00	306.00
S	MPa	Shear stress at the onset of shear damage	39.62	34.09
G_f^{1+} **	N.mm/mm²	Energy per unit area for tensile fracture along fibre direction 1	6.61	7.94
G_f^{1-}	N.mm/mm²	Energy per unit area for compressive fracture along fibre direction 1	4.35	5.56
G_f^{2+}	N.mm/mm²	Energy per unit area for tensile fracture along fibre direction 2	6.61	7.94
G_f^{2-}	N.mm/mm²	Energy per unit area for compressive fracture along fibre direction 2	4.35	5.56
α_{12}	-	Parameter in the equation of shear damage	0.38	0.31
$d_{12}^{\max}$	-	Maximum shear damage	0.67	0.72
$\overline{\sigma_{0y}}$	MPa	Initial effective shear yield stress	45.00	30.00
C	-	Coefficient in hardening equation	1326.42	2024.98
p	-	Power term in hardening equation	0.48	0.49

* $tr(\boldsymbol{\varepsilon}) = \varepsilon_{11} + \varepsilon_{22}$

** determined for element characteristic length of $2.5\ mm$ based on $G_f^{1+} = L_c g_0^{1+}$

- The novel X-braced hybrid composite laminates, despite having less of the much stiffer Carbon Fibre Reinforced Polymer plies, showed only marginally lower initial plate buckling performance and higher failure performance.
- The novel laminates exhibited significantly higher strain to failure compared to the conventional laminates, thanks to the X-bracing concept and the plastic deformation of the 0 deg Carbon Fibre Reinforced Polymer plies.
- Experimental and numerical studies show that standard and hybrid panels can withstand collapse shear loads 1.3 and 1.6 times, respectively, beyond their associated buckling load.
- Failure of the conventional laminates was dominated by both tensile and compressive fibre damage in the local 2 direction of the outermost and innermost plies. Whereas the novel X-braced hybrid laminates failed with shear damage and compressive fibre breakage in the ply local 2 direction of the outermost plies.

Using laminate hybridisation (CFRP-GFRP) and shaped CFRP plies to increase plate post-buckling strain to failure under shear loading

Mahdi Damghani [a,*], Christopher Wallis [a], Jerzy Bakunowicz [a], Adrian Murphy [b]

[a] Department of Engineering, Design and Mathematics (EDM), University of the West of England (UWE), Bristol, BS16 1QY, UK

[b] School of Mechanical and Aerospace Engineering, Queen's University Belfast (QUB), Belfast, BT9 5AG, UK

Abstract

Previous works have established the response and failure behaviour of hybrid (CFRP-GFRP) laminates when subjected to a wide range of destabilising loads. However, to date no works have quantified the influence of selective laminate shapes and hybridisation on plate post-buckling strain to failure. Thus, this paper investigates the plate collapse behaviour of a novel X-braced hybrid (CFRP-GFRP) twill woven laminate, subjected to in-plane shear loading. An experimental and numerical investigation is undertaken, including the consideration of a baseline pure CFRP laminate design. The experimental results illustrate that despite having less CFRP material, a hybrid laminate design with shaped CFRP plies can exhibit a greater strain to failure and buckling to failure load ratio, with only a marginally lower initial plate buckling load. Additionally, the experimental and numerical analysis reveals that the failure mechanism of the hybrid laminate is dominated by shear damage and fibre compressive breakage, whereas compressive and tensile fibre breakage dominate the conventional baseline laminate behaviour. Due to the prevalence of the shear damage and hence cracking and plastic deformation of the matrix, the novel hybrid laminate demonstrates a more gradual failure than the standard baseline laminate design, with failure strains significantly higher than that of the baseline laminate design.

Keywords: shear buckling, laminated composites, hybrid composites, post-buckling behaviour, nonlinear behaviour, failure criterion

* Corresponding author. Tel.: +4411732 87369
Email address: Mahdi.Damghani@uwe.ac.uk

1 Introduction

In recent years, there has been a significant increase in the use of Carbon Fibre Reinforced Polymer (CFRP) and Glass Fibre Reinforced Polymer (GFRP) in the design of highly loaded structural components, e.g. aircraft wing primary structure, and wind turbine blades. For instance, the Boeing 787 Dreamliner and the Airbus 350 XWB are reported to have respectively 52 and 53 per cent of their total weight resulting from the use of CFRP material. This is a markedly more substantial proportion than reported for the previous generation of aircraft, for example, 12 per cent for the Boeing 777 [1]. This marked increase is due to the superior strength/weight and stiffness/weight ratios of such material systems compared to conventional homogeneous isotropic materials, e.g. aluminium alloy [2]. Moreover, these materials also demonstrate enhanced fatigue performance [3] and corrosion resistance [4], particularly crucial for high-performance structures with long service life.

In aerospace applications, wing and fuselage CFRP panels are subjected to significant loading resulting from a vast range of combined aerodynamic pressures, manoeuvre induced inertial loads, and environmental fluctuations, e.g. temperature changes. Such panels are typically thin-walled, to minimise structural mass, but have large surface areas to generate the required lift or enclose the payload, crew, systems and fuel. Additionally, stiffness is a key requirement for such panels to maintain an aerodynamic form. As a result, wing skin and fuselage panels have their stressed skin supported and divided by internal stiffeners (stringers and ribs in a wing structure and stringers and frames in a fuselage). With the skin assumed as thin-walled plate elements between stiffeners, they need to resist significant direct and shear membrane loading [5]. Thus, understanding the behaviour of skin panel elements under various membrane loading actions is key to achieving a low mass design.

Skin panel elements under direct and shear stresses are prone to buckling instability [6], [7]. This topic is an essential area of research because it significantly influences design and structural mass. Furthermore, one of the leading design strategies generally adopted by the industry is to size structural components using simplified analysis assumptions [8]–[10] which generally give lower-bound buckling solutions. Hence, they give conservative (upper-bound) solutions in design. This is, of course, appropriate for conservative structural design and initial sizing, but where the

structure is weight critical, it is important to investigate lightweight structural configurations that have large strength reserves after structural buckling.

There is a large body of research which establishes the response and failure behaviour of hybrid (CFRP-GFRP) laminates when subjected to a wide range of destabilising loads [11]–[14]. However, these typically consider only complete plies and do not examine the tailoring of individual ply shapes. There is no works to date which investigate the benefits of combine selective laminate shapes and hybridisation to increase strain to failure and delay plate post-buckling collapse. In addition, most preceding work considers only plate compression and does not consider shear loading of plates which is a critical loading condition for many structures. Thus, this paper aims to examine if a hybrid CFRP-GFRP laminate with selective CFRP laminate shapes may be used to increase strain to failure and delay plate post-buckling collapse. However, it is necessary, that such additional post-buckling reserve is achieved without significantly impacting the load to cause initial plate buckling or to increase the unit mass of the plate (comparing against standard CFRP laminate stacking sequence designs).

To achieve the stated aim and quantify the potential for improved post-buckling reserve, an experimental program will be undertaken to compare a conventional laminate design against a CFRP-GFRP laminate with selective ply shapes. This will identify whether the condition of equivalent or equal initial buckling can be achieved while also achieving an increase in post-buckling reserve. Next, a finite element simulation will be developed to understand the damage mechanisms which occur between initial buckling and collapse. The purpose of the modelling work is to develop further understanding of the internal damage behaviour not visible/captured during the physical testing, and establish a method for future work to optimise the shape of plies and the laminate stacking sequence design. To represent the bi-directional nature of the twill materials employed in the experimental study, a novel constitutive material model from the literature, developed for fabric reinforced composites, is used. This approach is required because the most common material criteria in the simulation literature, for example criteria such as Hashin, which were originally developed for uni-directional polymeric composites, are not appropriate for fabric plies. The fabric ply failure model is necessarily implemented within a built-in VUMAT user subroutine in ABAQUS/Explicit. A single standard specimen will be tested (as there is established

understanding on standard laminate strength and stiffness repeatability), however for the novel laminate design two specimens will be tested to initially understand the repeatability of the novel hybrid laminate behaviour.

2 Literature review

There is a considerable body of literature about buckling and post-buckling behaviour of composite laminate structures. Early investigations on the shear buckling performance of composite panels took place in the early 1980s [11], [15], [16]. Since the late 1980s, most of the literature proposes efficient analytical methods or numerical methods and many works present accompanying validation experiments. Amongst the analytical methods is the work of Loughlan [7], who characterised the buckling behaviour of CFRP plates with an efficient Finite Strip Method (FSM). Fazzolari et al. [17] developed an exact dynamic stiffness theory for composite plate elements, using higher-order shear deformation theory, and studied the buckling behaviour of complex structures modelled as plate assemblies. Zhao et al. [18] used exact strip analysis to study post-buckling behaviour of anisotropic plates under shear loading. In this analysis, the mode shapes were assumed to be the sum of sinusoidal responses with different half-wavelengths, which were coupled together to satisfy the boundary conditions at the longitudinal ends. The resultant predictions demonstrated good agreement with Finite Element Analysis (FEA). Damghani et al. [19], [20] used a smeared method based on exact stiffness analysis derived from analytical solutions of the governing differential equations. Global buckling behaviour of delaminated rectangular composite plates were predicted and found to be in good agreement with FEA predictions. Wu et al. [21] developed a semi-analytical variational approach to perform post-buckling analysis of Variable Angle Tow (VAT) plates under uniform axial compression loading. They demonstrated that VAT laminates outperformed straight fibre laminates. The advantage of analytical, semi-analytical and strip analysis methods is their low computational expense (in comparison to FEA analysis). However, such methods are less appropriate for non-prismatic plate and panel geometries and the representation of progressive material damage, which will be studied herein.

Since the 1990s, combined numerical modelling and experimental studies have for decades enabled a better understanding of buckling and post-buckling behaviour of laminated composite structures. Such works have considered both damaged

(delaminated) and undamaged laminates. For example, Kolanu et al. [22] carried out an experimental and numerical study of a quasi-isotropic CFRP laminate under positive and negative shear loading. The study considered laminate collapse to understand the combined stability behaviour and material failure mechanisms. They used non-contact techniques like digital image correlation (DIC), Air-coupled ultrasonics and infrared thermography (IR) and other in situ damage monitoring techniques like acoustic emission (AE) for better understanding of the structural behaviour and complex damage characteristics of composite laminates. Zhang et al. [23] conducted experiments subjecting stiffened composite panels to shear loading. The study illustrated the potential for good agreement between FEA predictions and well controlled experiments. Reinoso et al. [24] carried out an experimental investigation on buckling and post-buckling behaviour of a stiffened cylindrical composite panel under uniform pressure load. Significantly, the study showed that no damage was developed in the structure up to 3.5 times the first buckling load and collapse only occurred after 4.1 times the design buckling load. Kumar et al. [25], [26] investigated the buckling and post-buckling responses, failure loads and failure characteristics of a simply-supported quasi-isotropic laminate under shear loading and combined in-plane loading. An extensive review of the buckling and post-buckling response of composite laminates is given in [27].

Despite considerable attempts in the literature, such as those mentioned above, the application of post-buckling design with composite structures has been limited, as current industrial analysis tools are not capable of accurately representing the damage mechanisms that lead to structural collapse.

Focusing on the hybridisation of composites, this topic has drawn the attention of many researchers for over four decades, with the objective to create composites possessing high strength, stiffness, toughness and thermal resistance [13]. The advantage of hybridisation on post-buckling performance of thin-walled laminated composite structures was demonstrated by Burgueno et al. [14]. They presented numerical and experimental studies that evaluated the elastic response of thin-walled laminated composite cylindrical shells in their post-buckling regime under axial loading and unloading. Two structural prototypes were considered: (1) a carbon/epoxy cylindrical shell and (2) a hybrid carbon/E-glass/epoxy cylindrical shell with various carbon ply shapes. The study illustrates the well-known challenges of predicting and

controlling cylindrical shell buckling and post-buckling response because of their high sensitivity to imperfections. Interestingly, the study demonstrates that by hybridising the cylindrical shell, the structure was able to withstand a load 1.26 times greater than the buckling load. Kubiak et al. [12] studied experimental and numerical post-buckling behaviour of thin-walled channel columns. The columns were made as a hybrid of Fibre Metal Laminate (FML) and GFRP. The failure loads of the hybrid columns were two times that of the GFRP columns. Al-Azzawi et al. [28], [29] established the potential for good agreement between numerical predictions of the instability behaviour of hybrid FML-Glare laminates and experimental tests. Petkune et al. [30] used hybridisation of shear walls in civil engineering, revealing that a hybrid of carbon and glass were superior to pure steel under repeated shear loading in terms of load bearing capacity, energy absorption and dynamic stiffness degradation. In fact, in civil engineering, X-braced frames are an alternative to shear walls, capable of stabilising structures under seismic loading, but having low cost, low weight, and quickness in construction. Although there has been limited work on the post-buckling behaviour of hybridized composite laminates there has been considerable work in other structural topics and the reader is referred to [31] for a comprehensive review of hybrid composites.

In summary, it is evident from the literature that composite laminates have considerable strength reserve after buckling. However, this strength reserve is not used in aircraft design due to limited understanding, a lack of robust and rapid prediction methods for composite damage mechanisms after buckling, loading complexity, and aerodynamic considerations for some zones of the aircraft. Additionally, the success of any developed understanding, analysis/design methodology and the potential of post-buckling composite structures will have applications for the next generation of lightweight aerospace structures.

Despite the developed knowledge on the buckling and post-buckling behaviour of composite laminates, there is very limited work on the damage mechanisms of hybrid CFRP-GFRP woven fabric composite laminates designed for optimal weight under in-plane shear loading. In particular, for such loading, there are very few combined experimental studies and numerical works which fully characterise hybrid laminate post-buckling damage behaviour. Hence, this paper presents a combined experimental and numerical simulation study. A conventional laminate and a novel

CFRP-GFRP laminate with selective laminate shapes will be designed and tested. Buckling, post-buckling and collapse behaviour will be experimentally captured and simulation will further examine the different design post-buckling damage behaviours. This will identify whether the condition of equivalent or equal initial buckling can be achieved while also achieving an increase in post-buckling reserve, and how damage in the post-buckling regime influences this performance.

Based on the literature review the remaining paper content is arranged as follows: Section 3 introduces the design of the novel CFRP-GFRP laminate with selective laminate shapes, and an appropriate baseline laminate design. Section 4 presents the Finite Element modelling approach which will be used to understand the differences in post-buckling damage mechanisms between the conventional and novel laminate designs. The experimental procedure for material characterisation and the laminate post-buckling testing is presented in section 5. Finally, results and discussions are given in section 6 and conclusions are made in section 7.

3 Laminate design

In civil engineering applications, X-bracing of steel frame structures has long been used to withstand the shear loads resulting from either seismic activities or lateral wind forces [32]. On the other hand, the current industrial practice makes use of hybrid CFRP-GFRP laminates in aircraft wing construction, e.g. AIRBUS A350-XWB. From this perspective, 1 to 2 GFRP plies are placed on the outer mould surfaces of a purely CFRP laminate wing skin where these plies act as a protective layer for the CFRP laminates against accidental impact. However, as the primary purpose of these additional plies is to reduce damage from impact, the load bearing capacity of the GFRP plies is typically ignored, thus adding extra weight to the structure [33]. Hence, in this study, the concept of X-bracing for a hybrid CFRP-GFRP laminate subjected to pure shear loading is explored.

Two structural configurations are considered. In the first configuration (type 1), the entire laminate is made of woven twill CFRP with a stacking sequence of $\left[\pm 45/\pm 45/0/0\right]_S$. This is the benchmark laminate in which all CFRP plies have a square shape of $200\,mm \times 200\,mm$. The second configuration (type 2) is a hybrid laminate in which woven twill GFRP plies are placed at the outer and inner mould surfaces. This is to ensure that the hybrid laminate of study mimics a civil aircraft wing

laminate. In this hybrid laminate design both the GFRP and CFRP plies of 0^o angle have a square shape with size $200\,mm \times 200\,mm$. However, the CFRP plies at angle 45^o have a X shape, as shown in Figure 1. Thus, the stacking sequence for the type 2 laminate is $\left[45G/\pm 45_X/\pm 45_X/0/0\right]_S$. The X shape is chosen to not only provide stiffness for shear loading but also reduce some mass to compensate for the addition of the GFRP plies, compared to benchmark type 1. In order to establish an appropriate width of the X-bracing, a parametric study is initially carried out to complete the design. By changing the width (W) of the X-bracing, Figure 1, and finding the minimum W which gives an equal or higher buckling load (both under pure shear and axial load) compared to the benchmark laminate (type 1) will finalise the laminate design.

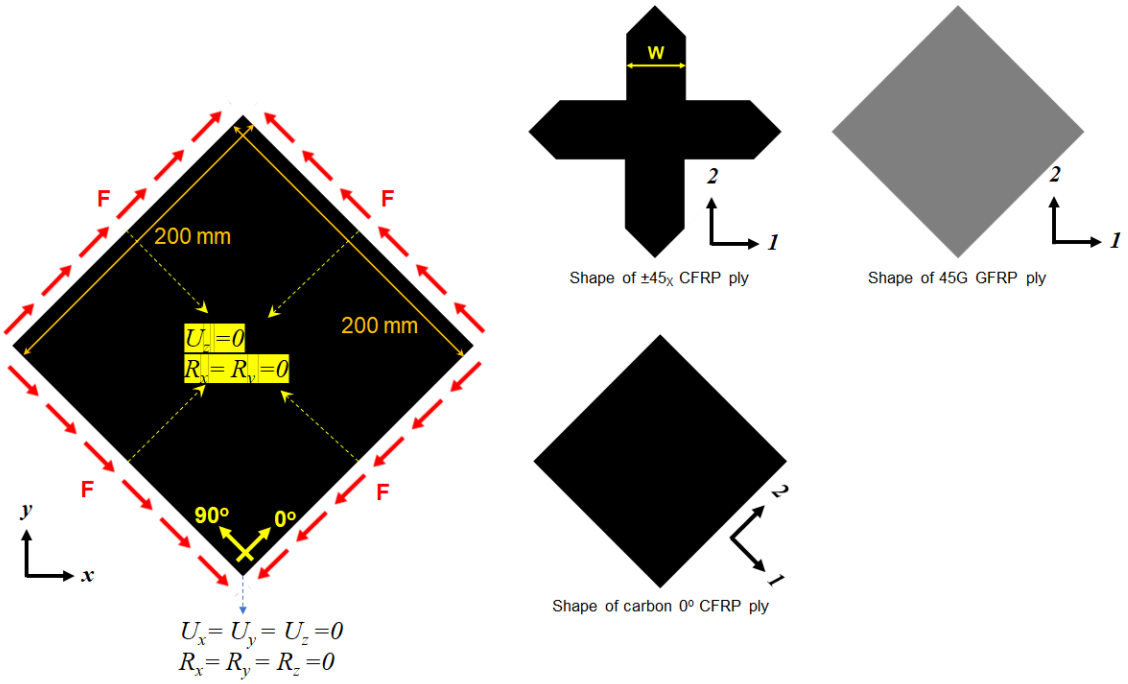

Figure 1: Loading (shear edge load in N/mm), boundary conditions and ply shapes of the laminates

The parametric study was carried out using ABAQUS software and linear eigenvalue analysis. S4R quadrilateral elements with reduced integration were used to model the laminate. Three integration points through the thickness were chosen for each ply. As shown in Figure 1, all edges of the laminates are constrained to displace in z direction and rotate about x and y axes. Multipoint constraints were incorporated on all four edges to ascertain they remain straight throughout the loading process [34]. Displacement and rotation of the node at the bottom of the laminate is constrained in all directions. The mesh used for the study is depicted in Figure 2a. As stated, the

objective was to match the buckling load of the hybrid laminate with the buckling load of the baseline laminate (type 1), whilst minimising mass. Figure 2 presents the simulation study results, with the non-dimensional buckling load plotted against the mass. Examining both the shear loading (Figure 2b) and compression loading (Figure 2c) it can be seen that a bracing width of $60\ mm$ yields slightly superior shear and axial buckling load of 1.05 and 1.12 times higher than type 1 laminate, respectively, and obviously with less mass compared to a width of $70\ mm$. Therefore, $W = 60\ mm$ is chosen to complete the hybrid laminate (type 2) design, which, together with the baseline laminate (type 1), will be manufactured, experimentally tested and its post-buckling behaviour modelled.

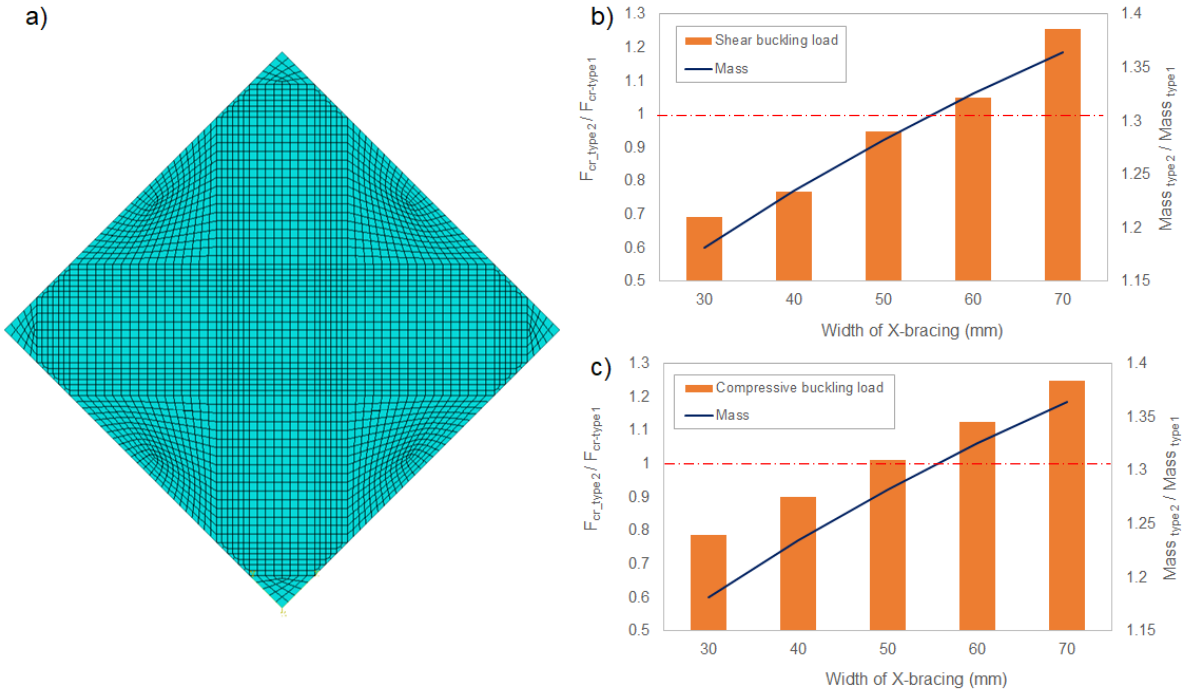

Figure 2: Meshing and critical buckling load of laminates; a) Mesh density; Ratios of buckling load of type 2 / buckling load of type 1 and mass of type 2 / mass of type 1 vs width of X-bracing subjected to b) shear loading only and c) axial compressive loading

4 Numerical analysis

4.1 Material model

The bi-directional nature of the twill materials employed in the study means that common conventional material failure criteria such as Hashin, which were originally developed for uni-directional polymeric composites, are not appropriate. Thus, a constitutive material model from the literature, developed for fabric reinforced composites, is used. The fabric ply failure model is necessarily implemented within a built-in VUMAT user subroutine in ABAQUS/Explicit.

Within the selected model, the fabric-reinforced ply is represented as a homogenous orthotropic elastic material, with the potential to sustain progressive stiffness degradation because of fibre and matrix cracking and plastic deformation under shear loading. Thus, it is assumed that there are two main failure mechanisms: fibre dominated failure in tension or compression in the two fibre directions; and matrix dominated failure in in-plane shear. The mechanisms of failure are discussed hereafter and further detailed in [35]. Furthermore, a summary of damage parameters used in this study are provided in the Appendix.

4.1.1 Elastic stress-strain relationship

The elastic stress-strain relations are given by orthotropic damaged elasticity. The relation is formulated in a local coordinate system aligned with the fibre direction as follows;

$$\begin{bmatrix} \varepsilon_{11} \\ \varepsilon_{22} \\ \varepsilon_{12}^{el} \end{bmatrix} = \begin{bmatrix} \frac{1}{(1-d_1)E_1} & \frac{-\upsilon_{12}}{E_1} & 0 \\ \frac{-\upsilon_{21}}{E_2} & \frac{1}{(1-d_2)E_2} & 0 \\ 0 & 0 & \frac{1}{(1-d_{12})2G_{12}} \end{bmatrix} \begin{bmatrix} \sigma_{11} \\ \sigma_{22} \\ \sigma_{12} \end{bmatrix} \quad (1)$$

where E_1 and E_2 are Young's moduli in the principal orthotropic directions, G_{12} is the in-plane shear modulus, and υ_{12} is the principal Poisson's ratio. Three scalar damage variables are used: d_1 $(0 \le d_1 \le 1)$ and d_2 $(0 \le d_2 \le 1)$ are associated to fibre fracture along the ply 1 and 2 directions, respectively; and d_{12} $(0 \le d_{12} \le 1)$ is related to matrix micro-cracking due to shear deformation. It is worth noting that fibre fracture damage variables consider the tensile and compressive fibre failure modes based on the stress state in the fibre direction.

4.1.2 Fibre response

The material response along the fibre directions is characterised with damage elasticity. It is assumed that the fibre damage variables are a function of the corresponding effective stresses as

$$
\begin{aligned}
d_{1+} &= d_{1+}\left(\overline{\sigma_{1+}}\right) \\
d_{1-} &= d_{1-}\left(\overline{\sigma_{1-}}\right) \\
d_{2+} &= d_{2+}\left(\overline{\sigma_{2+}}\right) \\
d_{2-} &= d_{2-}\left(\overline{\sigma_{2-}}\right)
\end{aligned}
\tag{2}
$$

where d_{1+}, d_{1-}, d_{2+} and d_{2-} are the tensile and compressive damages along the fibre in the ply directions 1 and 2, respectively. Effective stresses are updated stress states after damage initiation and are defined as

$$
\begin{aligned}
\overline{\sigma_{1+}} &= \frac{\sigma_{11}}{1-d_{1+}} \\
\overline{\sigma_{1-}} &= \frac{-\sigma_{11}}{1-d_{1-}} \\
\overline{\sigma_{2+}} &= \frac{\sigma_{22}}{1-d_{2+}} \\
\overline{\sigma_{2-}} &= \frac{-\sigma_{22}}{1-d_{2-}}
\end{aligned}
\tag{3}
$$

At any given time throughout the analysis, the elastic domain is defined in terms of the damage activation functions, F_i, as

$$
\begin{aligned}
F_i &= \phi_i - r_i \le 0 \\
\phi_i &= \frac{\overline{\sigma_i}}{X_i}; \left(i = 1+, 1-, 2+, 2-\right)
\end{aligned}
\tag{4}
$$

where X_i are the tensile (+) and compressive (-) strength for uniaxial loading along the fibre directions 1 and 2. The damage thresholds (r_i) are initially set to one. After damage activation ($\phi_i = 1$), the damage thresholds at any given time (t) increase based on

$$
r_i\left(t\right) = \max \phi_i\left(t^*\right); t^* \le t \tag{5}
$$

Thus, the model assumes that the ply material is non-healing. Therefore, on unloading, after damage, the damage parameters remain constant until a higher damaging load is re-applied. The evolution of damage variables are a function of the damage thresholds (r_i), the elastic energy density per unit volume at the point of

damage initiation (g_0^i), the fracture energy per unit area under uniaxial tensile/compressive loading (G_f^i) and the characteristic length of the FE mesh element (L_c). The damage variables are formulated as

$$d_i = 1 - \frac{1}{r_i} e^{\left(-\frac{2 g_0^i L_c}{G_f^i - g_0^i L_c} (r_i - 1) \right)} \tag{6}$$

The elastic energy density per unit volume at the point of damage initiation is given as

$$g_0^i = \frac{X_i^2}{2E_i} \tag{7}$$

In the current study, both carbon and glass fibres are assumed to behave in a brittle manner. Furthermore, $G_f^i \approx L_{\max} g_0^i$ where $L_{\max}$ is the maximum element length to avoid over prediction of energy dissipation. The reader may refer to [35] for further details.

4.1.3 Shear response

It is assumed that shear behaviour and the mechanism of ply in-plane shear degradation are mainly controlled by the resin [36]. Thus, in the adopted material model, fibre and shear damage modes are decoupled. The shear response is dominated by the nonlinear behaviour of the matrix, which may be inelastic and/or irreversible due to the presence of extensive matrix cracking or plasticity. On unloading, this can lead to permanent deformations in the ply. Various components of matrix elasticity, plasticity and evolution of damage are consequently modelled, each is described hereafter.

4.1.3.1 Elasticity

The elastic response of the matrix relates the effective stress to the elastic strain, as follows

$$\overline{\sigma_{12}} = \frac{\sigma_{12}}{1 - d_{12}} = 2G_{12}\varepsilon_{12}^{el} = 2G_{12}\left(\varepsilon_{12} - \varepsilon_{12}^{pl}\right) \tag{8}$$

where ε_{12}^{el} and ε_{12}^{pl} are elastic and plastic strains, respectively. It is worth noting that plasticity is only associated with the matrix and therefore, fibre plasticity is zero, i.e. $\varepsilon_{11}^{pl} = \varepsilon_{22}^{pl} = 0$.

4.1.3.2 Plasticity

An elastic domain function, otherwise known as a yield function, is introduced (F) that assumes only the effective shear stresses lead to plastic deformation, thus

$$F = \left|\overline{\sigma_{12}}\right| - R\left(\varepsilon^{pl}\right) \tag{9}$$

where $R\left(\varepsilon^{pl}\right)$ is an isotropic hardening function following a power rule, given as

$$R\left(\varepsilon^{pl}\right) = \overline{\sigma_{y0}} + C\left(\varepsilon^{pl}\right)^{p} \tag{10}$$

where $\overline{\sigma_{y0}}$ is the initial effective shear yield stress and C and p are coefficient and power terms in the hardening equation, respectively. It should be noted that the condition of $F < 0$ corresponds to stress states inside the elastic domain where the material undergoes elastic damage. Whereas $F = 0$ describes the plastic deformations. The evolution of the plastic work during yielding ($\dot{U}^{pl}$) is given as a function of the evolution of the plastic strain ($\dot{\varepsilon}_{12}^{pl}$), the shear damage parameter (d_{12}) and the effective shear stresses ($\overline{\sigma_{12}}$), as

$$\dot{U}^{pl} = 2\sigma_{12}\dot{\varepsilon}_{12}^{pl} = 2\left(1 - d_{12}\right)\overline{\sigma_{12}}\dot{\varepsilon}_{12}^{pl} \tag{11}$$

4.1.3.3 Damage

The elastic domain is defined in terms of the damage activation function (F_{12}) as

$$\begin{aligned} F_{12} &= \phi_{12} - r_{12} \le 0 \\ \phi_{12} &= \frac{\overline{\sigma_{12}}}{S} \end{aligned} \tag{12}$$

The function ϕ_{12} is the criteria for initiation of shear damage of the matrix and S is the shear strength of the ply. Damage thresholds (r_{12}) are initially set to one. After damage activation ($\phi_i = 1$), the damage thresholds at any given time (t) increase based on

$$r_{12}(t) = \max \phi_{12}(t^*); t^* \le t \tag{13}$$

It is assumed that the shear damage variable increases as a logarithm of r_{12} until a maximum value of $d_{12}^{\max}$ is reached. Thus

$$d_{12} = \min\left(\alpha_{12} \operatorname{Ln}(r_{12}), d_{12}^{\max}\right) \tag{14}$$

where $\alpha_{12} > 0$ and $d_{12}^{\max} \le 1$ are defined material properties.

4.2 Buckling and post-buckling analysis

In order to predict buckling, post-buckling behaviour and unstable collapse, eigenvalue buckling and explicit analysis were used. Initially, an eigenvalue buckling analysis is performed. The subspace method is used to extract the eigenvalues of the composite laminates, as the extraction of the eigenvalues in reduced space speeds convergence to the eigenvectors in full space. For the post-buckling prediction, geometric imperfections (typically less than 10% the thickness of laminates) are introduced to the model to trigger the unstable response within the explicit analysis. An initial qualitative comparison of the experimental buckling mode shapes and the eigenvalue mode shapes was undertaken (for both laminate types 1 and 2) to select the imperfections to be modelled. It was followed by a sensitivity study to select the imperfection magnitude.

Figure 3a shows that the type 1 laminate experimental out of plane deflections are symmetric about the centre line of the specimen and similar to the first numerical eigenvalue mode of the laminate, Figure 3b. Therefore, 10% of the laminate thickness times eigenvalue mode 1 is chosen as initial geometric imperfection after a series of imperfection sensitivity studies in which the minimum magnitude was identified which would produce the desired experimental mode shape. Similarly, close inspection of the experimental out of plane displacement for the type 2 laminate (see Figure 4a) shows that the displacements are un-symmetric with respect to the centre line of the specimen, and the mode shape has a larger wavelength on the left-hand side than the right-hand side of the geometric centreline. The sensitivity study identified that 8% laminate thickness of eigenvalue mode 2 (see Figure 4b) and 2% laminate thickness of eigenvalue mode 1 (see Figure 4c) was appropriate to recreate the experimental imperfection (see next Section).

Along with the initial imperfections, the material failure law, as defined in section 4.1, is used within each post-buckling analysis. Three integration points are considered for each ply for the calculation of stresses, strains and damage parameters. Elements are deleted when the damage parameter at all section points exceeds unity. For accuracy and efficiency, a quasi-static analysis was performed by applying the shear load using the ABAQUS/Explicit built-in load amplitude function called SMOOTH STEP. This uses a fifth order polynomial function to apply the load and eliminate significant energy changes at the start and end of loading. Additionally, mass scaling is employed to reduce the solution time without increasing the loading rate.

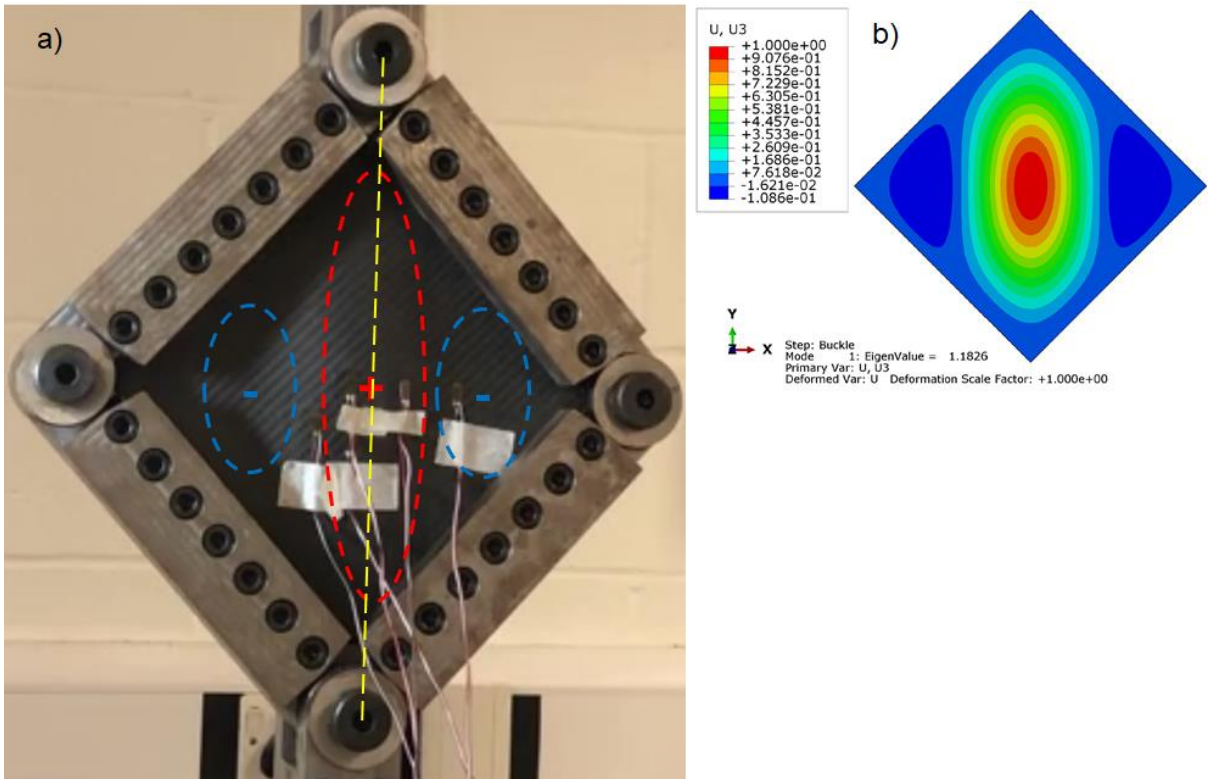

Figure 3: Qualitative comparison of experimental and numerical mode shapes for type 1 laminates; a) experimental mode shape, b) first mode shape (eigenvalue of 1.18) for applied shear load of $F = 100\ N/mm$

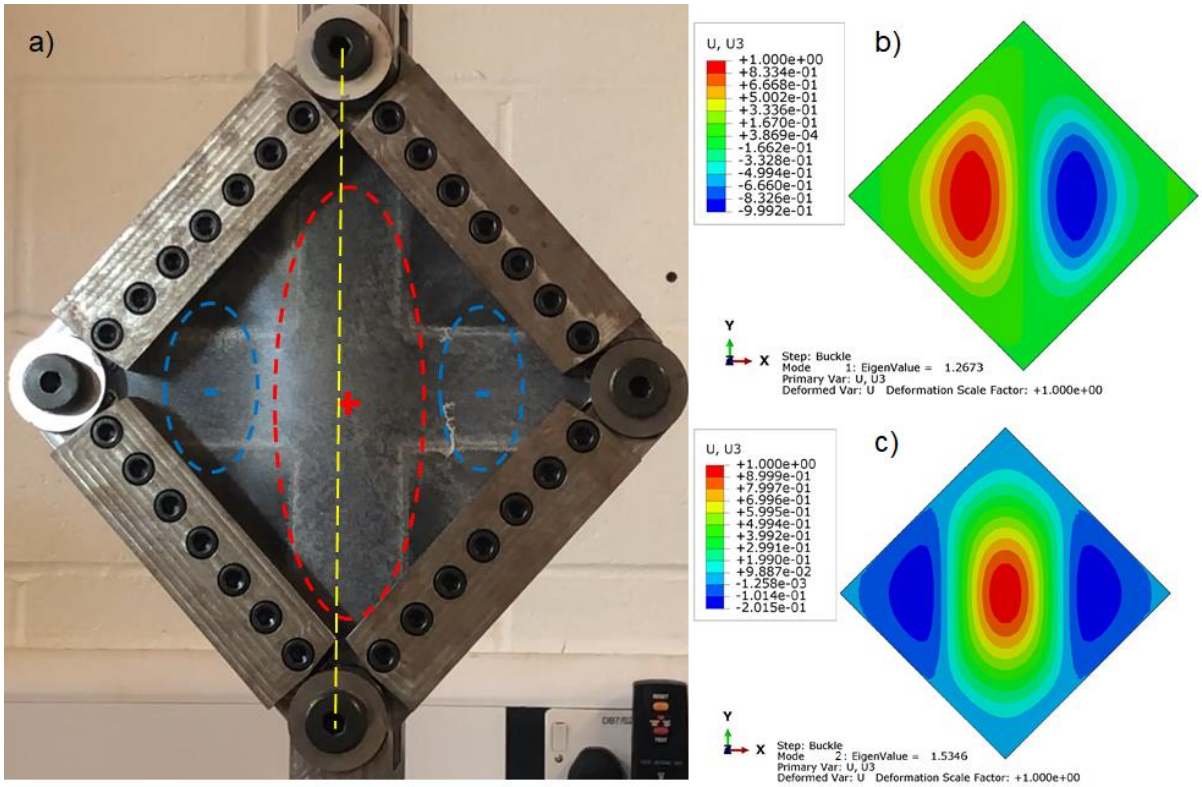

Figure 4: Qualitative comparison of experimental and numerical mode shapes for type 2 laminates; a) experimental mode shape, b) first mode shape (eigenvalue of 1.26) and c) second mode shape (eigenvalue of 1.53) for applied shear load of $F = 100\ N/mm$

5 Materials and experimental methods

5.1 Composite material and manufacture

The materials used in this study are twill woven pre-impregnated carbon fibre (AX-5180), and a twill woven pre-impregnated glass fibre (AX-3180) with mechanical properties given in Table 1. It is worth noting that in the absence of manufacturer's data, the mechanical properties have been obtained by the authors as detailed in the next section. Both carbon and glass prepregs consist of 54% fibre by volume (60% by weight) and have compatible resin contents enabling simultaneous hot press curing. Three laminates of each laminate type were initially hand laid to form a plate and cured in a heated press for an hour at 120^{O} Celsius under 1 bar pressure. The specimens were then abrasively cut to $200\ mm \times 200\ mm$.

Table 1: Mechanical properties of both woven CFRP (AX-5180) and GFRP (AX-3180) fabric plies

Mechanical properties	Units	AX-5180 CFRP	AX-3180 GFRP
$E_{11}=E_{22}$	MPa	67094.00	30083.00
G_{12}	MPa	4831.38	4954.60
S_t^*	MPa	595.50	437.16
S_c	MPa	393.00	306.00
S_s	MPa	87.00	62.00

Strain to failure	Strain	0.01	0.02
ϑ_{12} (Poisson's ratio)	N/A	0.04	0.14
t_{ply}^{**}	mm	0.224	0.288

* t, c and s subscripts denote the strength of ply in tensions, compression and shear respectively.
** cured ply thickness

5.2 Shear test

All testing was performed using a $100\ kN$ capacity INSTRON tensile machine and a picture frame test fixture. The laminate specimen is first clamped into the test fixture. On each edge the specimen is clamped via grip plates of width $10\ mm$, providing gauge dimensions of $180\ mm \times 180\ mm$. The specimen is held in position and loaded by constant static friction set initially by the clamping force of the bolts (which are set to a specific torque). The specimen and test fixture are located in the tensile machine, and a tensile load is applied under displacement control at a speed of 2 mm/min to the test fixture, as shown in Figure 5. This, in turn, induces a shear force on the test laminate. In addition, the test device is designed to ensure that the panel is under pure shear along the loading line.

To acquire strain data, the conventional laminate specimen and one of the novel laminate specimens were instrumented with six uniaxial Vishay strain-gauges (see Figure 5b). The locations of the strain gauges were determined based on the laminate eigenvalue simulations, with the areas of a high strain selected for gauging. Therefore, strain gauge 3 is positioned at the centre of the panel with strain gauge 6 on the opposite side to capture the effect of central laminate out of plane bending. All strain gauges measure strain in the y-direction (Figure 1), in the direction parallel to the applied tensile loading. Detailed positioning and spacing of each strain gauge and their numbering are given in Figure 5b.

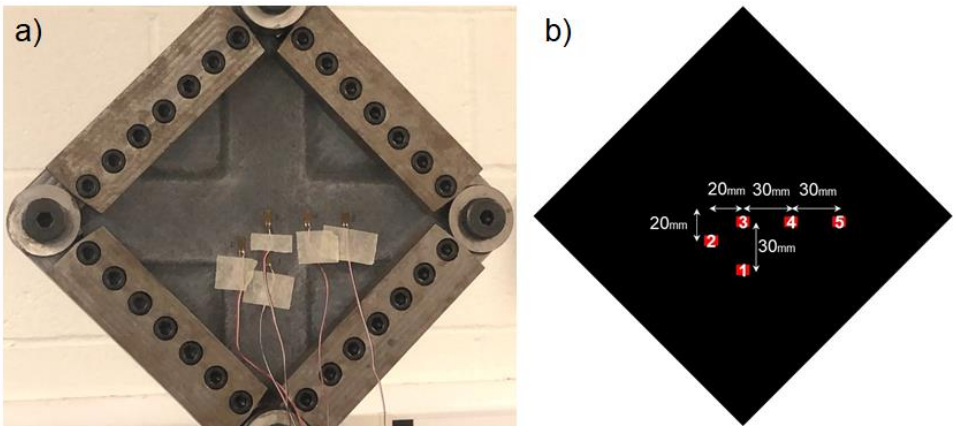

Figure 5: Shear test set-up; a) gauged type 2 and b) location of strain gauges and their numbering (strain gauge 6 is on the back of the laminate opposite to strain gauge 3)

5.3 Determination of fabric ply material model

In the absence of mechanical property data in the literature for the studied materials, and to find the material parameters for the material model proposed in section 4, a series of tensile and cyclic shear tests were performed. Incorporation of such data is expected to benefit future researchers in the field.

5.3.1 Tensile tests along the fibre

The parameters of the elastic damage model were derived from standard coupon tests under uniaxial tension/compression loading of $0/90$ laminates as summarised in Table 1. The compressive mechanical properties were estimated using data available in the literature [37]. The shear modulus values G_{12} were obtained from uniaxial tensile tests on ± 45 laminates, by calculating the Young' modulus (E_{45}) and using the equation [38]

$$\frac{1}{G_{12}} = \frac{4}{E_{45}} - \frac{1}{E_1} - \frac{1}{E_2} + 2\frac{\upsilon_{12}}{E_1} \tag{15}$$

The calibration of damage evolution in the fibre failure mode was not possible due to specimen abrupt and brittle failure for both the AX-5180 CFRP and the AX-3180 GFRP tests. Therefore, it can be assumed that $G_f^{\alpha} \approx 0$. However, for the stability of the post-buckling numerical model, the value of $G_f^{\alpha} = L_c g_0^{\alpha}$ will be used.

5.3.2 Cyclic shear tests

As a result of permanent plastic deformations, cyclic load, i.e. loading and unloading, an experimental test is required to characterise the shear response of both fabric materials. A typical idealised representation of a fabric laminate shear response is shown in Figure 6a. In order to obtain the damage parameters noted in Figure 6a, a tensile material specimen made of only angle plies, i.e. $\pm 45^o$, is tested. By testing such a material specimen, the strains along the fibre directions can be neglected. The resulting tensile test data is used to obtain the shear stresses and strains as below

$$\begin{aligned} \sigma_{12} &= \frac{\sigma_y}{2} = \frac{P}{2wt} \\ \varepsilon_{12} &= 0.5\left(1+\upsilon_{xy}\right)\varepsilon_y \end{aligned} \tag{16}$$

where P is the experimental tensile load, w and t are the laminate specimen width and thickness, respectively. ε_y is the experimental axial strain and υ_{xy} is the total homogenised Poisson's ratio of the cross-ply laminate (≈ 0.76 for carbon and 0.5 for glass laminates).

The calculated values of shear stresses against shear strains are plotted in Figure 6b-c for both CFRP and GFRP. The level of damage is measured from the ratio of unloading stiffness to the initial undamaged elastic stiffness. This allows the identification of a pair of (σ_{12}, d_{12}), for the unloading curve. This data is presented in terms of d_{12} and $\mathrm{Ln}\left(\overline{\sigma_{12}}\right)$ where $\overline{\sigma_{12}} = \sigma_{12} / (1 - d_{12})$. The linear fit of data then provides the parameters α_{12} and S. The schematic representation of this process is shown in Figure 7a. The experimental test results with all calculated damage parameters are shown in Figure 7b-c. Comparing the experimentally derived curves, it is clear that the GFRP plies are capable of sustaining more damage than the CFRP plies.

Finally, the plastic hardening function requires the calculation of the accumulated plastic strain. From the cyclic test data, it is possible to obtain a pair of $\left(\varepsilon_{12}^{pl}, \overline{\sigma_{12}}\right)$ to plot each hardening curve. The schematic representation of the hardening curve is illustrated in Figure 8a, and the experimentally determined hardening curves for CFRP and GFRP fabrics are shown in Figure 8b-c.

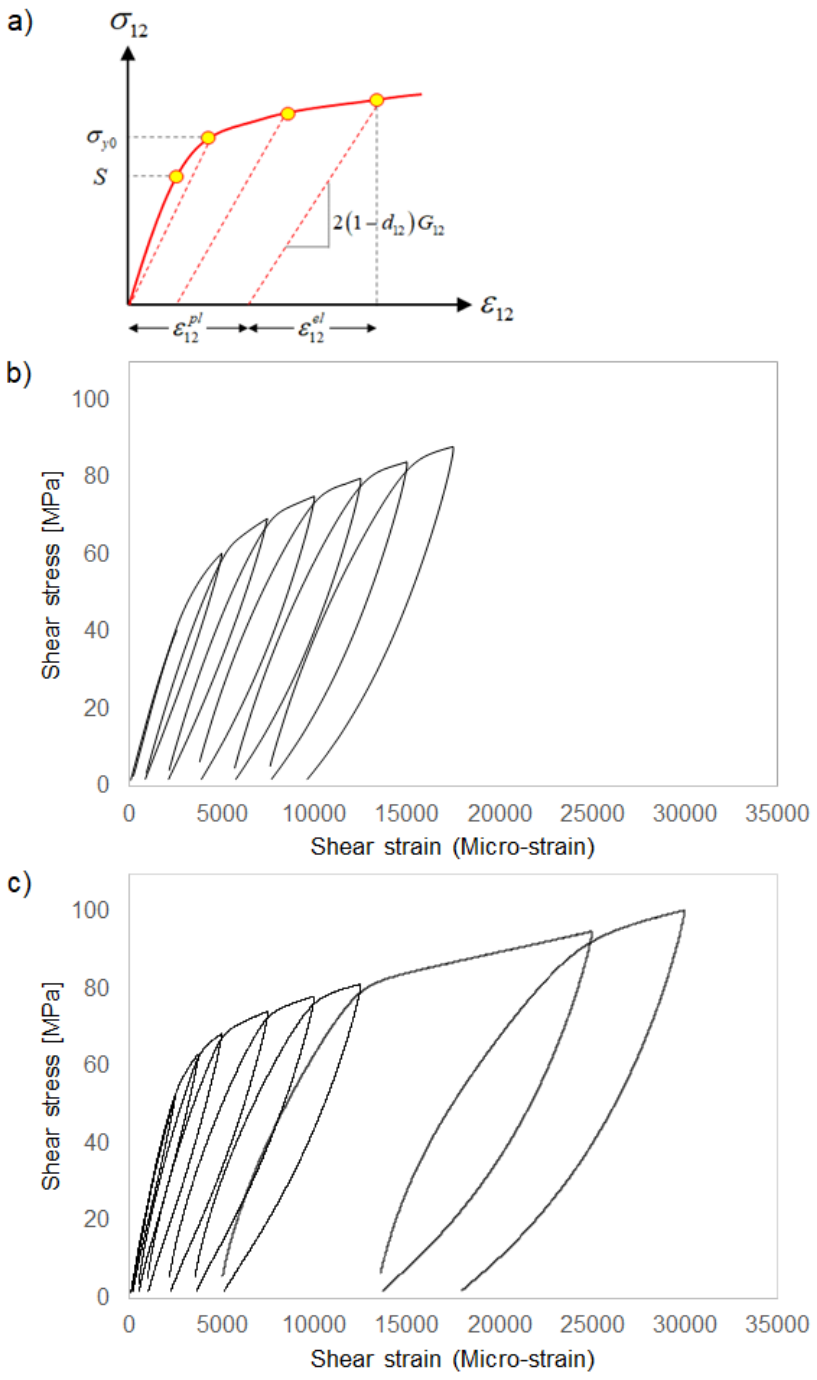

Figure 6: Shear response of a fabric reinforced composite. S is shear stress at the onset of damage and σ_{y0} is initial shear yield stress; a) schematic representation, b) experimental cyclic shear stress-strain for CFRP AX-5180 and c) experimental cyclic shear stress-strain for GFRP AX-3180.

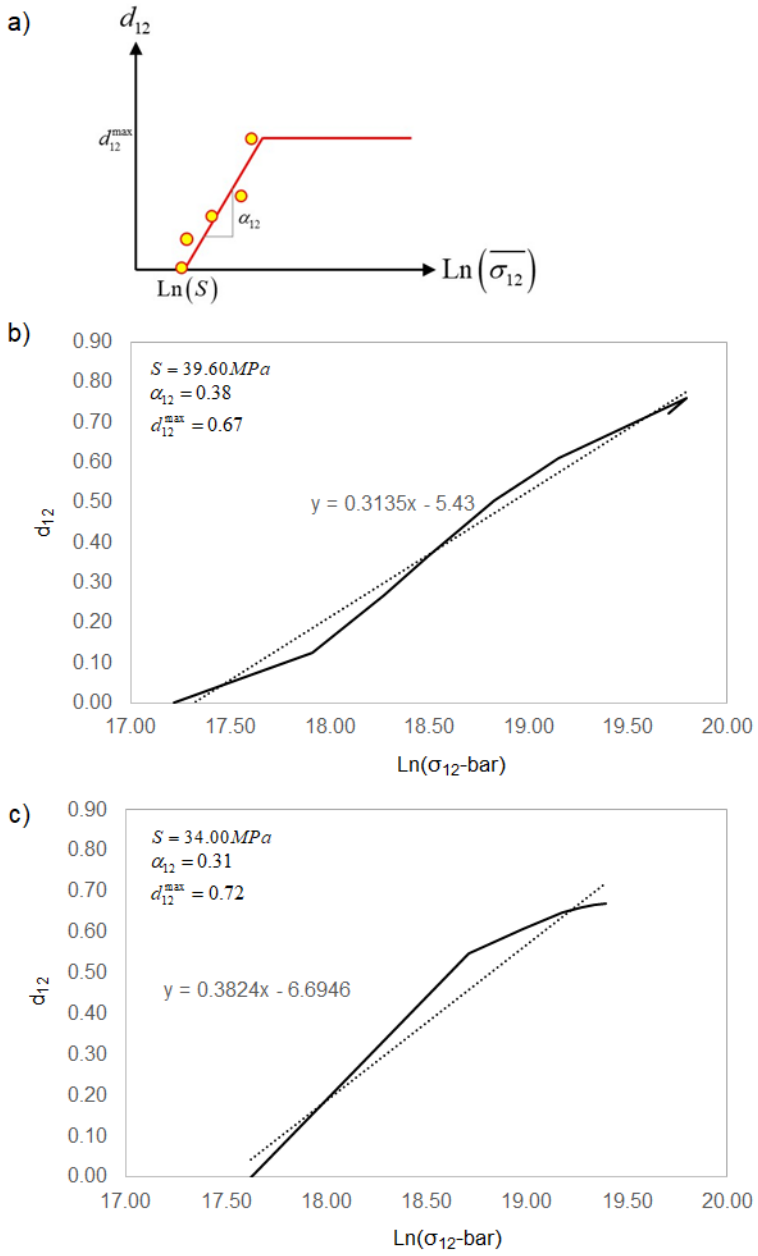

Figure 7: Shear damage parameters α_{12} and S ; a) schematic representation, b) experimental shear damage parameters for CFRP AX-5180 and c) experimental shear damage parameters for GFRP AX-3180

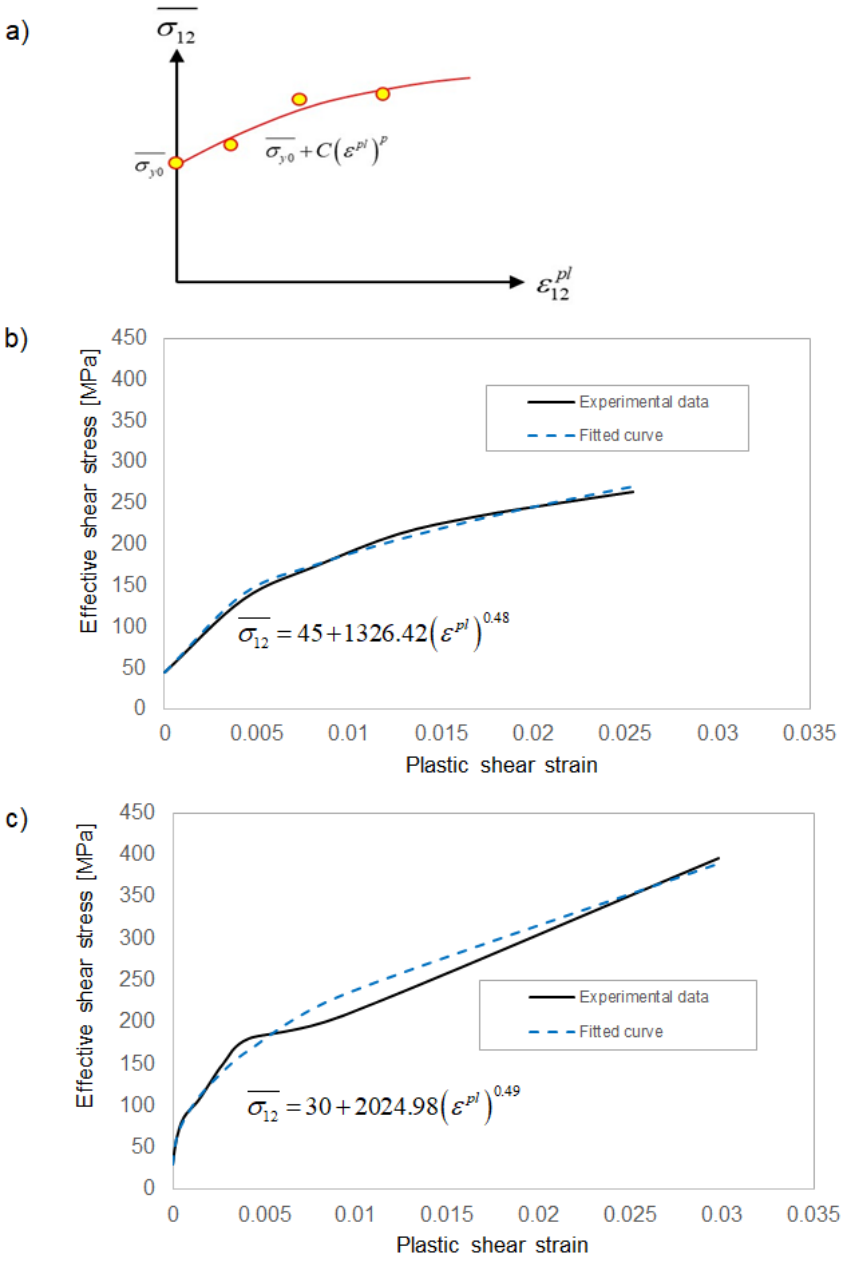

Figure 8: Shear hardening curve; a) schematic representation, b) experimental curve for CFRP AX-5180 and c) experimental curve for GFRP AX-3180.

6 Buckling/post-buckling results and discussions

Figure 9a demonstrates the theoretical plate buckling and post-buckling response for a composite laminate material. The behaviour is quite different from that of a homogenous isotropic material, due to the potential existence of specific composite laminate failure modes, i.e. delamination, fibre cracking, fibre debonding etc. In the theoretical illustration, the laminated composite deforms almost linearly up to the bifurcation point B. The bifurcation point corresponds to initial plate buckling and will lead to a collapse at A. However, the global buckling may be preceded or associated

with local buckling modes of delaminated sub-laminates, denoted by the point D. Additionally, the load path may be limited by material failure resulting from increasing deformations. Finally, the existence of geometric imperfections will influence each load path and the position of each point, i.e. A, B and D [27].

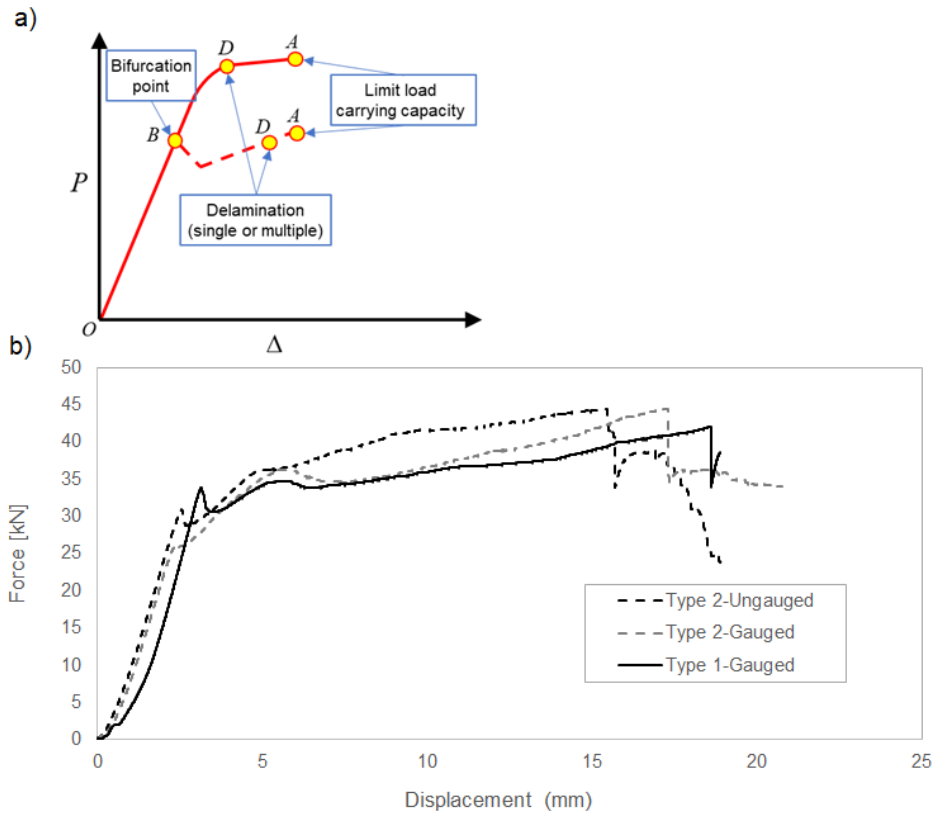

Figure 9: Buckling and post-buckling load-displacement curves for laminated composites; a) schematic representation for perfect structure (solid line) and structure with shape imperfections (dashed line), b) for type 1 and type 2 laminates of study under pure in-plane shear loading

The experimental load-displacement curves for the single conventional (type 1) and two novel (type 2) specimens are illustrated in Figure 9b. The measured load represents the tensile force applied to the test fixture, and the displacement is the resulting deflection at the loaded end of the test fixture. As expected, both laminate types, follow a linear equilibrium path up to the bifurcation point. The slopes of the linear portion of each curve (between 10-20kN) indicate specimen stiffnesses of $9.14\ kN/mm$ and $14.36\ kN/mm$ for type 1 and 2, respectively. For both laminate types, the applied shear force decreases immediately after buckling as a result of laminate out of plane bending. However, the force continues to increase up to the point of final collapse.

Table 2 summarises the experimental and numerical buckling and failure loads of both laminate configurations. It is worth noting that numerical strain values are extracted for elements and integration points associated to the location of strain gauges in the experiment. Both type 2 laminates exhibit a higher load bearing capacity than the type 1 laminate. The average failure load for the type 2 laminates was $43.94\ kN$, whereas the failure load for the gauged type 1 laminate was $41.8\ kN$. The average buckling load for the type 2 laminates was $27.9\ kN$, whereas the buckling load for the gauged type 1 laminate was $32.00\ kN$. Therefore, the hybrid X-braced laminate design (type 2) may have a marginally higher failure performance but a slightly lower buckling performance. The panels develop an approximate load carrying capacity of 1.3 and 1.6 times the critical buckling load for type 1 and type 2 laminates, respectively. This behaviour is similar to that of incomplete diagonal tension field panels for isotropic materials [5] in which the web of such beams retain, after buckling, some of their ability to support loads so that even near failure they are in a state of stress somewhere between that of pure diagonal tension and the pre-buckling stress. This underpins the importance of considering post-buckling behaviour for a lightweight design.

Table 2: Experimental and numerical buckling load

Laminate type	Number of specimens	Failure load (kN)	Average failure load (kN)	Numerical failure load (kN)	Experimental buckling load (kN)	Average experimental buckling load (kN)	Numerical buckling load (kN)
Type 1-Gauged	1	41.68	-	40.63	32.00	-	33.37
Type 2-Ungauged	1	44.30	43.94	46.45	29.80	27.90	35.84
Type 2-Gauged	1	43.58			26.00		

For a detailed analysis of the experimental post-buckling strain to failure, the measured strain gauge data is examined. Figure 10 presents strain gauge data for six locations (type 1 data in Figure 10a, type 2 data in Figure 10b). The numerical simulation results at extreme fibres are also shown on the figure as dashed lines. Based on the figures, the type 2 laminate endures greater strains than the type 1 laminate, due to the use of high strain to failure glass plies. For instance, as shown in Figure 11, strain gauge 3 on the type 2 laminate records a maximum strain of 7671 micro-strain, compared to a maximum of 5507 micro-strain for the type 1 laminate. This is a 40% higher failure strain. This demonstrates an improved strain to failure

response for the hybrid laminate over the pure CFRP laminate design. For both laminate types, there is good agreement between the numerical and experimental results up to the bifurcation point.

The prediction of failure load is in excellent agreement between the numerical and experimental results. It is observed that the predicted strain in the post-buckling region, at the strain gauge 4 location, shows a divergence from the measured strain results. This is due to the inability of the numerical model to capture the mode shape at failure fully. In the simulation, for the type 2 laminates, at the point close to collapse, the deflected shape tends to transit to the mode 1 shape with two lateral half wavelengths in the direction perpendicular to the loading direction (see Figure 4) which is not the case in the experiments. In fact, the change in the mode shape is not observed in the experiment. It is worth noting that consideration of a perturbed geometry (instead of the ideal perfect geometry) in the numerical model significantly contributes to a smoothing of the transition between the initial linear behaviour and the nonlinear post-buckling behaviour. In addition, it also smooths the transition between modes in the post-buckling regime, thus decreasing the severity of any convergence difficulties. This is in agreement with results obtained in [39], [40].

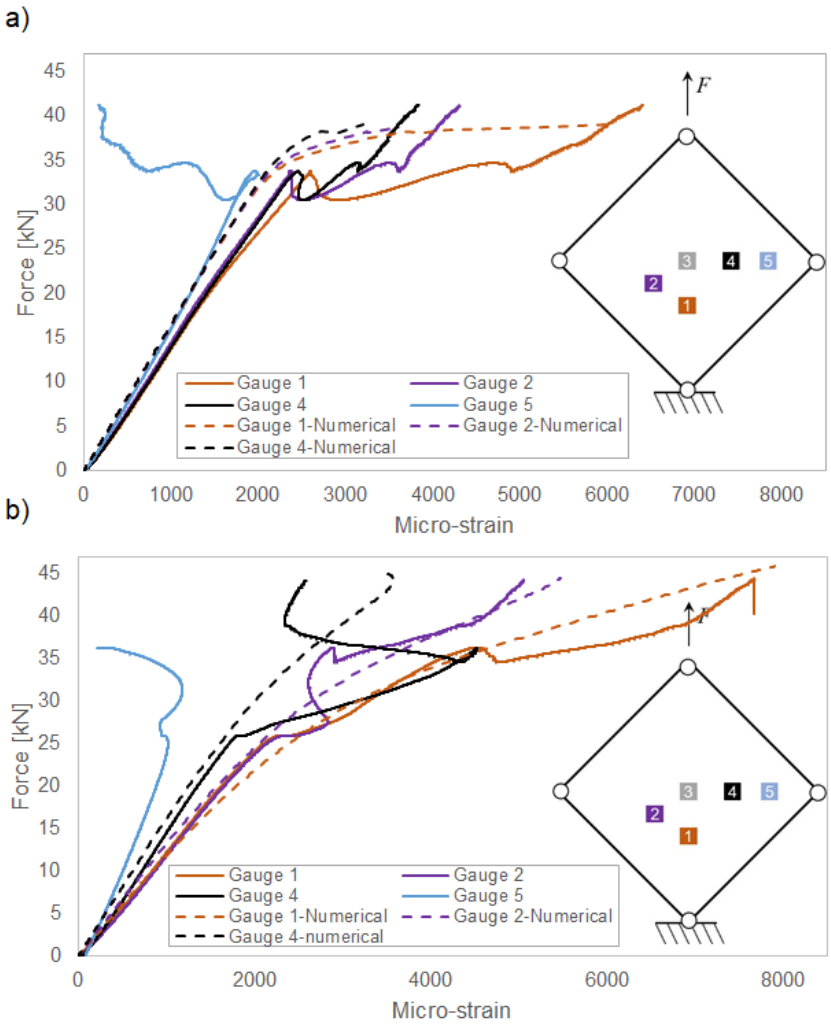

Figure 10: Experimental strain gauge readings and numerical values for; a) pure CFRP laminates (type 1) and b) X-braced hybrid laminates (type 2). FE results are extracted at through-thickness integration point locations equivalent to that of strain gauge locations in the experiment

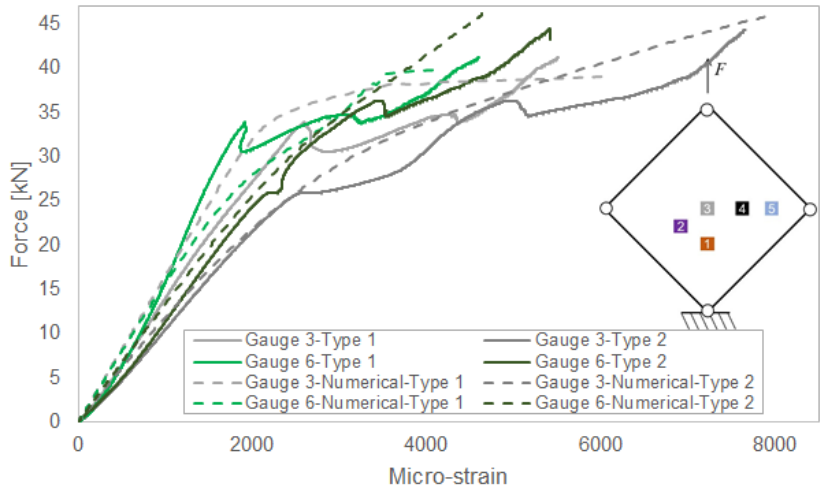

Figure 11: Experimental strains (solid lines) and numerical strains (dashed lines) for strain gauges 3 and 6 of both laminate types 1 and 2. Strain gauge 6 (green data) is on the opposite side of strain gauge 3

The numerical analysis has the advantage that it can provide insight into the internal specimen damage mechanisms, helping to identify differences in behaviour between the laminate designs. The failed specimens of type 1 and 2 laminates are shown in Figure 12 demonstrating a repeatable failure location and type for all specimens. Experimental examination of the failed laminates shows that the type 1 laminate failed along the centreline of the specimen, displaying a combination of matrix cracking and fibre breakage (see Figure 13). The failure in the direction of the main diagonal shows the well-known characteristic tension field panel behaviour under pure shear loading. A similar failure type is reported in [34]. After initial plate buckling, the specimen deforms into mode shape 1 (Figure 13a) and continues deforming in the same mode up to the point of failure (Figure 13c). As observed in the experiment, the fracture is sudden and brittle. Probing the numerical results suggests that although shear damage is present in the type 1 laminate (see Figure 14c), the failure is dominated by compressive and tensile fibre breakage along the local 2 direction of the outermost plies, i.e. plies 1 and 8 (see Figure 14a-b). In other words, the comparison of maximum and minimum principal stresses just before and after load drop (see Figure 15) for the outermost plies is comparable with those of material strength allowables ($595\,MPa$ for tensile and $393\,MPa$ for compressive strength) of Table 1. This shows that the initiation of damage is strongly correlated to the tensile damage of fibres focused along the geometric centreline of the tensile outermost ply in the laminate (ply 8). This is in good agreement with the observation of the experimental results.

Figure 16 illustrates the experimental failure process of the type 2 laminates. The experimental failure starts from the ply drop off of the X-brace CFRP plies (Figure 16a), which then joins up with the failure from the bottom grip location (Figure 16b). As the loading increases, the failure grows (Figure 16c-d) and reaches the top grip (Figure 16e-f). Examination of the predicted damage from the simulation, just before failure and throughout the failure process, shows that shear damage (SDV5) occurs far in advance of any damage mechanism, i.e. fibre tensile/compressive failure, and is present throughout the failure process as shown in Figure 17. Shear damage is mostly associated to the 0 deg carbon plies in the areas close to the boundaries of the laminate than the 45 deg carbon or glass plies. For the sake of brevity, shear stresses of the 0 deg carbon ply of the laminate are plotted in Figure 18 at various time steps.

Comparison of the numerical shear stresses of Figure 18 with those of Figure 8b illustrates the exceedance of shear stresses from $45\,MPa$ (threshold for plastic shear strain). This suggests that plastic deformation of the 0 deg carbon plies, under shear loading, could be a key contributing factor to the considerably higher strain to failure of the type 2 laminate design.

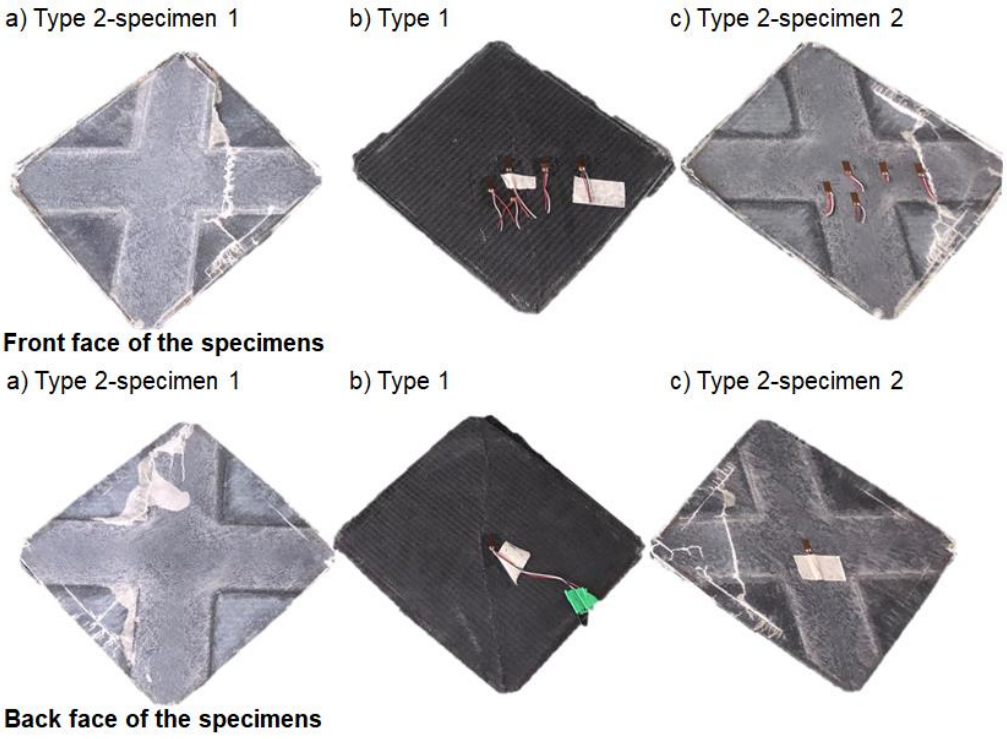

Figure 12: Failed specimens for type 1 and two of type 2 laminates. Top and bottom figures are for the front and back faces, respectively.

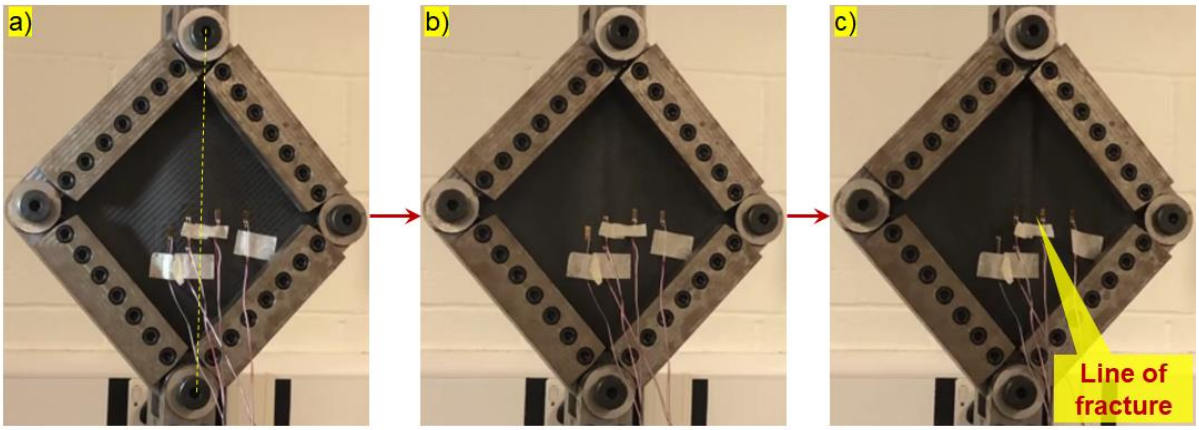

Figure 13: Experimental progression of failure in type 1 laminates (the yellow dashed line shows the centreline or axis of symmetry)

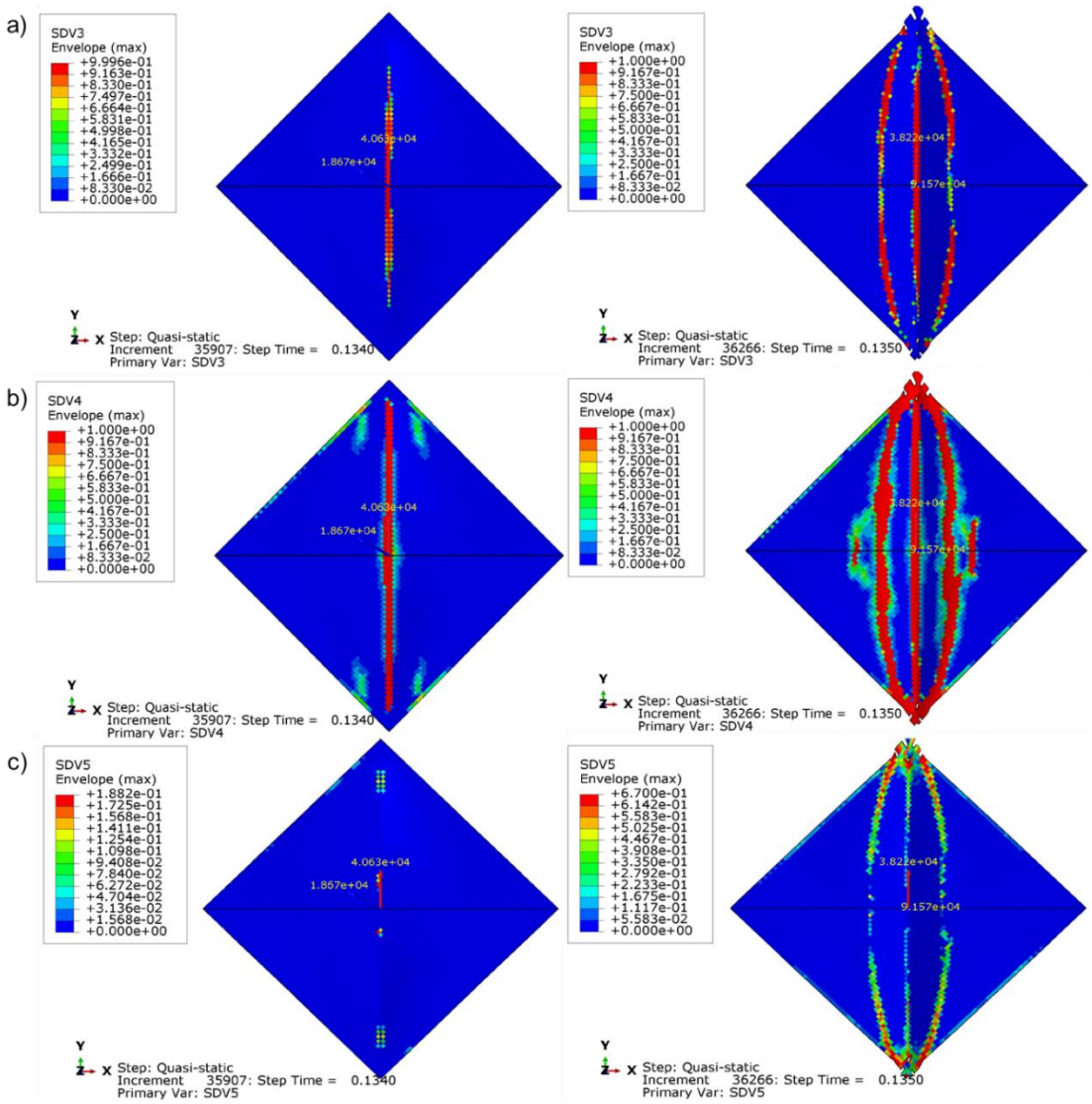

Figure 14: Damage parameters of type 1 laminates; a) fibre tensile damage in ply local direction 2, b) fibre compressive damage in ply local direction 2 and c) shear damage at the damage initiation (left images) and just prior to load drop and specimen collapse (right images)

It is worth noting that the shear damage parameter never exceeds 0.72 (maximum possible experimental shear damage parameter for CFRP and GFRP material as shown in Figure 7) and is present throughout the failure process. In fact, as shown in Figure 19, shear damage is often accompanied by a compressive failure (SDV4) of fibres along the 2 material direction. As shown in Figure 20, X shaped 45 deg carbon plies furthest away from the mid-plane of the laminates experience the highest compressive stresses as a result of out of plane bending deformation and fail first. Subsequently, the load is redistributed to the glass fibres located at the outer mould surfaces, giving rise to compressive stresses along the 2 material direction as shown in Figure 21. It is worth noting that, unlike the type 1 laminates, the numerical simulation does not predict tensile damage of the fibres, nor compressive damage in

the local 1 direction for the material. In general, the numerical model demonstrates good agreement with the experimental results, in terms of damage location, initiation and progression.

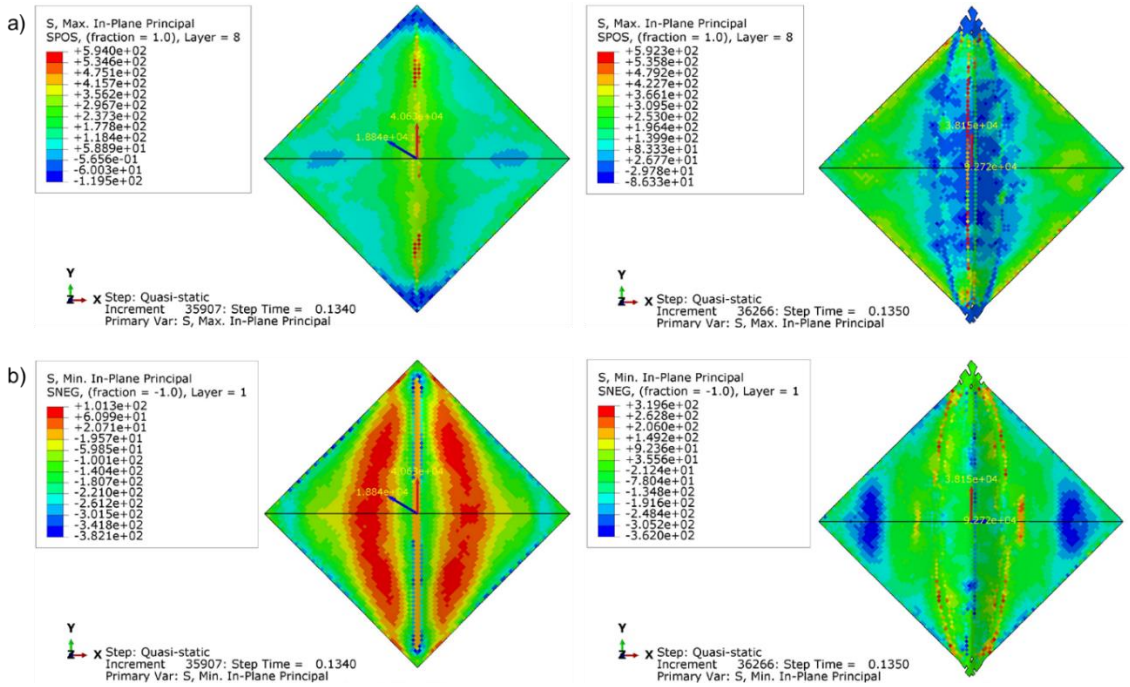

Figure 15: Principal stresses of type 1 laminates; a) maximum principal stress just before (left image) and after (right image) the load drop for tensile outermost ply (ply 8), b) minimum principal stress just before (left image) and after (right image) the load drop for compressive outermost ply (ply 1)

Unlike the conventional type 1 design, the type 2 laminates do not manifest the well-known characteristic behaviour of either complete or incomplete tension field plates. Instead, they demonstrate a gradual failure behaviour due to the dominance of the shear damage failure mechanism, as opposed to tension along the main diagonal of the plate and in the loading direction that could lead to sudden fibre breakage as evidenced in the type 1 design. This is a result of shear damage, cracking and plastic deformation of the matrix leading to a more gradual failure. It may be argued that this mode of failure is more desirable for flight critical components.

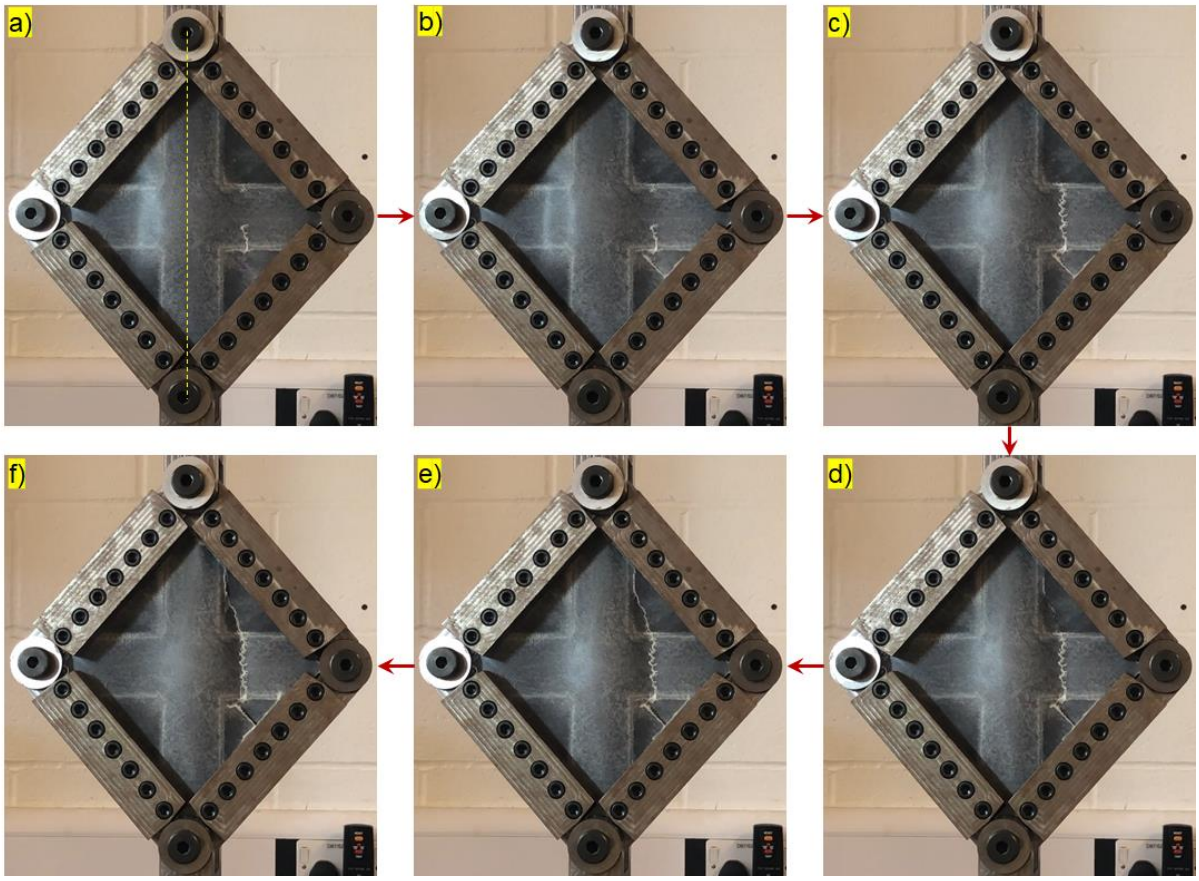

Figure 16: Experimental progression of failure in type 2 laminates (the yellow dashed line shows the centreline or axis of symmetry)

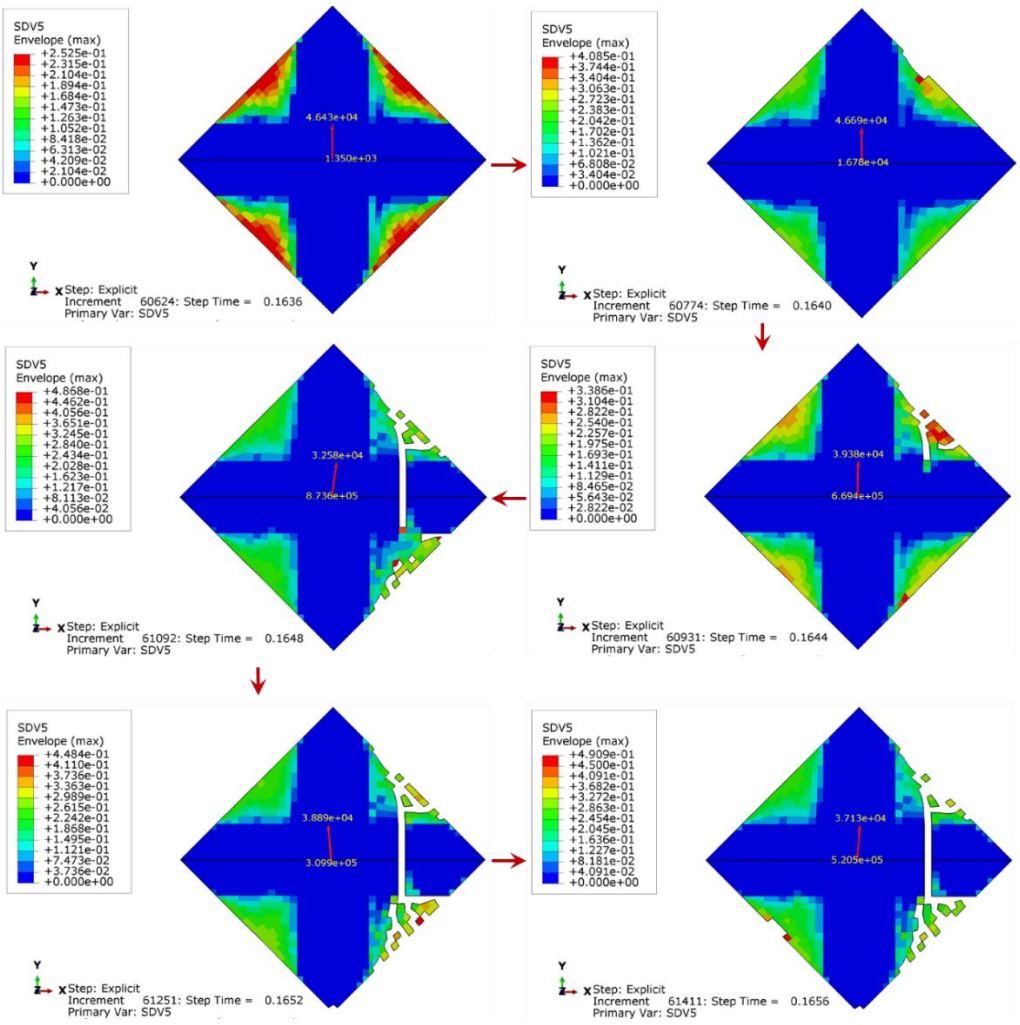

Figure 17: Progressive shear damage parameter (SDV5) for type 2 laminates throughout the failure process

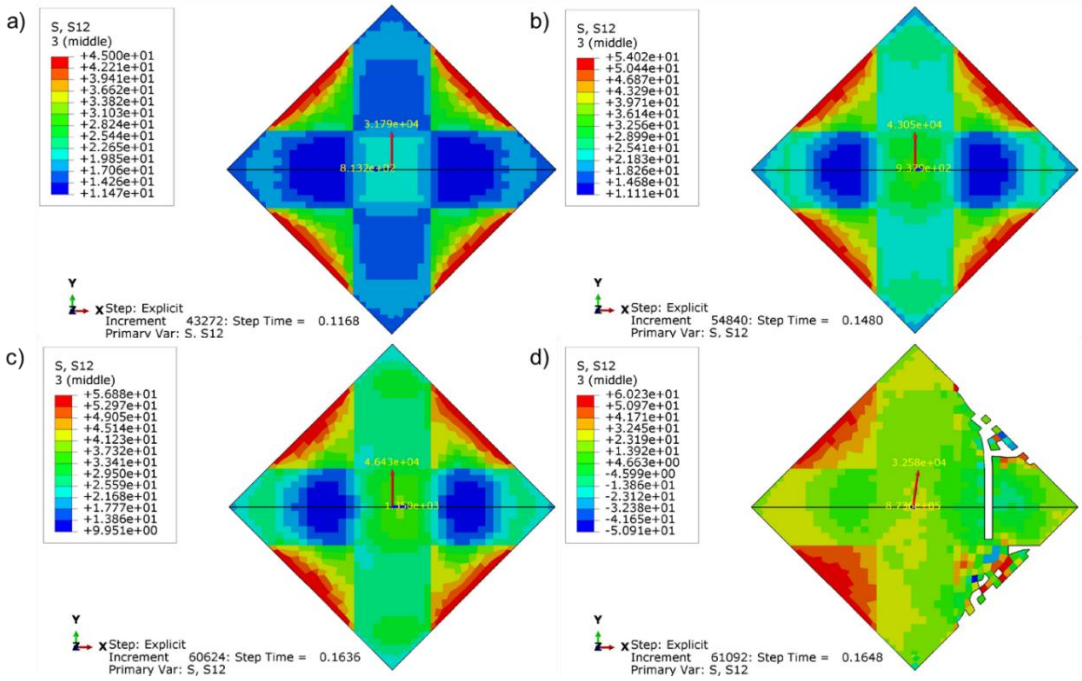

Figure 18: Progressive shear stresses of 0deg carbon plies for type 2 laminates before and throughout the failure process

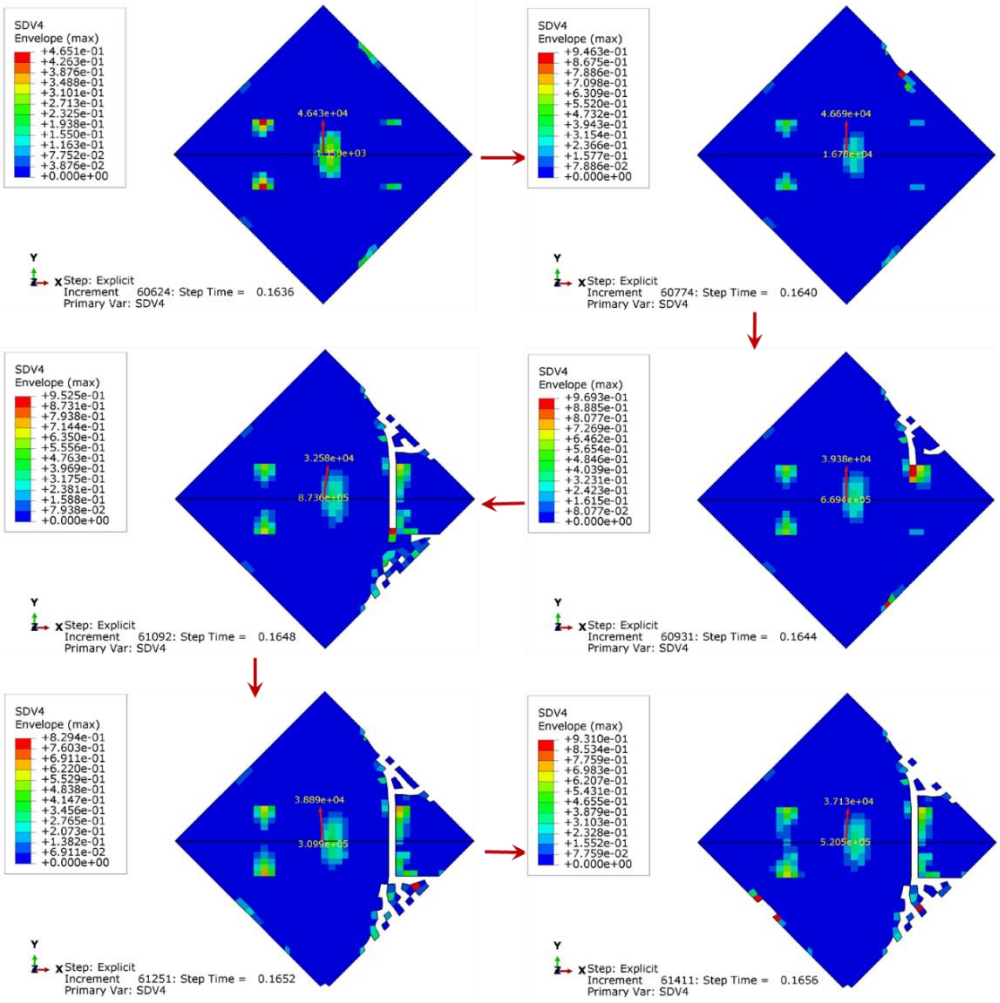

Figure 19: Progressive compressive damage parameter (SDV4) along fibre direction 2 for type 2 laminates throughout the failure process

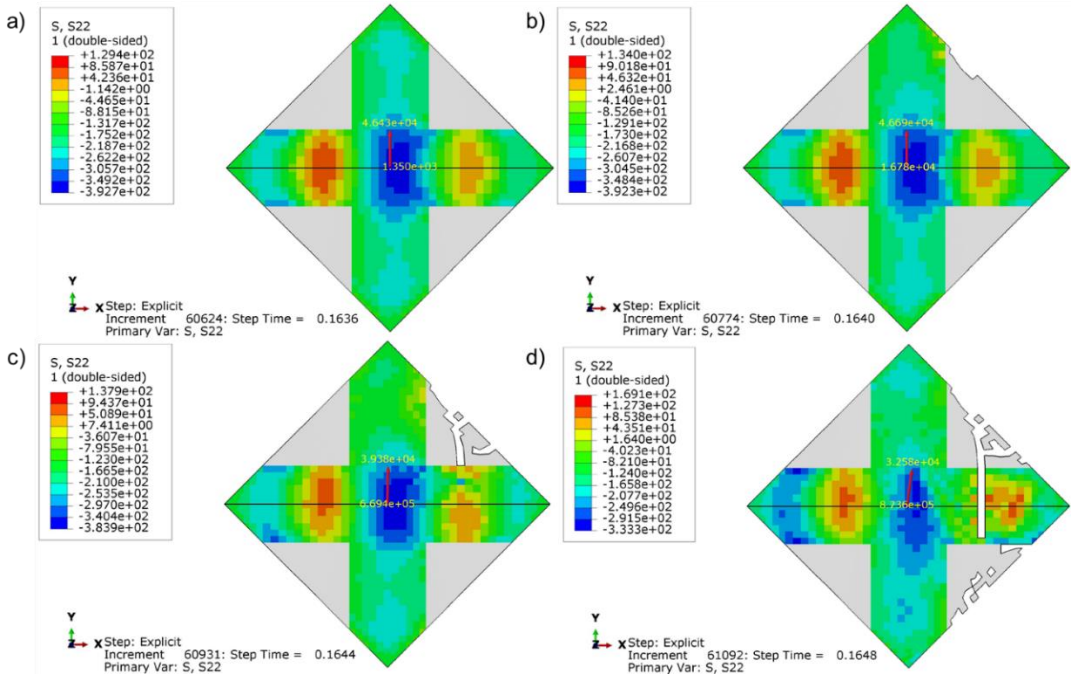

Figure 20: Progressive compressive stresses of X shaped carbon plies for type 2 laminates just before and throughout the failure process

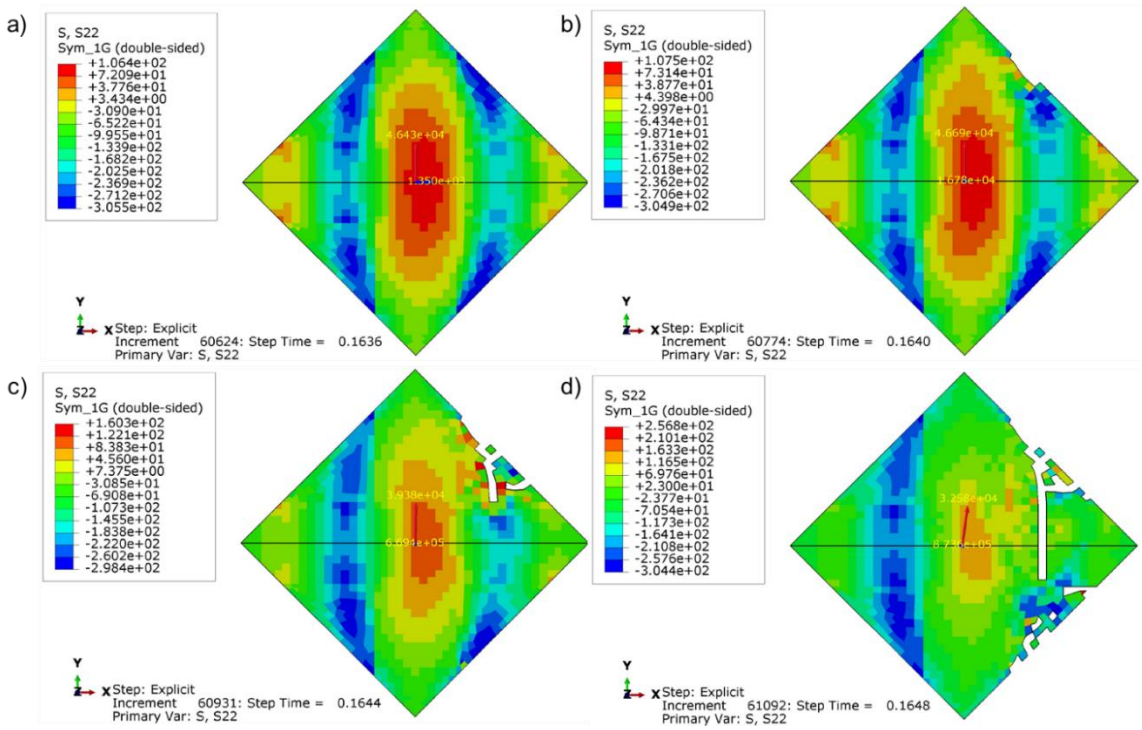

Figure 21: Progressive compressive stresses of glass plies for type 2 laminates just before and throughout the failure process

7 Conclusions

Buckling and post-buckling performance of pure twill woven CFRP (type 1) and a novel X-braced hybrid laminate design (type 2) have been investigated experimentally and numerically, considering pure shear loading. Type 1 and hybrid laminates failed at loads approximately 1.3 and 1.6 times higher than the initial plate buckling load, respectively, demonstrating the capability of composite laminates in resisting loads well beyond initial buckling. It is evident that the X-braced hybrid laminates benefit from 23% higher buckling to failure load ratio compared to type 1 laminate. The novel X-braced hybrid laminates, despite having less of the much stiffer CFRP plies, showed only marginally lower initial plate buckling performance and higher failure performance. In addition, the novel laminates also exhibited significantly higher strain to failure compared to the conventional laminates, thanks to the X-bracing concept and the plastic deformation of the 0 deg CFRP plies. The numerical models achieved close prediction of the experimental buckling and nonlinear post-buckling behaviour - predicting the bifurcation point, the failure load, the location of damage and the damage mechanisms all with reasonable accuracy. Due to the representation of initial imperfections within the numerical models, smooth transitions were consistently observed from the linear buckling to the post-buckling behaviour. Failure of the

conventional laminates was dominated by both tensile and compressive fibre damage in the local 2 direction of the outermost and innermost plies. Whereas the novel X-braced hybrid laminates failed with shear damage and compressive fibre breakage in the ply local 2 direction of the outermost plies. The combined experimental and numerical results illustrate the feasibility to tailor the shape of hybrid laminate plies to reduce weight and maximise their post-buckling strain to failure. Further studies and more test samples are required to evaluate the performance of such concepts under other loading conditions, particularly, their cyclic behaviour given the lower buckling mode of hybrid concept compared to the traditional type 1 laminate.

8 Declaration of conflicting interests

The authors declared no potential conflicts of interest with respect to the research, authorship, and/or publication of this article.

9 Acknowledgment

The authors received no financial support for the research, authorship, and/or publication of this article.

10 References

[1] Y. Feng, Y. He, X. Tan, T. An, and J. Zheng, “Experimental investigation on different positional impact damages and shear-after-impact (SAI) behaviors of stiffened composite panels,” *Compos. Struct.*, vol. 178, pp. 232–245, 2017, doi: 10.1016/j.compstruct.2017.06.053.

[2] D. G. Stamatelos, G. N. Labeas, and K. I. Tserpes, “Analytical calculation of local buckling and post-buckling behavior of isotropic and orthotropic stiffened panels,” *Thin-Walled Struct.*, vol. 49, no. 3, pp. 422–430, 2011, doi: https://doi.org/10.1016/j.tws.2010.11.008.

[3] M. Suresh Kumar, M. Ambresha, K. Panbarasu, I. Kishore, and V. R. Ranganath, “A comparative study of failure features in aerospace grade unidirectional and bidirectional woven CFRP composite laminates under four-point bend fatigue loads,” *Materwiss. Werksttech.*, vol. 46, no. 6, pp. 644–651, 2015, doi: 10.1002/mawe.201400278.

[4] M. H. Kabir, S. Fawzia, T. H. T. Chan, and M. Badawi, “Durability of CFRP strengthened steel circular hollow section member exposed to sea water,” *Constr. Build. Mater.*, vol. 118, pp. 216–225, 2016, doi: 10.1016/j.conbuildmat.2016.04.087.

[5] T. H. G. Megson, *Introduction to Aircraft Structural Analysis*. 2010.

[6] T. Kopecki, J. Bakunowicz, and T. Lisle, “Post-critical deformation states of composite thin-walled aircraft load-bearing structures,” *J. Theor. Appl. Mech.*, vol. 54, no. 1, pp. 195–204, 2016, doi: 10.15632/jtam-pl.54.1.195.

[7] J. Loughlan, “The buckling of CFRP composite plates in compression and shear and thin-walled composite tubes in torsion – The effects of bend-twist coupling and the applied shear direction on buckling performance,” *Thin-Walled Struct.*, vol. 138, pp. 392–403, 2019, doi: https://doi.org/10.1016/j.tws.2019.01.045.

[8] A. Murphy, F. Lynch, M. Price, and A. Gibson, “Modified stiffened panel analysis methods for laser beam and friction stir welded aircraft panels,” *Proc. Inst. Mech. Eng. Part G J. Aerosp. Eng.*, vol. 220, no. 4, pp. 267–278, 2006, doi: 10.1243/09544100JAERO51.

[9] D. Quinn, A. Murphy, and C. Glazebrook, “Aerospace stiffened panel initial sizing with novel skin sub-stiffening features,” *Int. J. Struct. Stab. Dyn.*, vol. 12, no. 5, p. 1250060, 2012, doi: 10.1142/S0219455412500605.

[10] X. Liu, C. A. Featherston, and D. Kennedy, “Buckling optimization of blended composite structures using lamination parameters,” *Thin-Walled Struct.*, vol. 154, p. 106861, 2020, doi: https://doi.org/10.1016/j.tws.2020.106861.

[11] B. E. Kaminski and J. E. Ashton, “Diagonal Tension Behavior of Boron-Epoxy Shear Panels,” *J. Compos. Mater.*, vol. 5, no. 4, pp. 553–558, Apr. 1971, doi: 10.1177/002199837100500416.

[12] T. Kubiak and R. J. Mania, “Hybrid versus FR laminate channel section columns – Buckling and postbuckling behaviour,” *Compos. Struct.*, vol. 154, pp. 142–149, 2016, doi: https://doi.org/10.1016/j.compstruct.2016.07.040.

[13] I. Papa, L. Boccarusso, A. Langella, and V. Lopresto, “Carbon/glass hybrid composite laminates in vinylester resin: Bending and low velocity impact tests,” *Compos. Struct.*, vol. 232, p. 111571, 2020, doi: https://doi.org/10.1016/j.compstruct.2019.111571.

[14] R. Burgueño, N. Hu, A. Heeringa, and N. Lajnef, “Tailoring the elastic postbuckling response of thin-walled cylindrical composite shells under axial compression,” *Thin-Walled Struct.*, vol. 84, pp. 14–25, 2014, doi: https://doi.org/10.1016/j.tws.2014.05.009.

[15] B. L. Agarwal, “Postbuckling Behavior of Composite Shear Webs,” *AIAA J.*, vol. 19, no. 7, pp. 933–939, Jul. 1981, doi: 10.2514/3.51022.

[16] S. Kosteletos, “Postbuckling response of laminated plates under shear load,” *Compos. Struct.*, vol. 20, no. 3, pp. 137–145, 1992, doi: https://doi.org/10.1016/0263-8223(92)90020-D.

[17] F. A. Fazzolari, J. R. Banerjee, and M. Boscolo, “Buckling of composite plate assemblies using higher order shear deformation theory—An exact method of solution,” *Thin-Walled Struct.*, vol. 71, pp. 18–34, 2013, doi: https://doi.org/10.1016/j.tws.2013.04.017.

[18] K. Zhao, D. Kennedy, and C. Featherston, “Exact strip postbuckling analysis of composite plates under compression and shear,” *Aeronaut. J.*, vol. 123, no. 1263, pp. 658–677, 2019, doi: https://doi-org.ezproxy.uwe.ac.uk/10.1017/aer.2019.27.

[19] M. Damghani, D. Kennedy, and C. Featherston, “Global buckling of composite plates containing rectangular delaminations using exact stiffness analysis and smearing method,” *Comput. Struct.*, vol. 134, pp. 32–47, Apr. 2014, doi: 10.1016/j.compstruc.2013.12.005.

[20] M. Damghani, D. Kennedy, C. C. A. C. Featherston, D. Kennedy, and C. C. A. C. Featherston, “Critical buckling of delaminated composite plates using exact stiffness analysis,” *Comput. Struct.*, vol. 89, no. 13–14, pp. 1286–1294, Jul. 2011, doi: 10.1016/j.compstruc.2011.04.003.

[21] Z. Wu, G. Raju, and P. M. Weaver, “Postbuckling analysis of variable angle tow composite plates,” *Int. J. Solids Struct.*, vol. 50, no. 10, pp. 1770–1780, 2013, doi: https://doi.org/10.1016/j.ijsolstr.2013.02.001.

[22] N. R. Kolanu, G. Raju, and R. M, “Post-buckling failure studies on quasi-isotropic CFRP panels under positive and negative in-plane shear loading,” *Compos. Struct.*, vol. 246, p. 112379, 2020, doi: https://doi.org/10.1016/j.compstruct.2020.112379.

[23] T. Zhang, S. Li, F. Chang, X. Shi, and L. Li, “An experimental and numerical analysis for stiffened composite panel subjected to shear loading in hygrothermal environment,” *Compos. Struct.*, vol. 138, pp. 107–115, 2016, doi: https://doi.org/10.1016/j.compstruct.2015.11.056.

[24] J. Reinoso, A. Blázquez, F. París, J. Cañas, and J. C. Meléndez, “Postbuckling behaviour of a pressurized stiffened composite panel – Part I: Experimental study,” *Compos. Struct.*, vol. 94, no. 5, pp. 1533–1543, 2012, doi: https://doi.org/10.1016/j.compstruct.2011.12.014.

[25] D. Kumar and S. B. Singh, “Postbuckling strengths of composite laminate with various shaped cutouts under in-plane shear,” *Compos. Struct.*, vol. 92, no. 12, pp. 2966–2978, 2010, doi: https://doi.org/10.1016/j.compstruct.2010.05.008.

[26] D. Kumar and S. B. Singh, “Stability and failure of composite laminates with various shaped cutouts under combined in-plane loads,” *Compos. Part B Eng.*, vol. 43, no. 2, pp. 142–149, 2012, doi: https://doi.org/10.1016/j.compositesb.2011.09.005.

[27] A. Muc, M. Chwał, and M. Barski, “Remarks on experimental and theoretical investigations of buckling loads for laminated plated and shell structures,” *Compos. Struct.*, vol. 203, pp. 861–874, 2018, doi: https://doi.org/10.1016/j.compstruct.2018.07.094.

[28] A. S. M. Al-Azzawi, L. F. Kawashita, and C. A. Featherston, “Buckling and postbuckling behaviour of Glare laminates containing splices and doublers. Part 2: Numerical modelling,” *Compos. Struct.*, vol. 176, pp. 1170–1187, 2017, doi:

https://doi.org/10.1016/j.compstruct.2017.04.063.

[29] A. S. M. Al-Azzawi, J. McCrory, L. F. Kawashita, C. A. Featherston, R. Pullin, and K. M. Holford, “Buckling and postbuckling behaviour of Glare laminates containing splices and doublers. Part 1: Instrumented tests,” *Compos. Struct.*, vol. 176, pp. 1158–1169, 2017, doi: https://doi.org/10.1016/j.compstruct.2017.04.030.

[30] N. Petkune, T. Donchev, H. Hadavinia, D. Wertheim, and M. Limbachiya, “Comparison of the behaviour of steel, pure FRP and hybrid shear walls under cyclic seismic loading in aspect of stiffness degradation and energy absorption,” *Constr. Build. Mater.*, vol. 165, pp. 621–630, 2018, doi: https://doi.org/10.1016/j.conbuildmat.2017.12.013.

[31] Y. Swolfs, L. Gorbatikh, and I. Verpoest, “Fibre hybridisation in polymer composites: A review,” *Compos. Part A Appl. Sci. Manuf.*, vol. 67, pp. 181–200, 2014, doi: 10.1016/j.compositesa.2014.08.027.

[32] E. A. Godínez-Domínguez and A. Tena-Colunga, “Behavior of ductile steel X-braced RC frames in seismic zones,” *Earthq. Eng. Eng. Vib.*, vol. 18, no. 4, pp. 845–869, 2019, doi: 10.1007/s11803-019-0539-0.

[33] M. Damghani, N. Ersoy, M. Piorkowski, and A. Murphy, “Experimental evaluation of residual tensile strength of hybrid composite aerospace materials after low velocity impact,” *Compos. Part B Eng.*, vol. 179, p. 107537, Dec. 2019, doi: 10.1016/J.COMPOSITESB.2019.107537.

[34] N. R. Kolanu, G. Raju, and M. Ramji, “Damage assessment studies in CFRP composite laminate with cut-out subjected to in-plane shear loading,” *Compos. Part B Eng.*, vol. 166, pp. 257–271, 2019, doi: 10.1016/j.compositesb.2018.11.142.

[35] A. F. Johnson, “Modelling fabric reinforced composites under impact loads,” *Compos. - Part A Appl. Sci. Manuf.*, 2001, doi: 10.1016/S1359-835X(00)00186-X.

[36] T. Lisle, C. Bouvet, M. L. Pastor, T. Rouault, and P. Marguerès, “Damage of woven composite under tensile and shear stress using infrared thermography and micrographic cuts,” *J. Mater. Sci.*, 2015, doi: 10.1007/s10853-015-9173-z.

[37] M.-G. Han and S.-H. Chang, “Draping simulation of carbon/epoxy plain weave fabrics with non-orthogonal constitutive model and material behavior analysis of the cured structure,” *Compos. Part A Appl. Sci. Manuf.*, vol. 110, pp. 172–182, 2018, doi: https://doi.org/10.1016/j.compositesa.2018.04.022.

[38] V. Munoz, M. Perrin, M. L. Pastor, H. Welemane, A. Cantarel, and M. Karama, “Determination of the elastic properties in CFRP composites: Comparison of different approaches based on tensile tests and ultrasonic characterization,” *Adv. Aircr. Spacecr. Sci.*, 2015, doi: 10.12989/aas.2015.2.3.249.

[39] K. A. Stevens, R. Ricci, and G. A. O. Davies, “Buckling and postbuckling of composite structures,” *Composites*, vol. 3, no. 26, pp. 189–199, 1995, doi:

10.1016/0010-4361(95)91382-F.

[40] A. Blázquez, J. Reinoso, F. París, and J. Cañas, “Postbuckling behavior of a pressurized stiffened composite panel - Part II: Numerical analysis. Effect of the geometrical imperfections,” *Compos. Struct.*, vol. 94, pp. 1544–1554, 2012, doi: 10.1016/j.compstruct.2011.12.013.

Appendix

The damage parameters used for the materials of study are obtained via experimental testing by the authors and are shown in Table A.

Table A: Damage parameters for the materials of study

Parameter	Unit	Description	Value	
			AX 5180	AX 3180
E_{1+}	MPa	Young's modulus along fibre direction 1 when $tr(\boldsymbol{\varepsilon}) \geq 0$ *	67094.00	30083.00
E_{2+}	MPa	Young's modulus along fibre direction 2 when $tr(\boldsymbol{\varepsilon}) \geq 0$	67094.00	30083.00
υ_{12+}	-	Poisson's ratio when $tr(\boldsymbol{\varepsilon}) \geq 0$	0.04	0.14
G_{12}	MPa	Shear modulus	4831.40	4954.60
E_{1-}	MPa	Young's modulus along fibre direction 1 when $tr(\boldsymbol{\varepsilon}) < 0$	67094.00	30083.00
E_{2-}	MPa	Young's modulus along fibre direction 2 when $tr(\boldsymbol{\varepsilon}) < 0$	67094.00	30083.00
υ_{12-}	-	Poisson's ratio when $tr(\boldsymbol{\varepsilon}) < 0$	0.04	0.14
X_{1+}	MPa	Tensile strength along fibre direction 1	595.00	437.16
X_{1-}	MPa	Compressive strength along fibre direction 1	393.00	306.00
X_{2+}	MPa	Tensile strength along fibre direction 2	595.00	437.16
X_{2-}	MPa	Compressive strength along fibre direction 2	393.00	306.00
S	MPa	Shear stress at the onset of shear damage	39.62	34.09
G_f^{1+} **	N.mm/mm^2	Energy per unit area for tensile fracture along fibre direction 1	6.61	7.94
G_f^{1-}	N.mm/mm^2	Energy per unit area for compressive fracture along fibre direction 1	4.35	5.56
G_f^{2+}	N.mm/mm^2	Energy per unit area for tensile fracture along fibre direction 2	6.61	7.94
G_f^{2-}	N.mm/mm^2	Energy per unit area for compressive fracture along fibre direction 2	4.35	5.56
α_{12}	-	Parameter in the equation of shear damage	0.38	0.31
$d_{12}^{\max}$	-	Maximum shear damage	0.67	0.72
$\overline{\sigma_{0y}}$	MPa	Initial effective shear yield stress	45.00	30.00
C	-	Coefficient in hardening equation	1326.42	2024.98
p	-	Power term in hardening equation	0.48	0.49

* $tr(\boldsymbol{\varepsilon}) = \varepsilon_{11} + \varepsilon_{22}$

** determined for element characteristic length of $2.5\ mm$ based on $G_f^{1+} = L_c g_0^{1+}$

Dr. Mahdi Damghani
(CEng MIMechE, PhD, MSc, BSc)
Senior Lecturer in Composites and Aero-structures
Room 3D26
Engineering Design and Mathematics Department
University of the West of England (UWE)
Frenchay Campus
Coldharbour Lane
Bristol
BS16 1QY
Tel: 0117 328 7369
Email: Mahdi.Damghani@uwe.ac.uk

Date: 06/01/2021

Dear Editor,

This letter is to declare no conflict of interest in carrying out the research by the authors titled as “Experimental and numerical analysis for buckling and postbuckling behaviour of hybrid composite laminates subjected to in-plane shear loading”.

Yours’ Sincerely

Dr Mahdi Damghani
Mr Christopher Wallis
Dr Jerzy Bakunowicz
Prof Adrian Murphy

CRediT author statement:

Mahdi Damghani: Conceptualisation, Methodology, Software, Validation, Formal analysis, Resources, Writing-Original Draft, Writing-Review & Editing, Visualisation, Supervision, Project administration **Christopher Wallis:** Investigation, Data Curation **Jerzy Bakunowicz:** Resources, Writing-Review & Editing **Adrian Murphy:** Writing-Original Draft, Writing-Review & Editing